PU/NE-05-17

(REPORT)

PCCS SEPARATE EFFECT TESTS IN THE PUMA FACILITY

by

M. Ishii, S. W. Choi, J. Yang, K. Vierow, PU

and

W. Wang, J. Han
U.S. NRC

Prepared for
U.S. Nuclear Regulatory Commission

PURDUE
UNIVERSITY

May 2006

PURDUE UNIVERSITY
SCHOOL OF NUCLEAR ENGINEERING

PCCS SEPARATE EFFECT TESTS IN THE PUMA FACILITY

by

M. Ishii, S. W. Choi, J. Yang, K. Vierow, PU

and

W. Wang, J. Han
U.S. NRC

Prepared for
U.S. Nuclear Regulatory Commission

PURDUE
UNIVERSITY

May 2006

PURDUE UNIVERSITY
SCHOOL OF NUCLEAR ENGINEERING

PCCS Separate Effect Tests in the PUMA Facility

by

M. Ishii, S. W. Choi, J. Yang ,

K. Vierow, PU

and

W. Wang, J. Han, U.S. NRC

May 2006

Prepared for

School of Nuclear Engineering, Purdue University

400 Central Drive, West Lafayette, IN 47907 USA

ACKNOWLEDGEMENTS

ABSTRACT

The development of a reliable Passive Containment Cooling System (PCCS) is one of the key areas in the design of advanced nuclear reactors. According to the GE ESBWR (2002) design, the cooling capacity of the PCCS must be sufficient to maintain the containment pressure below 0.48 MPa (55 psig) during any postulated Design Basis Accidents by removing the decay heat for at least 72 hours after the accident. The primary heat removal mechanism of the PCCS is steam condensation in vertical tubes. Since the condensation heat transfer rate can be significantly reduced when noncondensable gases are present, it is important to understand the condensation phenomena of steam-gas mixtures inside the PCCS tubes to evaluate the function of the PCCS.

Several experiments have been performed by other researchers to study the PCCS capacity for heat exchange. The existing correlations and models are mainly for the "bypass mode", in which the mixture may vent directly to the wetwell gas space. These correlations and models may not be applicable when there is no open passage for the steam to escape.

The purpose of the current work is to obtain experimental data for the downward co-current flow of a steam/air mixture through condenser tube bundles during the three operational modes of the PCCS, namely the bypass mode, the cyclic venting mode and the long-term cooling mode.

This report provides a set of separate-effect PCCS test data obtained for condensation heat transfer in the PCCS heat exchangers of the PUMA (Purdue University Multi-dimensional Integral Test Assembly) facility under a task sponsored by the U.S. Nuclear Regulatory Commission. Test conditions are for the long term cooling mode, the bypass mode and the cyclic venting mode, covering a wide range of LOCA conditions in terms of pressure, mass flow rate, noncondensable gases concentration, and PCCS pool level.

Experimental results showed that the condensate heat transfer rate in PCCS tubes would be affected by several factors. First, as the inlet pressure of the PCCS increases,

the condensate heat transfer rate increases, while the average condensation heat transfer coefficient decreases. Secondly, as the inlet noncondensable gas concentration increases, the average condensation heat transfer coefficient decreases. The experiment data showed that the cyclic venting frequency was proportional to the noncondensable gas fraction in the inlet mixture flow. The PUMA separate effect data exhibited similar trends to the data from other programs including the UCB single-tube tests and the PANTHERS tube bundle tests.

TABLE OF CONTENTS

LIST OF TABLES

LIST OF FIGURES

NOMENCLATURE

A	Flow area [m^2]
A_i	Inner surface area of a condenser tube [m^2]
c_p	Specific heat at constant pressure [J/(kg-K)]
D_0	Outside diameter [m]
D_i	Inside diameter [m]
g	Gravitational acceleration [m/s^2]
h_c	Condensation Heat Transfer Coefficient [W/m^{2}K]
h_p	Heat Transfer Coefficient in PCCS pool [W/m^{2}K]
i	Enthalpy per unit mass [J/kg]
$\dot{m}$	Mass flow rate [kg/s]
$\dot{m}_{air}$	Mass flow rate of air [kg/s]
$\dot{m}_{steam}$	Mass flow rate of steam [kg/s]
N_{tubes}	Number of PCCS condenser tubes [-]
N_{units}	Number of PCCS units [-]
P	Pressure [Pa]
ΔP	Differential pressure [Pa]
Q_{con}	Condensation power [W]
q''	Heat flux [W/m^2]
Q_{in}	Input power [W]
Q_{out}	Output power [W]
T	Temperature [K]
t	Time [s]
T_b	PCCS tube centerline temperature [$^\circ$C]
T_g	Tube centerline gas temperature [$^\circ$C]
T_{in}	Inlet temperature [$^\circ$C]
T_{out}	Outlet temperature [$^\circ$C]
T_p	PCCS pool temperature [$^\circ$C]

T_{sat}	Saturation Temperature [^{o}C]
T_{wo}	Wall outside temperature [^{o}C]
T_{wi}	Wall inside temperature [^{o}C]
U	Overall heat transfer coefficient [W/m^{2}K]
V	Voltage output of sensors [V]
v	Velocity [m/s]
z	Axial coordinate [m]

Greek Symbols

ρ	Density [kg/m^3]

Subscripts

f	Liquid phase
g	Vapor phase
in	Inlet
m	Mixture
sat	Saturation
sub	Subcooling
w	Wall

1. INTRODUCTION

1.1 Research Background

General Electric (GE) Nuclear Energy has developed a new passively-safe boiling water reactor shown in Figure 1.1(2002), the Economic Simplified Boiling Water Reactor (ESBWR), which is based on the previous Simplified Boiling Water Reactor (SBWR) design with some significant modifications of safety systems. Major differences between the ESBWR or SBWR and current Boiling Water Reactors (BWRs) include the simplification of the coolant circulation system and the implementation of passive safety systems. There are no recirculation pumps to drive the coolant flow in the vessel of the ESBWR. The Emergency Core Cooling System and Passive Containment Cooling System (PCCS) do not have active pump-driven flows.

The PCCS uses natural circulation to passively provide long-term cooling and no active devices are required for the PCCS to function. The driving force of the flow through the PCCS is the pressure difference between the drywell and the wetwell. The cooling capacity of the PCCS must be sufficient to maintain the containment pressure below 0.48 MPa (55 psig) during any postulated Design Basis Accident by removing the decay heat for at least 72 hours. A good understanding of condensation of steam-gas mixtures inside vertical tubes is necessary to evaluate the performance of the PCCS.

Of particular importance are the condensation heat transfer characteristics of the PCCS in the presence of a noncondensable gas. Since the condensation heat transfer rate can be significantly reduced when noncondensable gas exists, it is important to study this effect when considering using the PCCS as a primary containment cooling system.

1.2 Objectives

The first aim of these tests is to obtain experimental data for the downward co-current flow of a steam/air mixture through condenser tube bundles, during the three operational modes of the PCCS. These modes are the bypass mode during the initial blowdown phase, the periodic venting mode right after the blowdown phase and the long-term cooling mode.

The second aim is to compare system analysis code results (TRACE or RELAP5) with experimental data obtained from these PUMA tests, placing emphasis on the PCCS performance to determine whether there is any condensation modeling deficiency.

The third aim is to develop a model for local heat transfer coefficients for condensation in the presence of noncondensable gas and implement this model into a safety analysis code.

These tests are separate effect tests intended to provide fundamental data on the PCCS behavior. They are strict simulations of neither the SBWR nor the ESBWR, however the data is applicable to both designs.

This report documents final data for the first objective.

1.3 Literature Survey

1.3.1 Separate effect test in a vertical tube

In this chapter, literature review was carried out for the empirical correlations compared PUMA data and integral test which was used for a reference on the test matrix condition.

There are several complications in the calculation of heat transfer coefficients associated with condensation heat transfer in tube film condensation. The film originates at the top of the condensing tube and flows downward under the influence of gravity. The thickness, d, and the condensate mass flow rate, m, increase with increased distance down the tube. This is a result of the continuous condensation at the liquid-vapor interface, and heat transfer from the film to the tube surface which is maintained at $T_w < T_{sat}$. In the most general case, the vapor may be superheated and may be part of a mixture containing one or more noncondensable gases. Moreover, there exists a finite shear stress at the liquid-vapor interface contributing to a velocity gradient in the vapor as well as in the film. The shear stress, interfacial waviness, and turbulent transport in the condensate film (Hasanein et al. 1996) become important factors at high vapor velocities. The film thickness, boundary layer thickness, distribution of temperature, thermodynamic state of the vapor liquid interface and the mass concentration gradientwhich is normal to the surface, are strongly influenced by the velocity of the main vapor flow.

The main research objective of condensation heat transfer is to quantitatively clarify the effects upon condensation mass flux and the heat flux at the cooling surface to which the heat is transferred through the condensate.

Nusselt(1916) developed the theoretical analysis on the filmwise condensation problem for a vertical flat plate in stagnant steam. There are several assumption such as thermal equilibrium between liquid film and vapor, constant wall temperature, no interfacial shear effect (vapor is stagnant) and neglect of the heat and momentum transfer in the liquid film.
The average Nusselt number has the form:

$$\overline{Nu_L} = (\frac{\overline{h_L}L}{k_l}) = 0.943 \left[\frac{\rho_l g (\rho_l - \rho_v) h_{fg}' L^3}{\mu_l k_l (T_{sat} - T_s)} \right]^{1/4} \tag{1-1}$$

Other researchers considered the effect of interfacial shear but assumed constant interfacial shear along the axial direction. Sparrow included the role of subcooling, interface and diffusion based on Nusselt's problem of vertical plate. Chen accounted for the effect of surface waves and turbulence in turbulent film condensation.

For film condensation without shear stress at the interface and with cocurrent vapor flow numerous research exists with considerable deviations from author to author.

Vierow (1990) performed experiments to obtain the local condensation heat transfer coefficient along a vertical tube. A natural circulation loop was used to simulate the PCCS condenser with 22 mm tube I.D. and 2.1 m active heat transfer length. Steam was injected into a lower plenum and condensation occurred in the top most part of the loop. The experiment data were correlated as a correction factor to the heat transfer coefficient obtained by Nusselt theory. This correlation has been a basis for much other research on single-tube steam condensation. The correction factor is defined as the ratio of the experimental heat transfer coefficient to the theoretical Nusselt heat transfer coefficient. The correlation with the correction factor, f(z) , is as follows:

$$f(z) = \frac{h_{exp}(z)}{h_{Nu}(z)} = 0.005 (Re_L(z))^{0.45} (Ma_{bulk}(z))^{-1.1} \tag{1-2}$$

This preliminary version of the correlation was used to evaluate the TRAC-G code by analyzing the Toshiba tube average data. These comparisons resulted in underestimation of the data by as much as 30%

Vierow and Schrock (1991) developed the empirical degradation factor that contains two factors for the theoretical Nusselt value. The Nusselt theory was based on a stagnant pure steam environment and a film thickness neglecting the interfacial shear stress effect.

$$f = f_1 \cdot f_2 = (1 + 2.88 \times 10^{-5} \, \mathrm{Re}_m^{1.18})(1 - CM_a^b) \qquad (1\text{-}3)$$

where Ma is the bulk air mass fraction and

C=10,   b=1.0   for Ma<0.063
C=0.938, b=0.13 for 0.063<Ma<0.6
C=1.0,   b=0.22 for Ma>0.6

The first bracketed term in Eq. (1-3) shows the interfacial shear stress effect on the condensation and second one shows the noncondensable gas effect.This correlation is used as an "alternative model" in RELAP5/MOD3.2 and MOD 3.3 to evaluate wall film condensation.

Siddique et al. (1993) carried out an experiment to obtain the local heat transfer coefficient in the presence of air or helium with downward flow conditions. The condenser tube had a 22 mm I.D. and 2.1 m length. The empirical correlation was developed by using the governing equations of the air-vapor boundary layer which is used for producing the appropriate nondimensional groups.

$$Nu(x) = 1.137 \, \mathrm{Re}_{mix}^{0.404} (W_{air})^{-0.956} Ja^{-0.741} . \qquad (1\text{-}4)$$

The applicable experimental range is

$$0.1 < W_{air} < 0.95,$$
$$0.07 < X_{air} < 0.87,$$
$$415 < Re < 22700,$$
$$\text{and}\ \ 0.04 < Ja < 0.07.$$

From literature review, the strong dependence on the local gas concentration and flow conditions such as steam or liquid Reynolds number is apparent.

Khun (1995) performed condensation experiments in a vertical tube 2.4m in length and 47.5 mm in ID. Khun's experimental parameters are as follows: inlet air mass fraction (1.0%~40%); steam flow rate (8.2~17 g/sec) and system pressure (114~517 kPa).

The venting flow rate was not measured and the effect of venting was not considered, but the results showed that the mixture should be forced to be vented to maintain a steady state condition

along the condenser tube. Khun evaluated the degradation factor f_1 by taking into account the interfacial shear thinning effect and the waviness effect instead of using the mixture Reynolds number as in Vierow and Schrock (1991):

$$f = f_1 \cdot f_2 = f_{1,shear} \cdot f_{1,other} \cdot f_2 \qquad (1\text{-}5)$$

$$f_{1,shear} = \frac{\delta_{Nu}}{\delta_{shear}} \qquad (1\text{-}6)$$

$$f_{1,other} = 1 + 7.321 \times 10^{-4} \cdot (\text{Re}_L / 4) \qquad (1\text{-}7)$$

$$f_2 = \begin{cases} 1 - 2.601 \cdot W_{bulk}^{0.708} & for \ W_{bulk} < 0.1 \\ 1 - W_{bulk}^{0.292} & for \ W_{bulk} \geq 0.1 \end{cases} \qquad (1\text{-}8)$$

where δ_{Nu} and δ_{shear} are the film thickness based on the Nusselt theory. The factor $f_{1,other}$ is obtained from pure steam data and f_2 term includes the effect of noncondensable gas.

Park (1999) carried out a condensation experiment with a vertical tube 47.5 mm ID and 2.4 m length. Using experimental data, he developed the degradation factor-type empirical correlation. The meaning of f is defined by the ratio of the total heat transfer coefficient to the film heat transfer coefficient as follows:

$$f = \frac{h_{tot}}{h_L} = \frac{q_{wi}'' / (T_{bulk} - T_{wi})}{q_{wi}'' / (T_L - T_{wi})} = 0.0012 (W_{bulk})^{-1.4} Ja^{-0.63} \cdot \text{Re}_L^{0.24} \qquad (1\text{-}9)$$

The applicable experimental range is

$$0.1 < W_{air} < 0.7,$$
$$12.4 < \text{Re}_L < 633.6,$$
$$and \quad 0.01654 < Ja < 0.07351.$$

To apply the condensation data obtained from the experimental facilities with a cooling jacket in place of a secondary pool and by pass mode experimental outlet conditions, there were some limitations of simulation of a real PCCS system. These separate-effect tests were not intended to replicate actual containment conditions.

First, due to bypass mode conditions, the effect of NC gas accumulation inside tube during venting period was not observed. Most of the PCCS operation conditions correspond to the

cyclic venting mode or long term cooling mode. Those conditions can be also classified by venting frequency according to the inlet NC gas fraction. Without having a large mixture dome inventory to simulate the DW, the earlier experimental loops had shortcomings in having a constant NC gas fraction. To simulate the NC gas fraction, they merged the steam supply line with air supply line before the PCCS inlet section. As the noncondensable gas accumulates inside condenser tube due to condensation, the inlet steam flow rate should decrease inducing system pressure build-up until NC gas venting happens. It is therefore impossible to control the air mass flow rate according to the cyclic change of steam flow rate in the previous separate test loops.

Another limitation of these experiment facilities comes from the secondary cooling jacket design. The prototype PCCS is submerged in the pool water and water temperature reaches saturation conditions quickly at 0.1 MPa pressure during the blowdown period. The heat transfer mechanism between the condenser tube and pool is the boiling heat transfer. However, the cooling jacket can't simulate the saturation boiling conditions and it may have a large error in determination of the bulk temperature to calculate the condensation heat flux.

One experimental facility with pool boiling conditions for the PCCS condensing system has been discussed in the literature. Kim& No's (2000) experiment were conducted with high pressure steam at a maximum pressure of 7.5 MPa in a single vertical tube with an inner diameter of 46 mm. However, the test conditions were restricted to high pressure steam condensation with turbulent film.

Oh (2004) performed experiments for three PCCS flow conditions. The secondary side pool was in pool boiling. The experimental parameters were tube diameter with 2.54 cm and 5.08 cm , noncondensbale gas fraction (0~10%) , inlet steam flow rate (2~6 g/sec) and operating pressure conditions (101~450 kPa). He developed a boundary layer model which suggests the possibility of combining all three PCCS operation modes into one universal condensation heat transfer model and an empirical correlation was suggested for laminar film and turbulent film respectively.

Oh's cyclic venting mode data has a limitation for direct application to the prototype since the DW volume is not properly scaled. If the large DW volume exists, it will take a longer time period to accumulate the NC gas in the condenser, which results in a longer venting period and

more degradation of PCCS condensation capability. Furthermore, error is introduced when simulating the venting frequency by opening the PCCS venting line manually.

PUMA experiment data have meaningful value in terms of simulating the cyclic venting mode and pool boiling condition as the prototype.

1.3.2 Integral Test Experiments

Leonardi (2000) developed an empirical correlation using inlet mixture flow rate and the inlet noncondensable gas concentration in the PUMA integral tests such as Main Steam Line Break (MSLB) and Bottom Drain Line Break (BDLB). This eliminated the complexity of previous models that depended on detailed local data that are extremely difficult to measure accurately and usually not available. Instead, the simple measurements of the inlet mixture flow rate and NC concentration enabled the determination of an empirical model that correlated the heat transfer coefficient in terms of the Nusselt and Reynolds numbers. The empirical model was of the form:

$$Nu(z) = \frac{h_c(z)L(t)}{k_g} = \mathrm{Re}^{0.35}(1-\chi)^{2.5} f(z/L(t), \chi) \qquad (1\text{-}10)$$

$$f(z/L(t), \chi) = \left(\frac{\chi_{in}}{\chi(z)}\right)^{0.35} \left(\frac{1-\chi(z)}{\chi_{in}}\right)^{2.5} g(z/L(t)) \qquad (1\text{-}11)$$

The summary of Leonardi research work is as follows:

1. a comprehensive PUMA data analysis for mass and energy balance was performed

2. an empirical model based on entrance conditions for the global heat transfer was developed

3. an analysis comparing against other researchers data

4. the global analysis correlation was extended to local criteria

5. the local analysis was implemented to a systems analysis code

6. Verification of improvement for the code calculation predictions was achieved.

GIRAFFE with a full-height and reduced-volume scale facility was an experimental program conducted by the Toshiba Corporation to investigate the thermal-hydraulic aspects of the SBWR passive heat removal safety systems and to support SBWR design certification in the

US and TRACG code qualifications. Both separate effects and system response tests were performed in order to investigate the ability of the PCCS heat exchanger tubes to condense steam in the presence of noncondensable gases, demonstrate venting of the noncondensable gases from the tube to the suppression pool and simulate the MSLB, BDLB and GDLB events. There was also a test to demonstrate the operation of the PCCS in the presence of lighter-than-steam noncondensable gas. GIRAFFE data have been used to substantiate PANDA and PANTHERS data at a different scale. It also provide a database to confirm the adequacy of TRACG to predict the SBWR containment system response in the presence of a lighter-than-steam noncondensable gas, including potential systems interaction effects.

PANDA is a test facility at the Paul Scherrer Institute (PSI) in Switzerland used to study the long term SBWR PCCS performance. It has a full height and 1/25 system scale for volume and power. A series of steady state test was conducted using one of the PANDA PCC condensers with various air flows and a constant steam flow of 0.195 kg/sec. The test performed included three tests that investigated the effect of the water level of the PCCS pool inventory on the system performance. Further tests were to investigate the PCCS start-up and long term heat removal capabilities. PANDA data have been used directly to evaluate certain features of TRACG.

PANTHERS is an experimental program performed at SIET in Italy, to provide data for TRACG qualification and demonstrate testing of the prototype PCCS heat exchangers. It had full-size prototype heat exchangers which has a single condenser unit with two modules with each module having 248 tubes. The tests are for low and high noncondensable gas concentrations and they were analyzed using the RELAP5.

This study showed that RELAP5 code was unable to model the natural convection that occurred in the PCCS pool. Steam and noncondensible gas were supplied to prototype heat exchangers over the complete range of SBWR conditions. A series of experiments were performed at the same thermal hydraulic conditions as in GIRAFFE and PANDA.
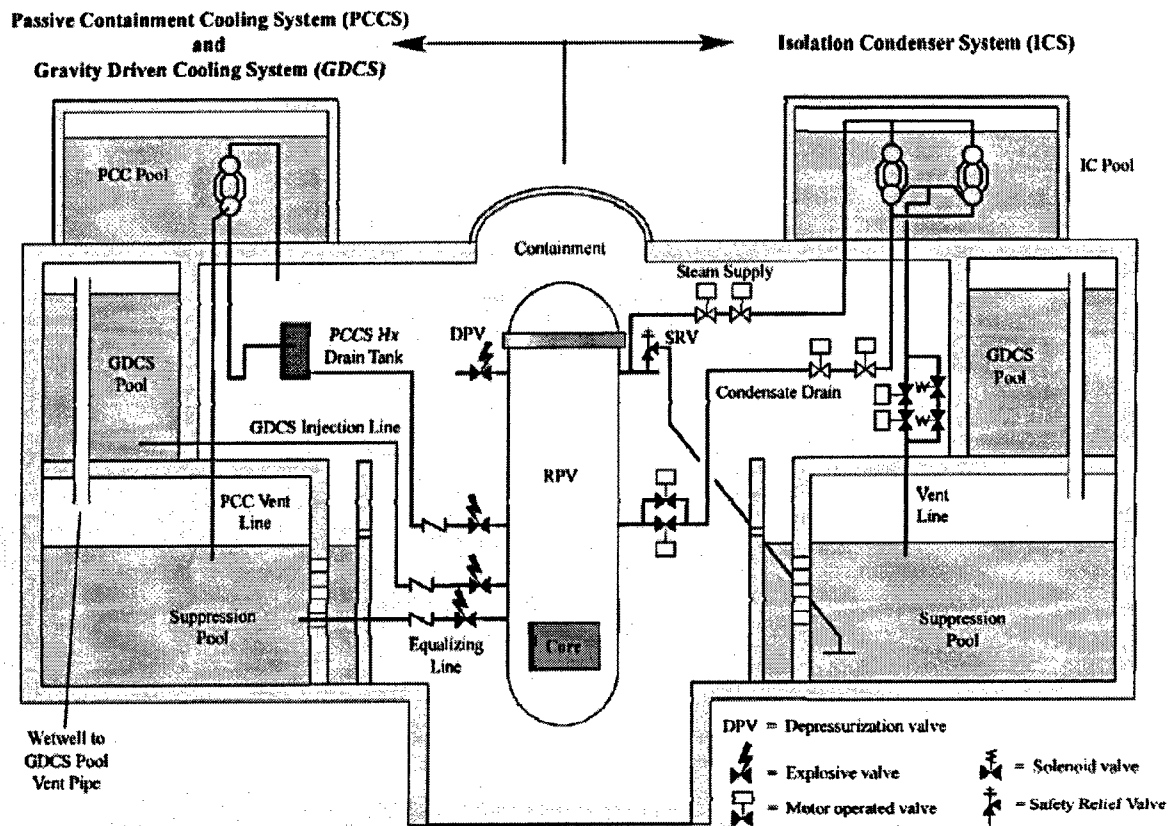
Figure 1.1 PCCS in ESBWR (NEDC-33084P, 2002)

2. EXPERIMENT

2.1 Facility Description

The PUMA facility was built to study the functionality of the SBWR safety systems and to obtain confirmatory integral test data for the U.S. Nuclear Regulatory Commission (NRC). The PUMA facility was modified to simulate the GE ESBWR design(2002) for the GDCS and PCCS components. PUMA test facility is consistent with ESBWR design as shown in Figure 1.1.

As shown in Figure 2.1, steam is supplied from the Reactor Pressure Vessel (RPV) to the drywell and the inlet noncondensable gas concentration is controlled by injecting preheated noncondensable gas into Main Steam Line (MSL) B upsteam at a predetermined flow rate. The drywell and wetwell pressure determine the pressure boundary conditions for the PCCS tests. An air injection line and vent valve are used to adjust conditions in the wetwell gas space. These valves can also be used to control the drywell initial pressure condition.

As shown in Figure 2.2, the noncondensable gas injection line is installed on MSLB downstream of the steam flow rate measurement. As shown in Figure 2.3, to have a well mixed flow with steam, there are three holes of 5/8-inch diameter facing toward the drywell side to prevent back flow and a ⅛-inch hole is at the bottom of the pipe to prevent the condensate water from collecting in the bottom of pipe. The preheater, with a capacity of 12 kW, was used for heating the air to prevent condensation of steam.

The air mass flow rate may be measured with one of three flow meters. For high air flow rates, a vortex flow meter with a ¾-inch diameter is used. The range is 13 ~ 171 g/sec at 280 kPa. Two air mass flow controllers have the measurement ranges of 0 ~ 1.96 g/sec and 0 ~ 9.8 g/sec respectively. The range of air mass flow rates in the test matrix is 0.07~27.7 g/sec.

As shown in Figure B.3 and Figure B.4, three PCCS units are simulated, each having 13 tubes. As shown in Figure B.19, three non-active condenser tubes per unit have been installed for design flexibility, but they are insulated by wrapping the outside surface area of the PCCS condenser tubes with insulating sheets of material such as Teflon to prevent condensation for this test. In addition to that, upper header and lower harder were also insulted with 0.5-inch thick rubber to minimize any condensation. Table 2.1 shows the PCCS pool and condenser design parameters.

2.2 Instrumentation

The instrumentation for the experimental system is summarized in Table 2.2-A and Table 2.2-B as well as in Appendix A and Appendix B respectively.

2.2.1 PCCS Unit and Inlet Instrumentation

The three PCCS units are located in a common pool that is partitioned into 3 sections. Each unit is provided with a measurement of pool side water temperature and level. As shown in the side view of the condenser units, Figure B.4, one condenser tube in each unit has three thermocouples on the outer tube wall and three tube centerline thermocouples placed along the pipe length at approximately equal distances. To obtain the overall heat transfer coefficient, the temperature, pressure and flow rate are measured at the inlet and outlet of the PCCS condenser as shown in Figure B.3 and Figure B.4.

The air mass flow controllers are designed to indicate flow rates and also to set flow rates of the noncondensable gas from the air supply tank into the upper drywell. The specifications of the two air mass flow controllers are shown in Table 2.3.

It is important to know the amount of noncondensable gas in the condensing vapor. The efficiency of the condenser decreases with an increase in the amount of noncondensable gas. In a closed system, the presence of the noncondensable gas degrades the condensation heat transfer and may eventually stop the condensation process if the noncondensable concentration is sufficient to block the diffusion of the vapor onto the condensing film or wall. In most industrial systems, air is always present in condensers. To estimate the concentration of air in a vapor mixture, first the oxygen concentration is measured. Then the air concentration is calculated assuming the oxygen concentration in air is 20.95% (NUREG/CR-5578, p. 4-1).

2.2.2 Drain line temperature

Among the PCCS drain line temperature measures, some of data in PCCS line B is not available due to the malfunction of thermocouples. Figure B.16 shows the isometric drawing for PCCS drain line B. The temperature of TE-PCB-14 was recorded for every test but the quality of the data is questionable and it has been removed from the instrumentation list. TE-PCB-12 shows a very similar temperature profile to TE-PCA-12 and TE-PCC-12 as expected. For some tests, TE-PCB-12 thermocouple has bad connections for the entire test data. In this case, TE-PCB-12 was removed from the data list. These temperatures are used for data reduction to obtain the condensate water density by averaging the three TE-PC-12 temperatures. Under normal measurement conditions, these three temperature readings are almost the same as the other drain line temperature reading. The average temperature of condensate water in the drain line for test in which TE-PCB-12 data is unavailable may therefore be estimated from other thermocouple data. In Table C.1, availability of TE-PCB-12 was summarized for each test.

2.2.3 Centerline temperature

The center line temperature profile for a mixture flow with noncondensable gas in a PCCS pool water level around 60 % shows large fluctuation at the middle of the condenser tube. These phenomena could be explained by the PCCS pool water inventory effect. These high pool void fractions near by TE-PC-07 locations caused transient condenser tube wall temperatures, which induce fluctuations of condensation boundary conditions in the tube.

For high mixture flow rates in the blowdown mode, the three centerline thermocouple shows almost the same high temperatures, which is close to the PCCS inlet line temperature.

However, the temperature profile of cyclic venting and blowdown mode with almost pure steam conditions shows fluctuations or sudden change of temperature trend. This is because accumulated noncondensable gas in the condenser tube has been vented out and the condensation rate increases which reduces the steam partial pressure. These phenomena can be observed for high steam flow rates with very low noncondensable gas concentrations that have shorter cyclic venting periods compared with the long term cooling mode.

The mixture flow with a very low NC gas condition corresponds to the long term cooling mode. Therefore, the average of the centerline temperature along the axial direction was made by selecting the low temperature region which has the same pattern of long term cooling.

2.2.4 Magnetic flow meter

The magnetic flow meters installed at the PCCS drain lines were calibrated using the water level change of the drain tank. Appendix D shows the results and equations of the data calibrations. By using calibrated readings from the magnetic flow meter, a more accurate heat and mass balance can be obtained and data from calibrated magnetic flow meter show good agreement with flow rates obtained by the drain tank water level measurement.

2.2.5 LT-PCX-02 Calibration

LT-PCX-02 is differential pressure gauge to measure the pressure difference between drywell and wetwell. Appendix D shows the LT-PC-02 calibrations results. The DP gauge have the error range of 0.46 kPa. The trend of bias error from the calibration results is seen from Figure D-3 to D-5.

2.3 Test Matrix

To obtain a comprehensive data set, references for choosing the pressure, noncondensable gas and steam flow rate conditions are following:

- PUMA integral test results: Obtain the steam flow rate for MSLB (Main Steam Line Break), BDLB (Bottom Drain Line Break) and GDLB (GDCS Drain Line Break) according to the bypass mode, cyclic venting mode and long-term cooling mode.
- RELAP5: Perform a calculation for the pressure in the bypass mode.
- Previous experimental conditions: Obtain appropriate data such as the pressure, steam flow rate and noncondensable gas concentration from PANTHERS, PANDA and GIRAFFE.

As shown in Figure 2.4, the pressure trends can be categorized into three groups: the blowdown period, the GDCS period, and the long-term PCCS period. For each period, the performance of PCCS has different characteristics.

In Table 2.3, a comparison of test conditions between PUMA and other integral tests is summarized. To compare with PUMA test conditions, inlet mass flow rates are scaled down based on the PUMA power scaling ratio, 1/200.

For the bypass mode, the PCCS condenser inlet and outlet have continuous flow. In this mode, the noncondensable gas is continuously vented through the vent lines. As shown in Figure 2.5, pressure conditions are determined from RELAP5 code calculations because the previous experimental research confirmed that code predicts the pressure trend well. As shown in Figure 2.6 and Figure 2.7, the steam flow rate and noncondensable gas concentration are based on the PUMA integral test results for a MSLB, BDLB and GDLB. In Table 2.4-A, test conditions are summarized for the bypass mode.

For the cyclic mode, the periodic venting of noncondensable gas to wetwell was simulated. For this operation the PCCS vent lines are submerged in the wetwell water to a depth of 200 mm and the noncondensable gas is injected through the PCCS inlet. The venting behavior varies depending on the noncondensable gas concentration. As the noncondensable gas accumulates in the tube, the condensation becomes inhibited because the noncondensable gas acts as a resistance to the condensation process. As shown in Figure 2.8 and Figure 2.9, pressure conditions, steam flow rates and noncondensable gas concentrations are based on PUMA integral test results for a MSLB, BDLB and GDLB scenarios. In Table 2.4-B, test conditions are summarized for the cyclic venting mode.

The long-term cooling mode simulates the continuous cooling mode which happens at the final stage of an accident. There is a very low noncondensable gas concentration in the drywell because most of noncondensable gas has been vented into the wetwell. As shown in Figure 2.10, pressure conditions and steam flow rate are based on the PUMA integral test results for a MSLB, BDLB and GDLB. Due to the small change of the mixture flow rate in the long-term cooling mode, only two steam flow rates were chosen and the noncondensable gas concentrations are very low so that pure steam conditions are assumed. The secondary water level is a parameter to be considered due to evaporation of water. The test conditions are summarized for the long-term cooling mode in Table 2.4-C.

2.4 Data Analysis Method

The PCCS condensers provide decay heat removal by condensing steam from the drywell and supplying condensate water to the RPV. The scaling of the heat transfer rate through the condenser is given by (NUREG/CR-6309, p. 5-58):

$$Q_{pccs} = N_{tubes} N_{units} \overline{U} A_i (\overline{T}_g - \overline{T}_P) \qquad (2.1)$$

where N_{tubes} is the number of PCCS condenser tubes, N_{units} is the number of PCCS units, $\overline{U}$ is the overall heat transfer coefficient, A_i is the inner surface area of a condenser tube, and $\overline{T}_g$ and $\overline{T}_p$ are the average steam and PCCS pool temperatures, respectively. The overall heat transfer coefficient is given by

$$\overline{U} = \left[\frac{1}{\overline{h}_c} + \frac{ln(D_o/D_i)D_i}{2k_w} + \frac{D_i}{\overline{h}_p D_o} \right]^{-1} \qquad (2.2)$$

In the right hand side of Equation 2.2, the first term corresponds to the tube side condensation heat transfer resistance, the second term corresponds to the tube wall conduction heat transfer resistance, and the third term corresponds to the secondary side pool heat transfer resistance. The condensation heat transfer resistance is for the condensation of steam and air mixture in a vertical tube.

The condensation heat transfer coefficient for the PCCS condenser tube must be estimated. The tube centerline temperature and tube outer wall temperature are used in calculating the condensation heat transfer coefficient. The effect of the noncondensable gas on condensation heat transfer is studied for different inlet flow rate conditions. The inputs to this model are the inlet temperature, outlet temperature, centerline steam bulk temperature, inlet pressure, outlet pressure, inlet steam flow rate, outlet condensed mass flow rate, and inlet noncondensable gas concentration. The analysis method is as follows:

- Calculate $Q_{in} - Q_{out} = Q_{con} \approx \dot{m}_{con} h_{fg}$ (2.3)

  where

$$Q_{in} = \dot{m}_{air} C_p T_{in} + \dot{m}_{steam} h_g \qquad (2.4)$$

  and

$$Q_{out} = \dot{m}_{air} C_p T_{out} + \dot{m}_{con} h_f \qquad (2.5)$$

- Calculate heat flux $q'' = Q_{con} / A$ (2.6)

where total inner surface area of a condenser tube

$$A = N_{tubes} N_{units} A_i \qquad (2.7)$$

- Find average overall heat transfer coefficient

$$\overline{U} = \frac{q''}{(\overline{T}_g - \overline{T}_p)} \qquad (2.8)$$

- Use equation 2.2 to obtain average condensation heat transfer coefficient $\overline{h}_c$

  where, the heat transfer coefficient for the pool is given by:

$$\overline{h}_p = \frac{Q_{con}}{A_o (\overline{\overline{T}}_{Wo} - \overline{T}_P)} \qquad (2.9)$$

Here $\overline{T}_g$, $\overline{T}_w$ and $\overline{T}_p$ are averages of the temperatures taken at the discrete vertical locations for each PCCS. Since q'' is a tube-average value, $\overline{T}_g$, $\overline{T}_w$ and $\overline{T}_p$ are also tube-average values. This method provides an average total heat transfer coefficient for the PCCS, which can be determined the average Nusselt number.

$$Nu = \frac{\overline{h}_c L}{k_l} \qquad (2.10)$$

where L is the tube length and k_l is liquid thermal conductivity.

2.5 Experimental Procedures

Test runs were carried out with pure steam and a mixture of air and steam. The test procedure was divided into the following phases: pre-test, test initialization and test mode. The pre-test operation involved setting up proper water inventory in each vessel, assuring power availability, performing DP (differential pressure) cell sensing line purging, carrying out DAS (Data Acquisition System) system check, and confirming the valve positions. The initial conditions for the tests included the RPV power, drywell pressure, wetwell pressure, PCCS inlet temperature, PCCS venting line temperature, oxygen analyzer signals and PCCS pool temperature. When the

initial mode became stable, the data acquisition was started and data were taken for at least 10 minutes.

- Pure steam experiment

First, the RPV was filled with water up to the level of 4.23 m. The wetwell was filled with water up to the 1.65 m level. This is somewhat less than the test condition water level due to water level increase during the initial condition preparations. This water level indicates the PCCS vent line is submerged about 0.2 m. The valves on the PCCS supply line were closed before blowing down the drywell air into the wetwell. The RPV was pressurized up to 40 psig by heating the water. After this, the main steam line was opened to blow the drywell gas into the wetwell through the horizontal vent line. The wetwell pressure was increased by the air and steam from the drywell. The PCCS line was opened when the drywell pressure reached close to 70% of the desired test condition. If the PCCS supply line were to be opened at the beginning of blowdown, it would prevent the system pressurization and decrease the water level of the PCCS pool by evaporation.

Initial conditions of each component were checked. These are the wetwell water level at 1.67 m, the voltage signal of the oxygen analyzer at 1 volt for the case of pure steam, the condensation drain tank water level of PCCS and PCCS pool water level. After this, a steady state condition for the drywell, RPV and wetwell pressures, and oxygen analyzer were maintained for more than 5 minutes. The PCCS condenser tube centerline temperature was checked to determine whether it reached the saturation temperature. Finally data acquisition was started and data were taken for at least 10 minutes.

- Steam and air mixture flow experiment

Similar to the pure steam tests, the test procedures for the mixture flow cases were divided into the following phases; pre-test, test initialization and test mode. The pre-test operation involved setting up proper water inventory in each vessel, assuring power availability, DP cell sensing line purging, DAS check, and valve positions. The initial conditions for the tests included the RPV power, drywell pressure, wetwell pressure, PCCS inlet temperature, PCCS venting line temperature, air mass flow rate, preheater power control, oxygen analyzer signals and PCCS pool temperature. The initial conditions of the components were obtained in the same

way as the pure steam case. The drywell pressure was increased by blowing steam from the RPV. The PCCS supply lines were opened after the drywell pressure reached nearly 60% of the desired test conditions. After more than 10 minutes, the drywell, RPV and wetwell pressure reached a steady state. While the drywell pressure was at the desired test condition, the noncondensable gas fraction reached the test condition.

Before taking data, initial conditions of each component were checked again such as the wetwell water level at 1.67 m, the voltage signal of oxygen analyzer, the water level of the PCCS condensation drain tank and the PCCS pool water level. The PCCS condenser tube inlet, outlet and center temperatures were checked by DAS program and temperatures were maintained at a constant value. Finally, the data acquisition was started and data were taken for at least 10 minutes.

Table 2.1 PCCS Pool and Condenser Design Parameters

Component	Parameter in PUMA
No. of PCCS Condenser Units	3
No. of PCCS Condenser Tubes per Unit	13
No. of PCCS condenser tubes insulated per Unit	3
PCCS Condenser Tube Inside Diameter	47.5 mm
PCCS Condenser Tube Length	450 mm
No. of Pools	1 (3 condensers each)
Pool Height	1450 mm
Pool Diameter	1225 mm

Table 2.2-A Instrumentation

Component	Quantity measured	Instruments
RPV	Power	Heat Controller
	Temperature	Type K TC
	Pressure	Pressure transducer
	Water level	Differential Pressure Gauge
Main Steam Line B	Flow rate	Vortex Flow Meter
	Temperature	Type K TC
	Pressure	Pressure transducer
Air Supply Line	Air mass flow rate	Mass Flow controller
	Temperature	Type K TC
Drywell	Water level	Differential Pressure Gauge
	Temperature	Type K TC
	Pressure	Pressure transducer
Wetwell	Temperature	Type K TC
	Pressure	Pressure transducer
	Water level	Differential Pressure Gauge

Table 2.2-B PCCS Instrumentation

Component	Quantity measured	Location	Instrument
PCCS	Temperature	Supply line	Type K TC
		Drain line	Type K TC
		Venting line	Type K TC
		Condenser pool	Type K TC
		Tube surface	Type K TC
		Centerline of condenser tube	Type K TC
	Differential pressure	PCCS inlet and outlet	Differential pressure gauge
		PCCS outlet and wetwell	Differential pressure gauge
	Water level	PCCS Drain Tank	Differential pressure gauge
	Steam flow rate	Supply line	Vortex flow meter
	Condensate Flow Rate	PCCS Drain Line	Magnetic flow meter
		PCCS Drain Tank	Differential pressure gauge

Table 2.3 Test Ranges for Integral Test Loop Experiments

Integral Test Loop	Steam flow rate (kg/sec)	Pressure (kPa)	T_{sat} (^{o}C)	Noncondensable gas mass fraction (%)
PANTHER	0.025, 0.007	296, 330, 380, 546	133, 136, 141, 155	14.6, 1.5, 1.06
PANDA	0.039, 0.053	300, Self adjusting	133	0, 1.5, 3, 7.5, 14
GIRAFFE	N/A	214, 281	117~132	4.4, 27.2
PUMA	0.098~0.043 (bypass)	235~293 (bypass)	117~132	0~16
	0.013~0.033 (cyclic and long-term cooling mode)	185~263 (cyclic and long-term cooling mode)		

Table 2.4-A Test Ranges for the Bypass Mode

PCCS Inlet				PCCS Pool water level (m)
Steam flow rate (kg/sec)	Pressure, kPa (psia)	$T_{sat}(^{o}C)$	Noncondensable gas mass fraction (%)	
0.065 ~ 0.75	220 (32)	123	0, 10 , 15	0.92 (100%)
	260 (38)	128		
	300 (44)	133		

Table 2.4-B Test Ranges for the Cyclic Venting Mode

PCCS Inlet				PCCS Pool water level (m)
Steam flow rate (kg/sec)	Pressure, kPa (psia)	T_{sat} (^oC)	Noncondensable gas mass fraction (%)	
0.029 ~ 0.032	220 (32)	123	0, 0.3, 2 , 4 and 6	0.92 (100%)
	240 (35)	126		
	260 (38)	128		0.62 (50%)
0.039 ~ 0.042	220 (32)	123	0, 2 and 4	0.92 (100%)
	240 (35)	126		
	260 (38)	128		

Table 2.4-C Test Ranges for the Long-term Cooling Mode

PCCS Inlet				PCCS Pool water level (m)
Steam flow rate (kg/sec)	Pressure, kPa (psia)	T_{sat} (^{o}C)	Noncondensable gas mass fraction (%)	
0.025	200 (29)	120	Less than 1 %	0.92 (100%)
	230 (34)	124		
	260 (38)	128		0.62 (50%)
0.031	220 (32)	123	Less than 1 %	0.92 (100%)
	240 (35)	126		
	260 (38)	128		
0.02	230	124	Less than 1 %	0.92 (100%)
	260	128		

Table 2.5 Air Mass Flow Controllers

Type	Volume flow rate (lit/min)	Mass flow rate (g/sec)	Error range
1	0 - 100	0 – 2.12	1.5 % (± 0.032 g/sec)
2	0 - 500	0 – 10.78	1.5 % (± 0.162 g/sec)
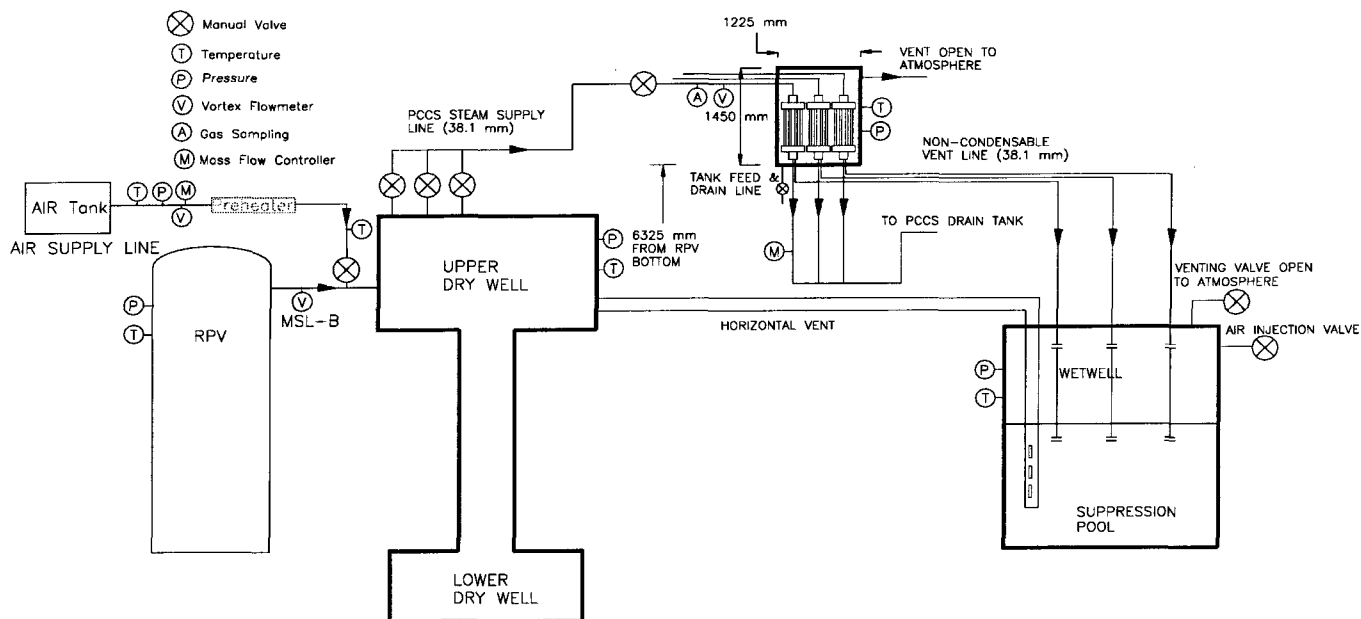
Figure 2.1 Schematic Diagram of PUMA Facility
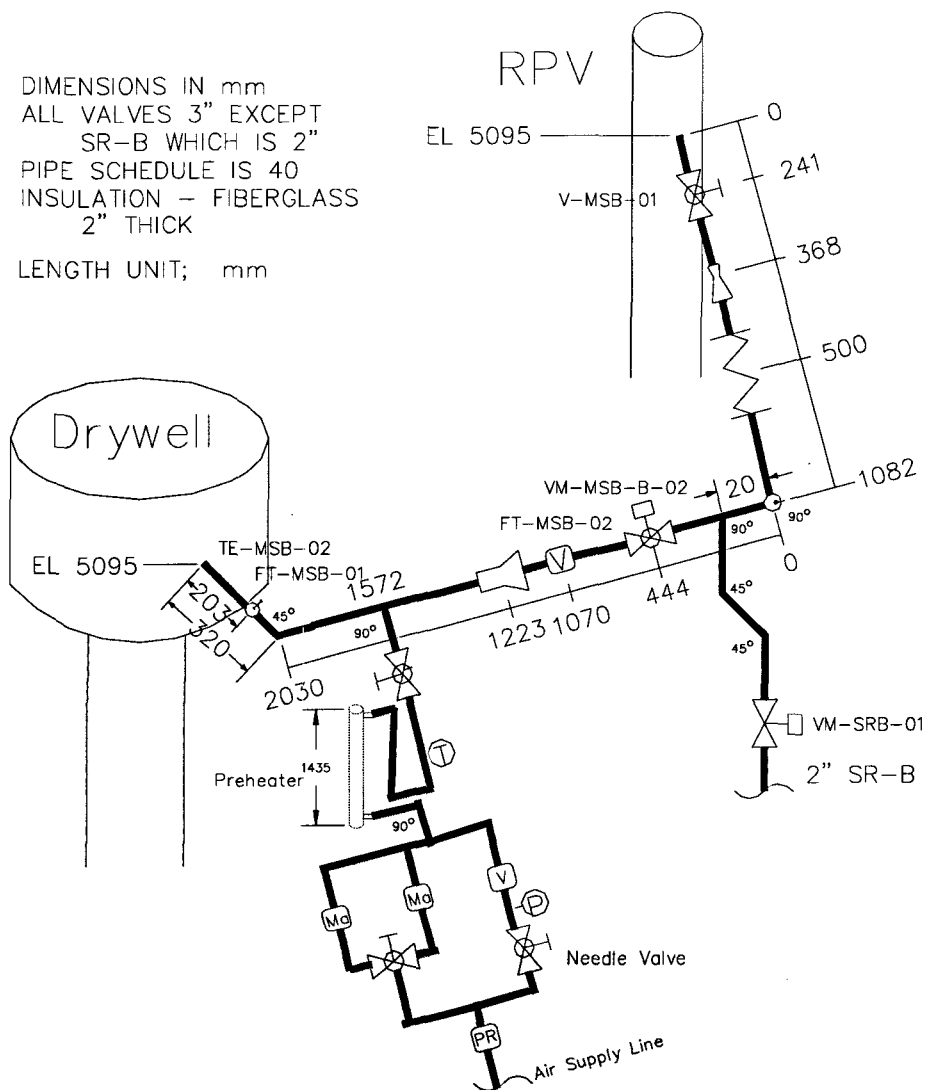
Figure 2.2 Layout of Air and Steam Line

1 inch Tube Air Supply Line

1 inch Tube Fitting

1 inch Flange

1 Inch Pipe

Ø0.6250 ($\frac{5}{8}$ inch size 3 Holes)

3 Inch MCLB Pipe

To Drywell

0.125 Dia Hole
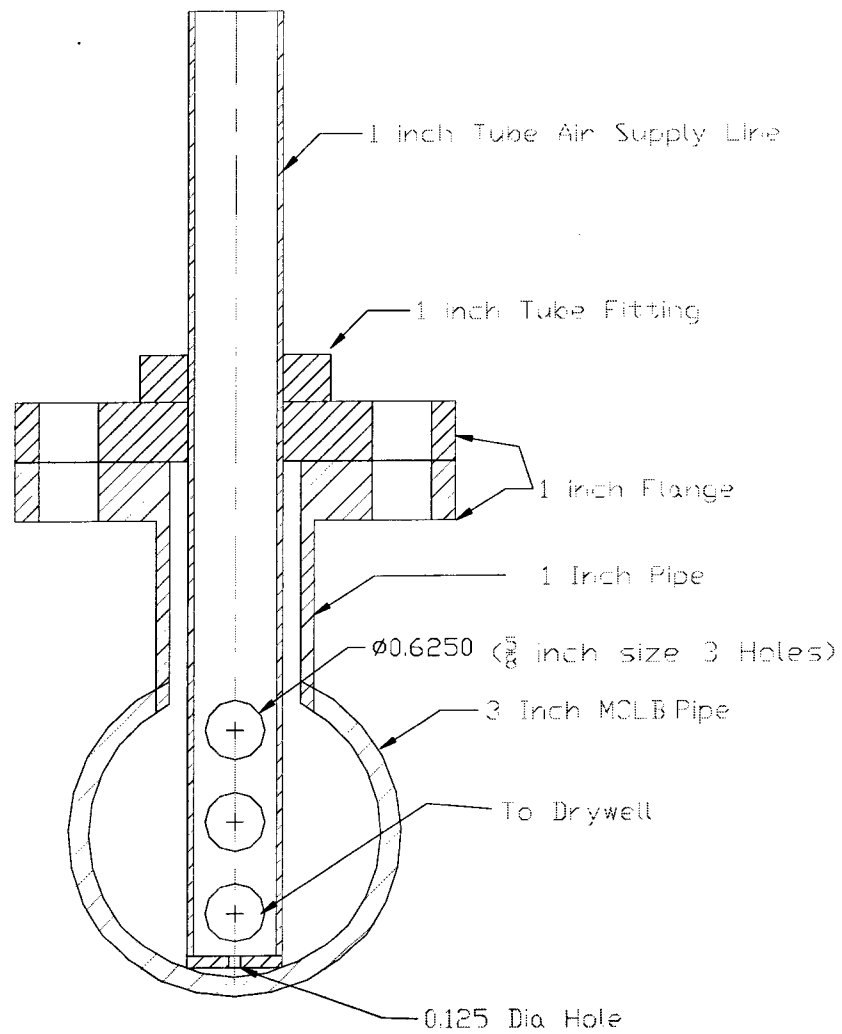
Figure 2.3 Air Sparger
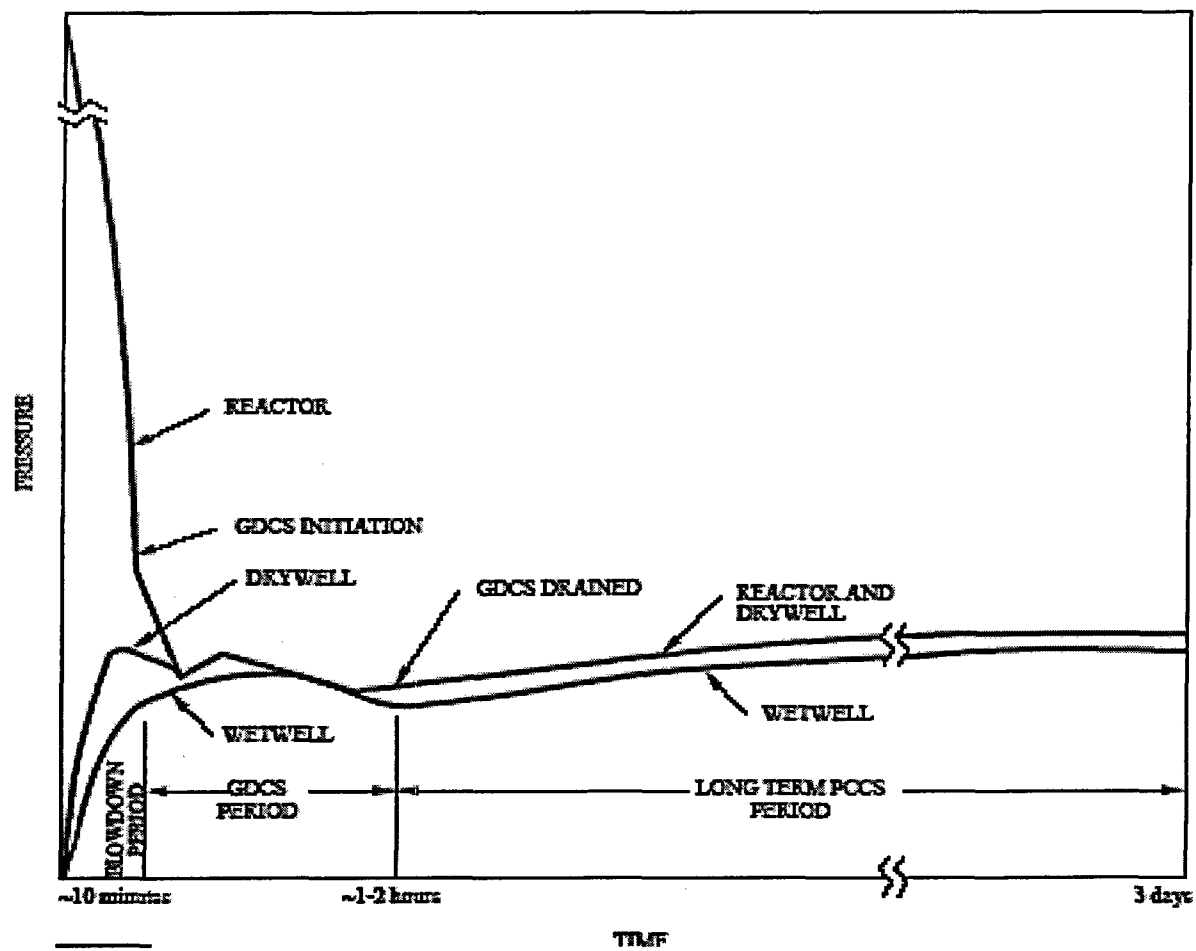
Figure 2.4 Typical Pressures Trend of Reactor, Drywell and Wet well (NEDC-33084P, 2002)
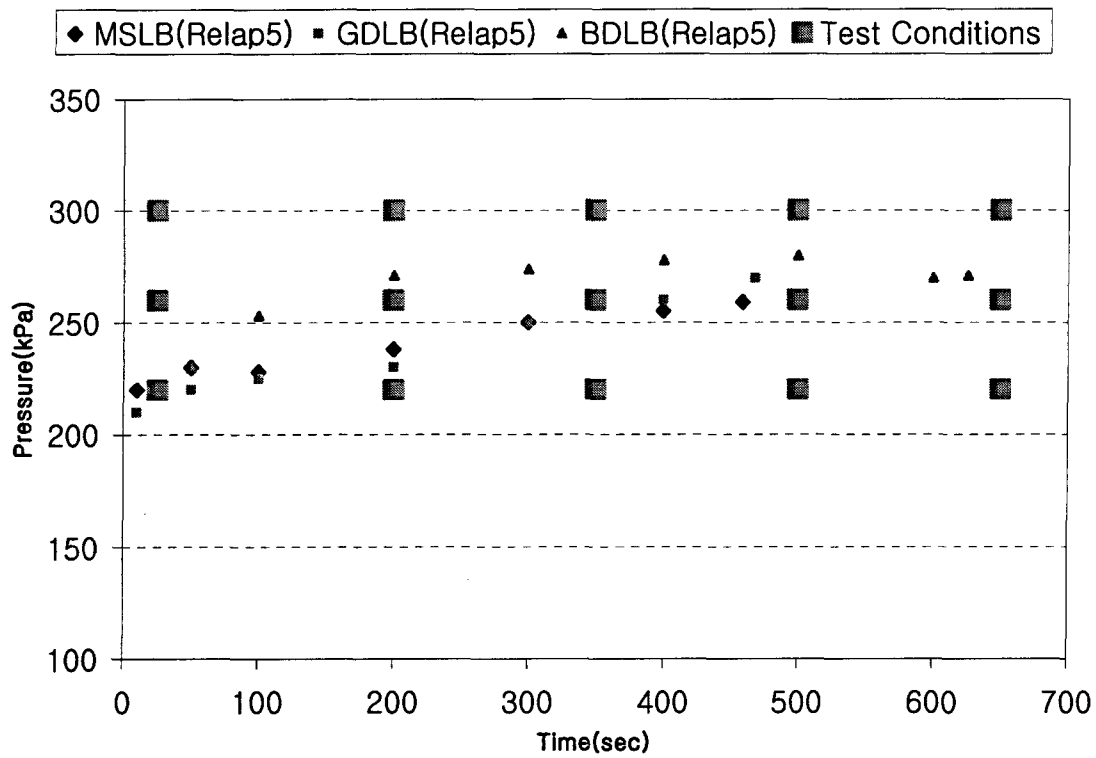
Figure 2.5 Pressure Condition for the Bypass Mode Based on the RELAP5 Code Calculation in the Plant Cases
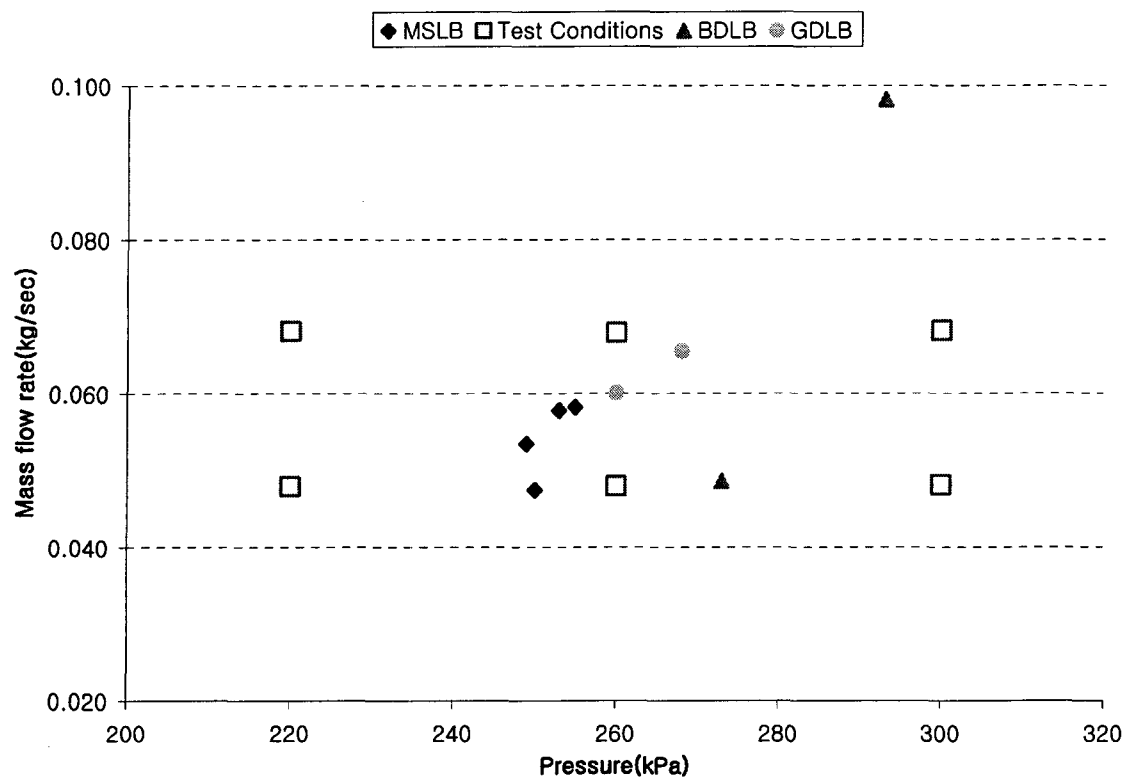
Figure 2.6 Test Conditions for the Pressure to Steam Flow Rates for the Bypass Mode

Figure 2.7 Test Conditions for the Pressure to Noncondensable Gas Concentrations for the Bypass Mode
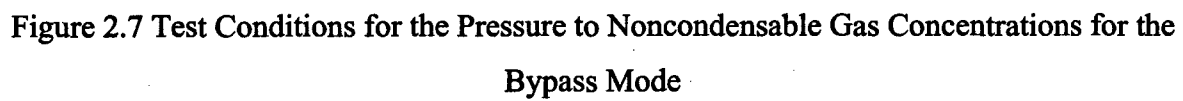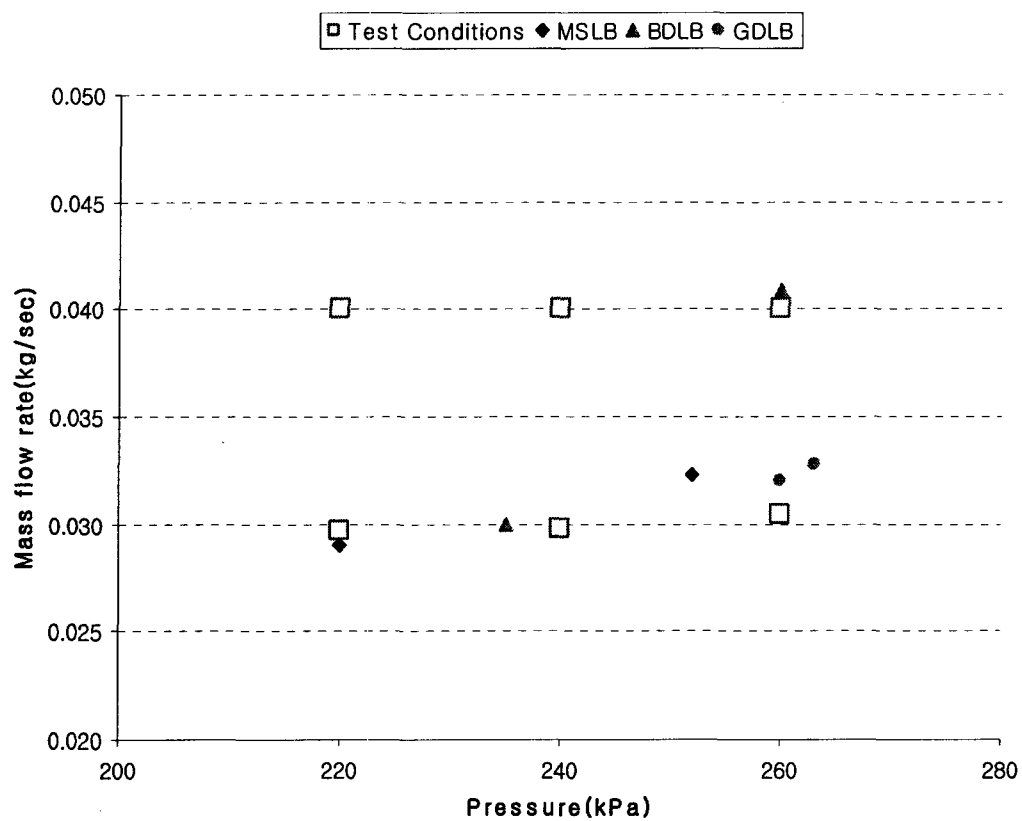
Figure 2.8 Test Conditions for the Pressure to Steam Flow Rates for the Cyclic Venting Mode
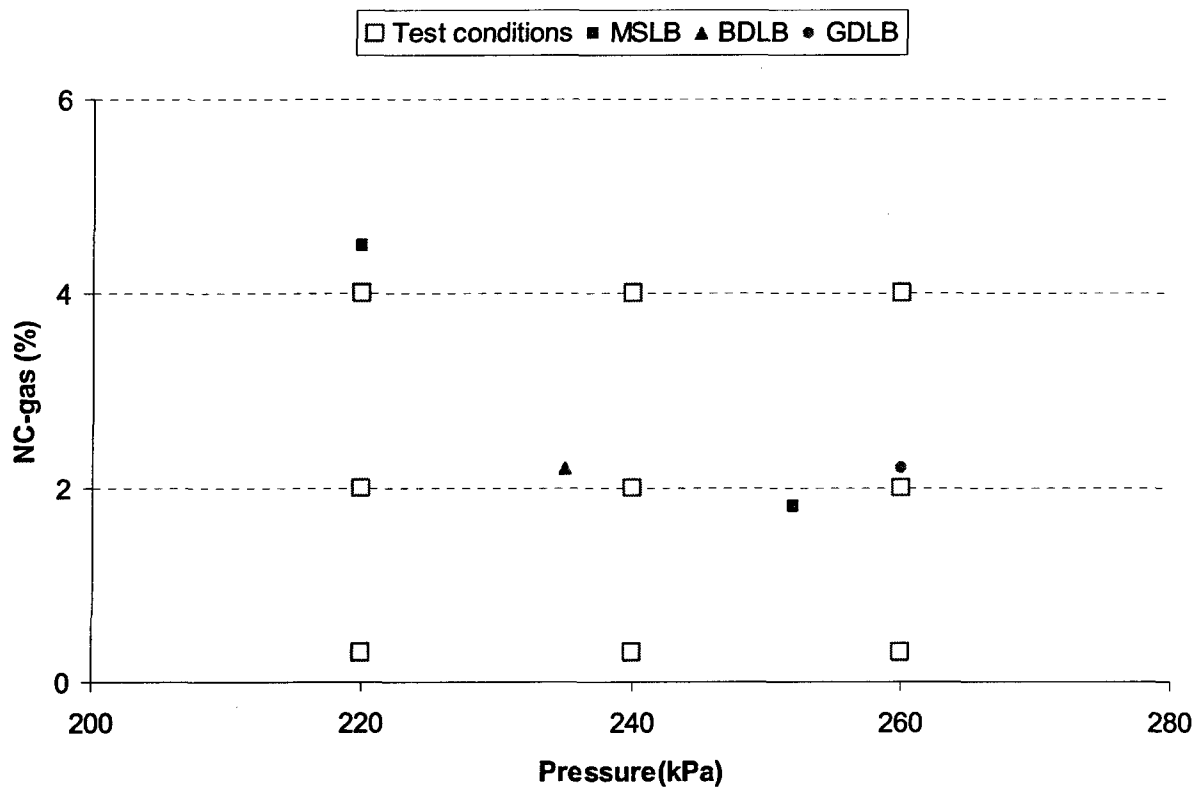
Figure 2.9 Test Conditions for the Pressure to Noncondensable Gas Concentrations for the
Cyclic Venting Mode
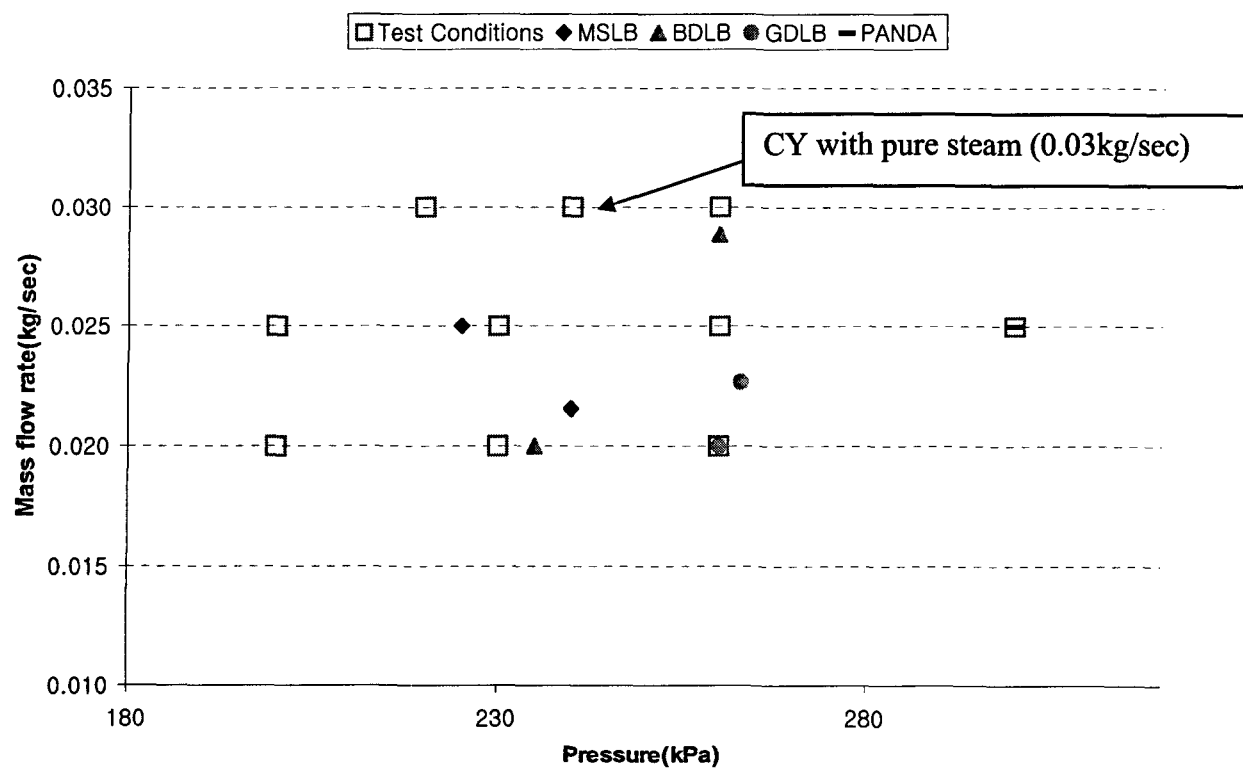
Figure 2.10 Test Condition for the Pressure to Steam Flow Rates for the Long-term Cooling Mode

3. LONG-TERM COOLING MODE EXPERIMENTS

3.1 Test Matrix

A total of 9 long-term cooling mode experiments were carried out mainly covering the high inlet steam flow conditions. The test condition parameters are pressure, steam flow rate and PCCS pool water level. The test matrix addressed in Table 2.3-C for the long-term cooling mode covers a wide range of steam flow rates. The inlet steam mass flow rates were kept almost same for all tests at 0.025 and 0.032 kg/sec as shown in Table 3.1. From high steam flow rate case, 0.032 kg/sec pure steam condition in the cyclic venting test matrix, the effect of high steam flow rate can be shown by comparing with other low steam flow cases, 0.025 kg/sec.

The PCCS pool water temperature was at saturation temperature, about 101°C, during the experiments. Due to evaporation of the pool-side water, it was initially thought that it might be necessary to fill preheated water into the PCCS pool. However the two-phase water level is around 5.5 cm higher than the collapsed water level. The change in the water level is proved to be negligible on the pool inventory effect.

3.2 Experimental Data

The long-term cooling mode simulates the continuous cooling mode which happens at the final stage of a hypothesized accident. There is a very low noncondensable gas concentration because most of the noncondensable gas has been vented into the wetwell. Therefore it can be assumed that noncondensable gas concentration into the PCCS inlet header is less than 1% (volumetric fraction).

Assurance of an almost pure steam flow from the drywell is a key criterion for the initial conditions. Such flow conditions were obtained by blowing steam into the drywell until the oxygen analyzer shows less than 1% volumetric gas concentration for more than 30 minutes before taking data in 2004 experiments. The same procedures were carried out to obtain initial conditions in the latest tests without measuring the oxygen concentration. None of oxygen analyzers in PUMA is available due to malfunction. Based on the previous experimental experience, the PCCS supply line temperatures and noncondensable gas venting line temperature can be used to confirm that the PCCS inlet gas concentration is low enough. In this case, the

PCCS supply line temperature should be the same as the main steam line steam temperatures. The noncondensable gas venting line temperature decreased continuously due to complete condensation in the condenser tube.

The system is considered to have achieved a steady state when several key parameters have been steady for more than 10 minutes. For each PCCS pool, PC-A, PC-B and PC-C, the steam volumetric flow rate and the condensate water flow rate are shown in Figure 3.1 and Figure 3.2, respectively. Figure 3.3 shows a typical water level change in the PCCS pool in the long-term cooling mode. Figure 3.4 shows a water level increase in the PCCS drain tank. Figure 3.5 shows the pressure condition of the drywell and wetwell. PCCS inlet steam temperatures, tube wall temperatures, tube centerline temperatures and pool temperatures are shown in Figure 3.6, Figure 3.7 and Figure 3.8.

For long term cooling mode with 50% of PCCS pool inventory experiment, the same measurement figures for normal PCCS pool level case are shown from Figure 3.9 to Figure 3.16. Figure 3.14 to Figure 3.16 show the temperature profile of PCCS inlet line, tube centerline and tube surface temperature, respectively. Due to water uncoverage in the z=745 elevation, the tube surface temperature is close to the tube centerline temperature. Because of high void fraction water condition near by thermocouple location z=580, the temperature fluctuations of tube centerline are observed in every PCCS pool inventory with 0.62m height tests such as LM and CM serials.

In Table 3.2, the test results are summarized including the average overall heat transfer rate ($\bar{U}$), the average heat transfer coefficient in the pool ($\bar{h}_p$), and the average of the condensation heat transfer coefficient ($\bar{h}_c$) at the inside tube over the PCCS condenser. Here $\bar{T}_g$, $\bar{T}_w$ and $\bar{T}_p$ are the average values of the tube-averaged temperatures for all PCCS. For 0.6 m pool height condition, temperature data near the inlet of condenser tube (z=745 mm) was not used for calculating the average heat transfer coefficients due to the uncoverage of condenser tubes in the PCCS pool. By calibration of two phase water level using the tube surface temperature (z=580 mm), the two phase water level was used to calculate the condenser tube surface area in the heat transfer rate calculation. A more detailed explanation is provided in Chapter 5.

Since the vortex flow meters on the PCCS supply lines are not capable to measure the low steam flow rate, steam flow rates measured on main steam line B are used as the total inlet steam flow rate (about 0.025 kg/sec) which can be compared with the total condensate flow rate in the

drain line. An accurate average PCCS supply steam flow rate can be also obtained by subtracting the drywell and system heat loss (3.38 kW) from the RPV power and converting this to an RPV steam flow rate. Steam flow rates from the RPV to the drywell are cross-checked by calculating the evaporation rate from RPV water level changes.

For the test LT718B and LT711C, energy balance were confirmed by comparison with energy by total condensate drain flow rate with energy by evaporation rate in the PCCS pool because the steam flow rate from RPV into Drywell was lower than the minimum range of vortex flowmeter in the main steam line B.

Figures 3.1 and 3.9 show the PCCS supply flow rate measured by vortex flow meters on each of PCCS supply lines during experiments. This reading can be used to verify steady inlet flow conditions. The flow rate readings are not accurate due to limitation of measurement for low flow rate.

From Figures 3.6 and 3.7, we can see TE-PCB-09, the temperature of the condenser tube surface, is lower than TE-PCA-09. These measurements are obtained by thermocouples soldered on the tube surface. The discrepancy is believed to be caused by the condition of the thermocouple-to-tube connection. The local measurement data of PCCS are not suitable for the analysis of local heat transfer coefficients. To eliminate the need for the difficult measurements of local parameters or their uncertain simulation, it is possible to correlate the heat transfer rate in terms of simple and more accurate measurements of inlet conditions for flow rate and noncondensable gas concentration. Using these parameters, an average heat transfer coefficient can be obtained for the PCCS system. From this average heat transfer coefficient, the local heat transfer rate distribution can be estimated (Leonardi, 2000).

The tests are named as AB123a, where the first two letters (AB) stands for the experiment type, the 3 digits in middle refer to the experiment date and the last letter means the test serial number.

3.3 Data Discussion

To perform a mass balance check on the system, the steam mass flow rate from the RPV and the sum of condensate mass flow rates from the three PCCS were compared. The total steam mass flow rate varies between 0.025 and 0.032 kg/s as determined by condensate water flow rate

measured by PCCS drain tank and the steam flow rate measurement from the vortex flow meter installed on the main steam line. As shown in Figure 3.17, the comparison of mass flow rate from drain tank water level and from the vortex flow meter installed at the Main Steam Line B shows a good agreement. Considering the RPV heat loss (2 kW) the average error is just 3%. It is believed that the vortex flow meter installed on Main Steam Line B provides the most reliable inlet mass flow rate condition among the available instrumentations.

To perform an energy balance check on the system, the energy calculated by drain tank inventory change and energy by PCCS pool were compared. As shown in Figure 3.18, the comparison of the energy calculated by drain tank and energy by water evaporation rate in the PCCS pool shows a good agreement.

In Figure 3.19 and Figure 3.20, the experimental data demonstrate the effects of the drywell pressure and PCCS pool height. As shown in Figure 3.19, when the pressure increases, the average condensate heat removal rates also increase, but average condensation heat transfer coefficients decrease as seen in Figure 3.20. This trend can be explained physically as following. The total heat removal rate is composed of condensed steam flow rate multiplied by the temperature difference between the pool and inside tube temperature. Pool temperature is almost constant saturation temperature with an atmospheric pressure condition while the saturation temperature is increased with DW pressure increase. Therefore, as the DW pressure increases which induces the temperature difference between PCCS pool and tube center line, heat removal rate is increasing. On the other hand, heat transfer coefficient is proportional to the inverse of liquid film layer thickness that presents a thermal resistance to heat transfer. As the heat removal rate increases, the liquid film thickness also increases. Therefore, the average condensation heat transfer coefficients decrease with pressure increase.

As shown in Figure 3.20 to show the effect of the PCCS pool inventory, heat removal rates for a pool height of 0.6 m collapsed water level case(LM) are lower than for a 0.92 m pool height case(LT). This shows that the coolant inventory of the PCCS pool is also one of the key parameters that determine the PCCS cooling capacity. However in terms of average heat transfer coefficients(HTC), LM test has a little higher HTC value compared with LT case. That can be explained by the average values of HTC with shorter active condenser tube length can be higher value than longer active condenser tube length ones. These facts can be also confirmed by UCB model calculation as shown in Figure 3.21.

3-4

The data is evaluated with the assumption that an equal amount of steam goes into each PCCS unit. This steam flow rate is equal to one-third the measured main steam line flow rate, and the steam is fully condensed within the heat exchanger in the long term cooling mode.

Data quality can be evaluated not only by the mass and energy balance in the system but also by comparing with other separate effect tests such as Vierow and Kuhn data. As shown in figure 3.21, average heat transfer coefficients obtained by the Vierow and Kuhn correlations demonstrate the effect of the variation of the inlet mass flow rate. The mass flow rate varies between 0.017 and 0.04 kg/sec during the long-term cooling period of the test. The inlet noncondensable gas concentration, though, remains approximately constant on the order of 1%.

Figure 3.22 shows the experiment data in terms of the average heat transfer coefficient and the inlet Reynolds number. The variations in the inlet mass flow rate become apparent when the average heat transfer coefficient is plotted against the Reynolds number, noting that as the inlet flow rate increases the heat transfer coefficient increases.

To compare current data with the single tube separate effect test data, two long term cooling data were selected with steam flow rates of 0.02 kg/sec and 0.025 kg/sec data at a pressure of 200 kPa. It shows the same trend with other experimental case and heat transfer coefficient is less than Khun's model. The data with the similar inlet Reynolds number conditions show the same trends. To obtain a more reliable comparison with the Vierow and Khun data, more experimental cases need be compared but it can be said that the data sets provide average heat transfer coefficients on the same order of magnitude.

Table 3.1 Test Matrix for the Long-term Cooling Mode

Test No.	$\dot{m}_{msl}$ (kg/Sec)	Pressure kPa (psia)	PCCS Pool water level (m)	PCCS inlet noncondensable gas mass fraction (%)
LM807AR	0.0254	200 (29)	0.62	<1%
LT912AR	0.0257		0.92	
LM807B	0.0264	230 (33)	0.62	
LT727B	0.0273		0.92	
LM807C	0.0278	260 (38)	0.62	
LT727C	0.0276		0.92	
LT823D	0.0278	300 (44)	0.92	
LT718B	0.017	230 (33)	0.92	
LT711C	0.021	260 (38)	0.92	

Table 3.2 Summary of the Long-term Cooling Mode Tests Data

Test No.	$\dot{m}_{msi}$ (kg/Sec)	Pressure (kPa)	NC Gas	Q_{con} (Kw)	$\bar{U}$ (W/m²K)	$\bar{h}_p$ (W/m²K)	$\bar{h}_c$ (W/m²K)	$\bar{T}_s$ (°C)	$\bar{T}_w$ (°C)	$\bar{T}_p$ (°C)
LM807A	0.0254	200	<1%	51.35	3052	20291	5422	114.9	103.7	101.9
LT912A	0.0257	200	<1%	55.66	2707	17212	4621	111.6	102.9	101.5
LM807B	0.0264	230	<1%	53.94	2989	33547	4810	116.1	102.9	101.7
LT727B	0.0273	230	<1%	58.11	2697	22487	4537	112.6	103.1	101.9
LM807C	0.0278	260	<1%	55.94	2825	34791	4380	117.4	102.8	101.6
LT727C	0.0276	260	<1%	57.33	2588	26622	3959	113.3	103.6	102.3
LT823D	0.0278	300	<1%	58.75	2334	24802	3424	114.6	103.2	102.1
LT718B	0.017	230	<1%	35.4	2047	27437	2811	110.0	101.8	101.4
LT711C	0.021	260	<1%	45.21	2363	34990	3360	110.8	101.9	101.3
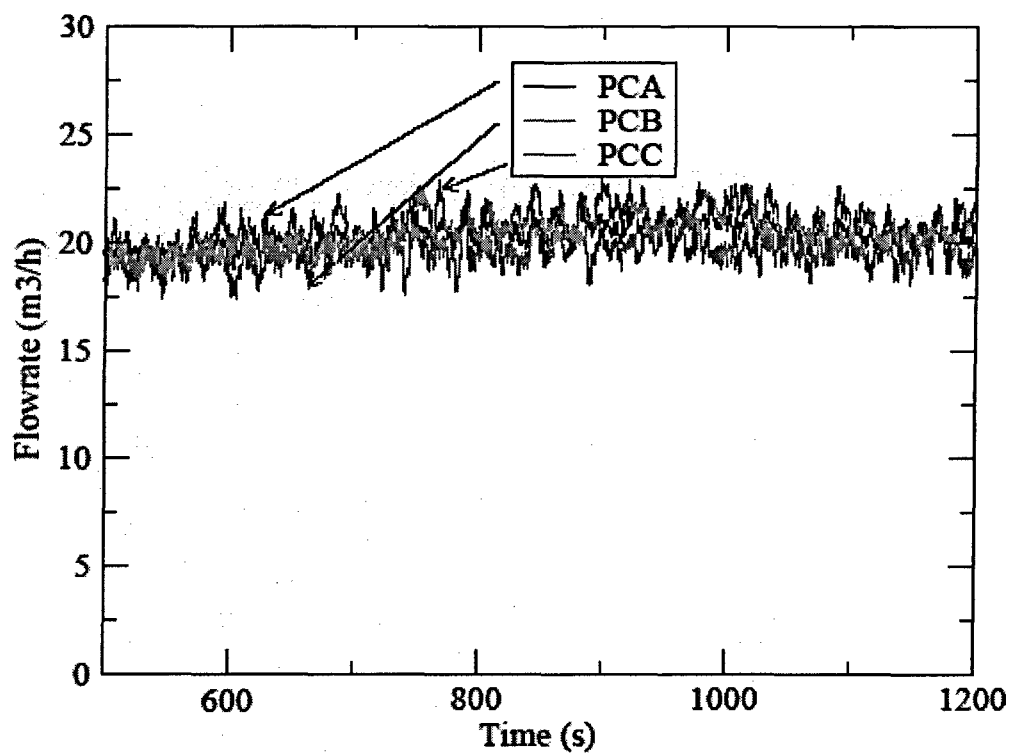
Figure 3.1 Steam Volumetric Flow Rates in PCCS Supply Lines from Vortex Flow Meter

PCCS Separate Effect Test

Test No.:	LT727B
Mode:	Long-term Cooling
Pressure Setting:	230 kPa
Noncondensable Gas Concentration:	<1%

Figure 3.2 Water Volumetric Flow Rates in PCCS Drain Lines

PCCS Separate Effect Test

Test No.:   LT727B
Mode: Long-term Cooling
Pressure Setting: 230 kPa
Noncondensable Gas Concentration: <1%
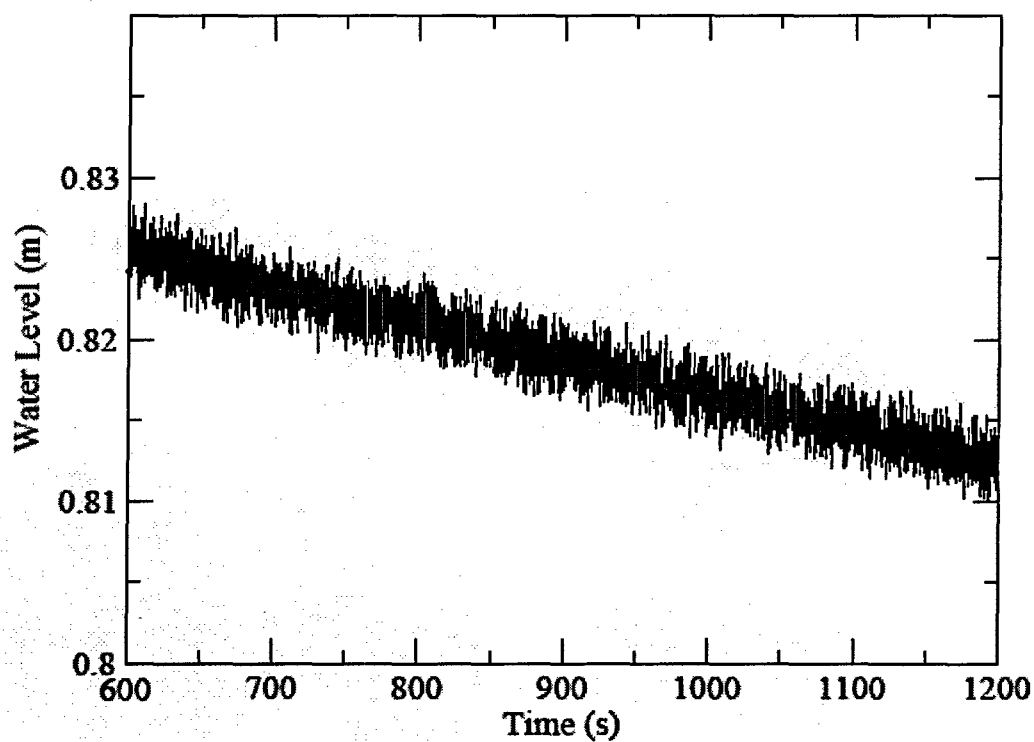
Figure 3.3 Water Level in the PCCS Pool

PCCS Separate Effect Test

Test No.:	LT727B
Mode:	Long-term Cooling
Pressure Setting:	230 kPa
Noncondensable Gas Concentration:	<1%

Figure 3.4 Water Level in the PCCS Drain Tank

PCCS Separate Effect Test

Test No.:	LT727B
Mode:	Long-term Cooling
Pressure Setting:	230 kPa
Noncondensable Gas Concentration:	<1%

Figure 3.5 Upper Drywell and Wetwell Gas Space Pressures

PCCS Separate Effect Test

Test No.:   LT727B
Mode: Long-term Cooling
Pressure Setting: 230 kPa
Noncondensable Gas Concentration: <1%

PT-DW-01: Upper drywell pressure
PT- SP -01: Wetwell pressure in gas space
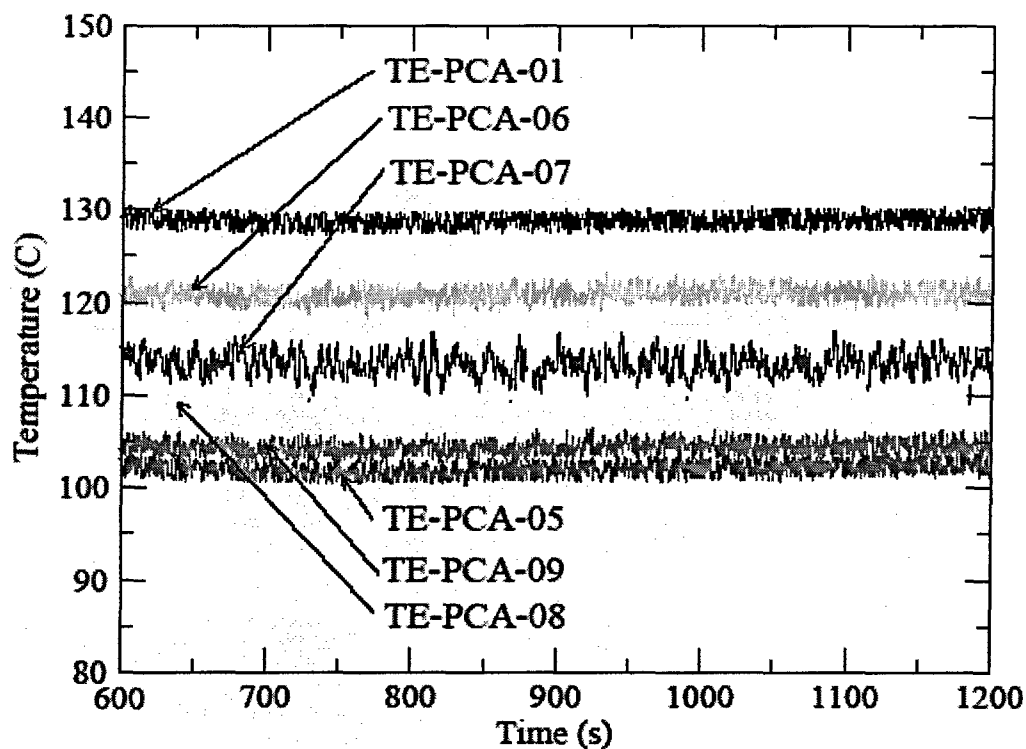
Figure 3.6 Temperatures in PCCS-A

PCCS Separate Effect Test

Test No.:	LT727B
Mode:	Long-term Cooling
Pressure Setting:	230 kPa
Noncondensable Gas Concentration:	<1%

TE-PCA-01:	Temperature of steam in PCCS supply line A
TE-PCA-05:	Temperature of water in PCCS pool A (z=254)
TE-PCA-06:	Temperature of condenser tube centerline in PCCS-A (z=745)
TE-PCA-07:	Temperature of condenser tube centerline in PCCS-A (z=580)
TE-PCA-08:	Temperature of condenser tube centerline in PCCS-A (z=415)
TE-PCA-09:	Temperature of condenser tube surface in PCCS-A (z=745)

Figure 3.7 Temperatures in PCCS-B

PCCS Separate Effect Test

Test No.:	LT727B
Mode:	Long-term Cooling
Pressure Setting:	230 kPa
Noncondensable Gas Concentration:	<1%

TE-PCB-01:   Temperature of steam in PCCS supply line B
TE-PCB-05:   Temperature of water in PCCS pool B (z=254)
TE-PCB-06:   Temperature of condenser tube centerline in PCCS-B (z=745)
TE-PCB-07:   Temperature of condenser tube centerline in PCCS-B (z=580)
TE-PCB-08:   Temperature of condenser tube centerline in PCCS-B (z=415)
TE-PCB-09:   Temperature of condenser tube surface in PCCS-B (z=745)

Figure 3.8 Temperatures in PCCS-C

PCCS Separate Effect Test

Test No.:	LT727B
Mode:	Long-term Cooling
Pressure Setting:	230 kPa
Noncondensable Gas Concentration:	<1%

TE-PCC-01:	Temperature of steam in PCCS supply line C
TE-PCC-05:	Temperature of water in PCCS pool C ($z=254$)
TE-PCC-06:	Temperature of condenser tube centerline in PCCS-C ($z=745$)
TE-PCC-07:	Temperature of condenser tube centerline in PCCS-C ($z=580$)
TE-PCC-08:	Temperature of condenser tube centerline in PCCS-C ($z=415$)
TE-PCC-10:	Temperature of condenser tube surface in PCCS-B ($z=580$)

Figure 3.9 Steam Volumetric Flow Rates in PCCS Supply Lines from Vortex Flow Meter

PCCS Separate Effect Test

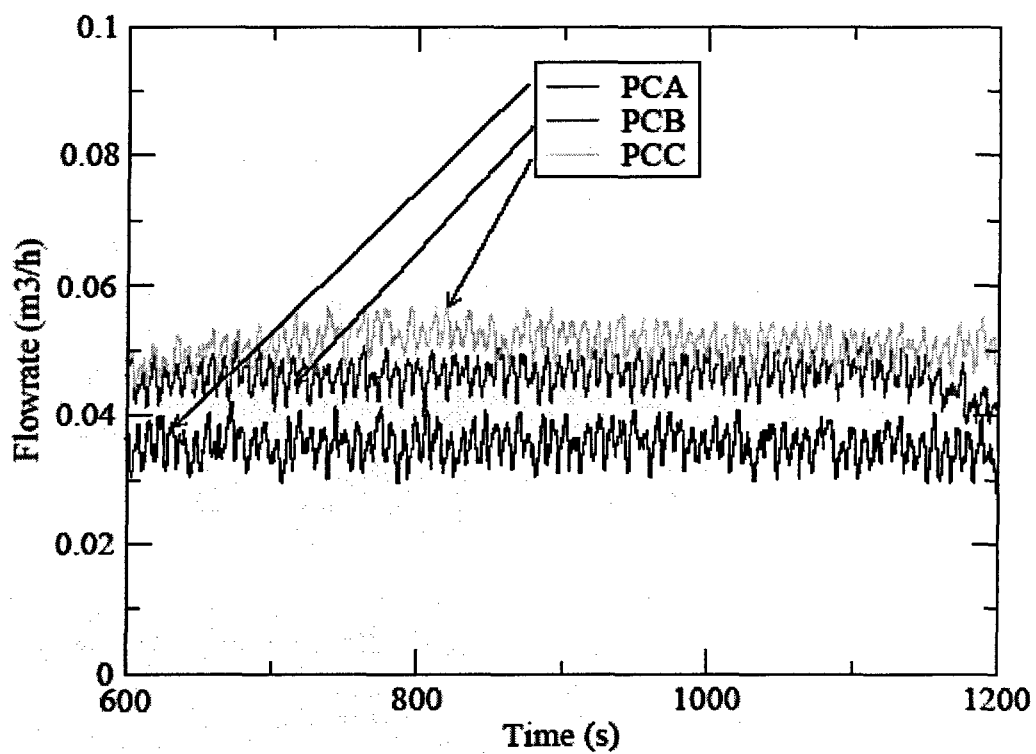|	
Test No.:	LM807B
Mode:	Long-term cooling with low pool level
Pressure Setting:	230 kPa
Noncondensable Gas Concentration:	<1%
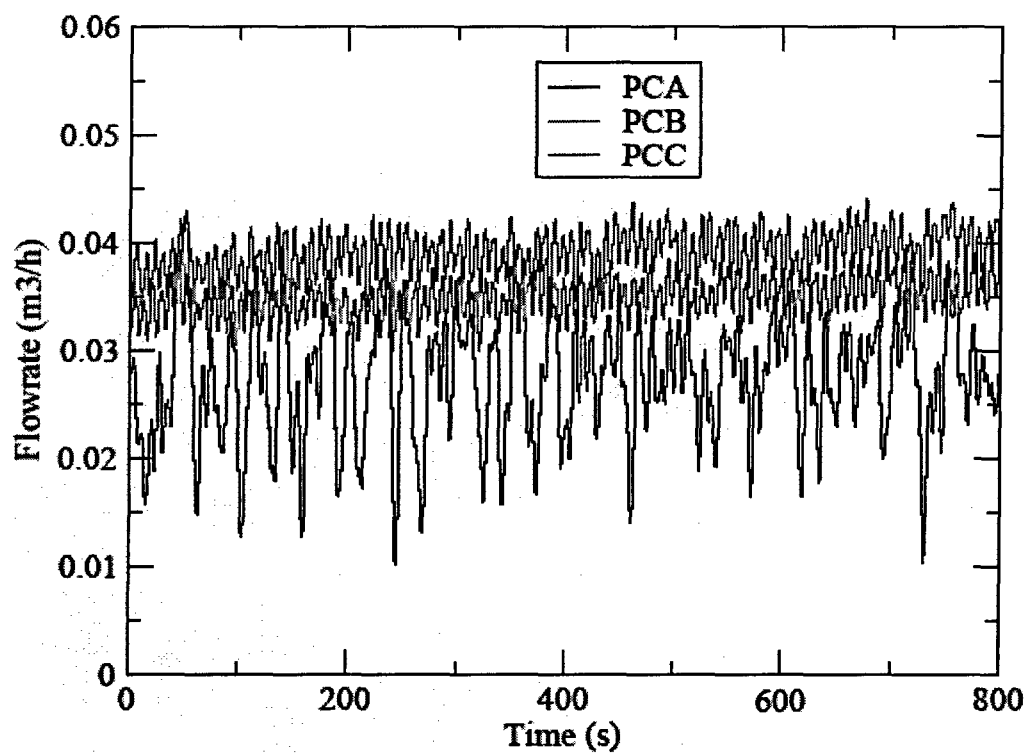
Figure 3.10 Water Volumetric Flow Rates in PCCS Drain Lines

PCCS Separate Effect Test

Test No.:   LM807B
Mode: Long-term cooling with low pool level
Pressure Setting: 230 kPa
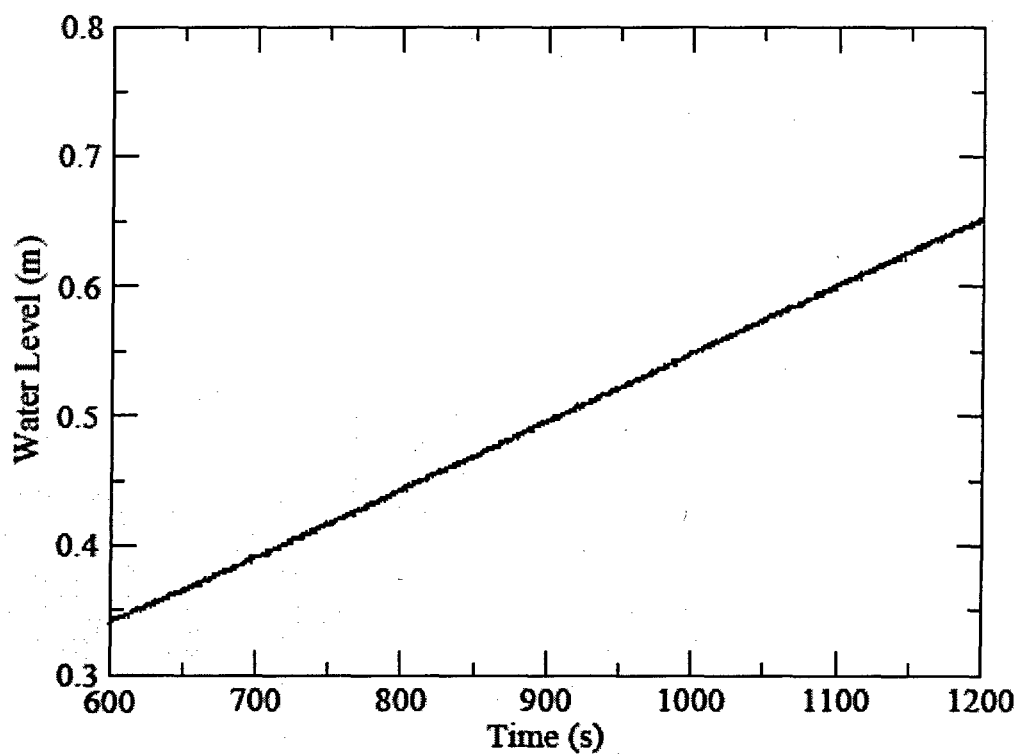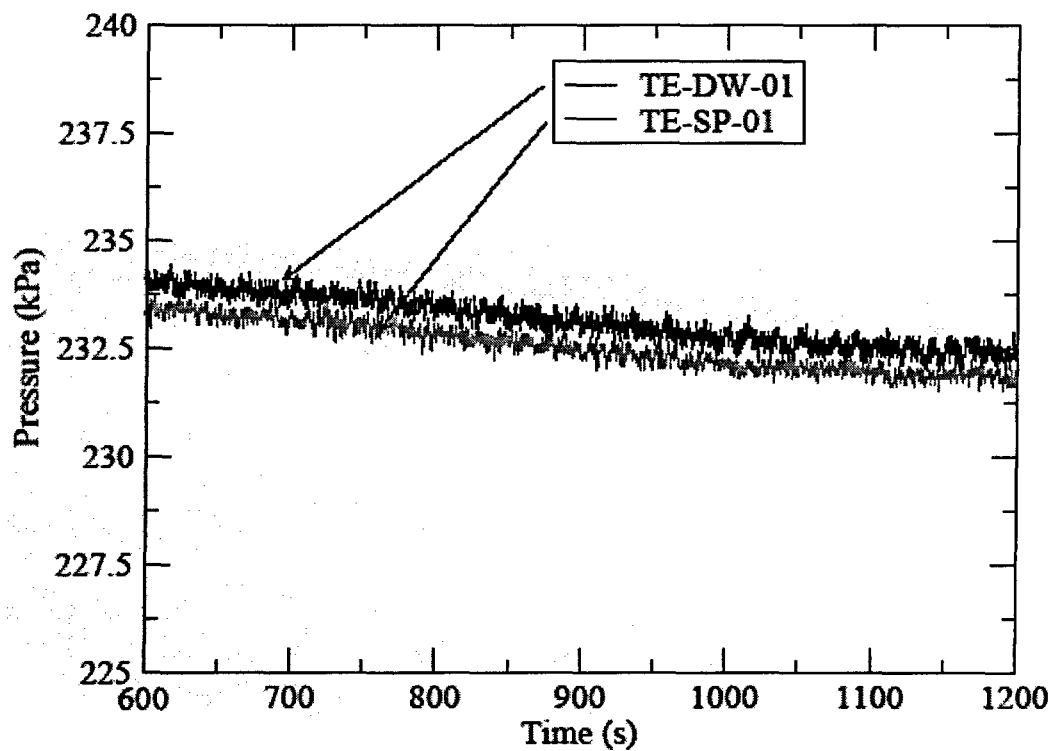Noncondensable Gas Concentration: <1%
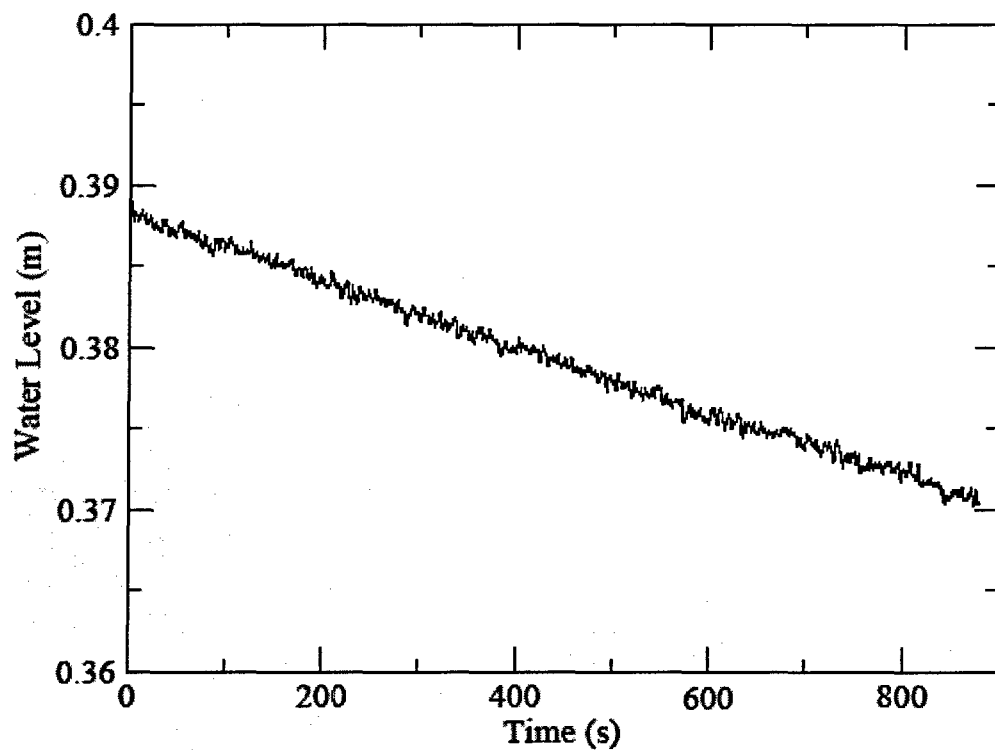
Figure 3.11 Water Level in the PCCS Pool

PCCS Separate Effect Test

Test No.:   LM807B
Mode: Long-term cooling with low pool level
Pressure Setting: 230 kPa
Noncondensable Gas Concentration: <1%

3-18
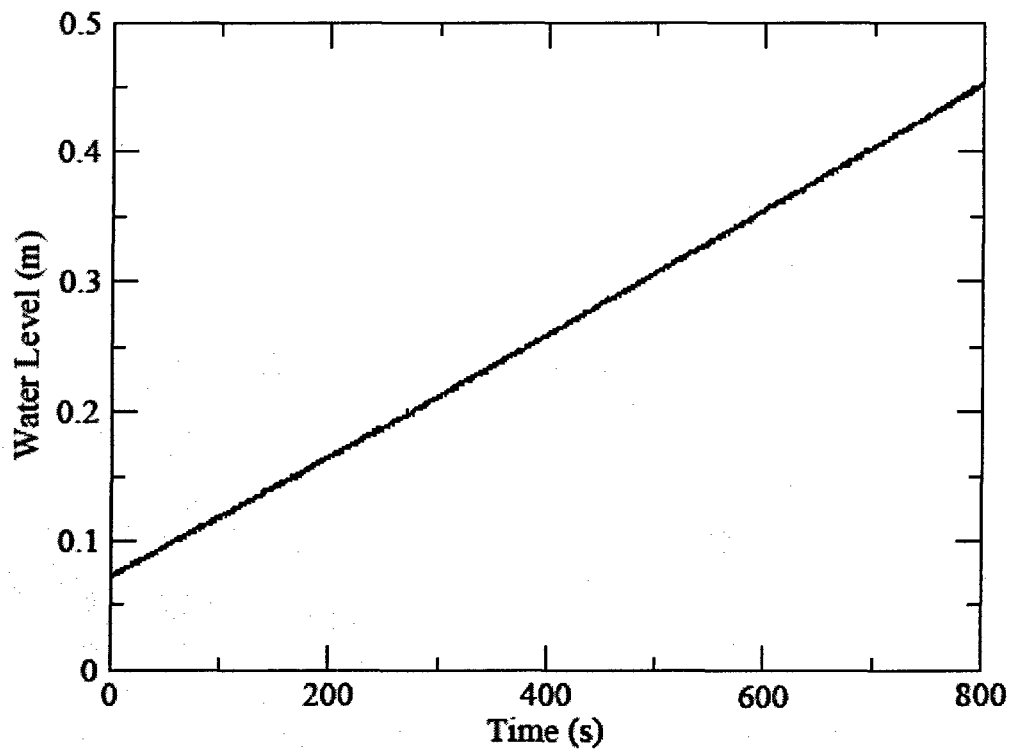
Figure 3.12 Water Level in the PCCS Drain Tank

PCCS Separate Effect Test

Test No.:	LM807B
Mode:	Long-term cooling with low pool level
Pressure Setting:	230 kPa
Noncondensable Gas Concentration:	<1%
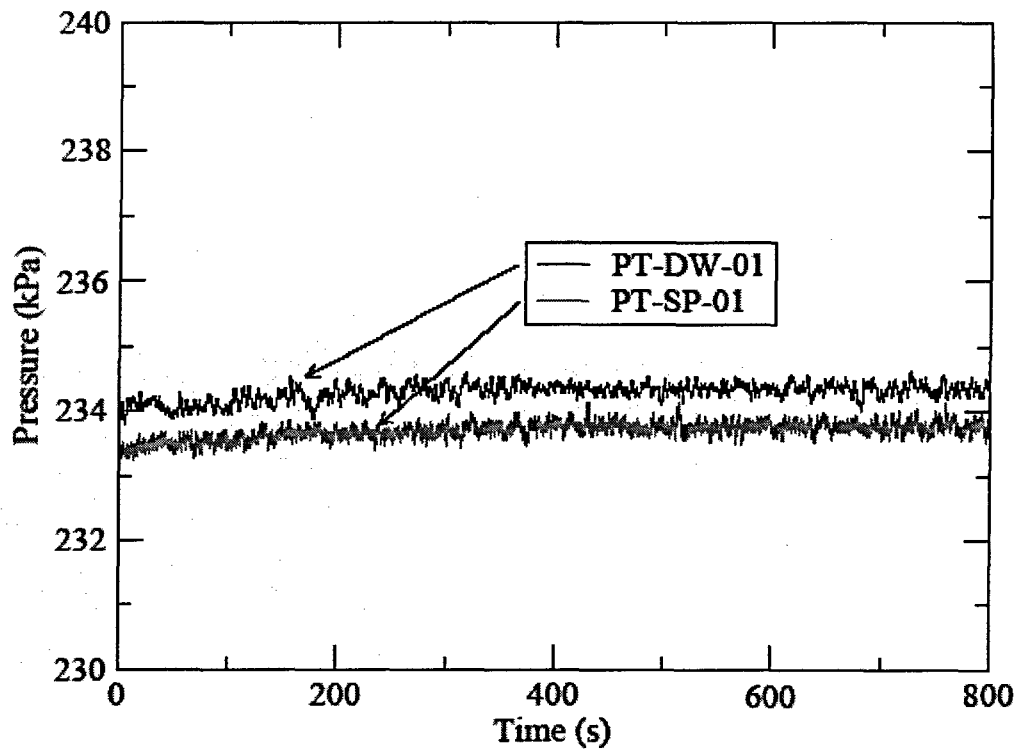
Figure 3.13 Upper Drywell and Wetwell Gas Space Pressures

PCCS Separate Effect Test

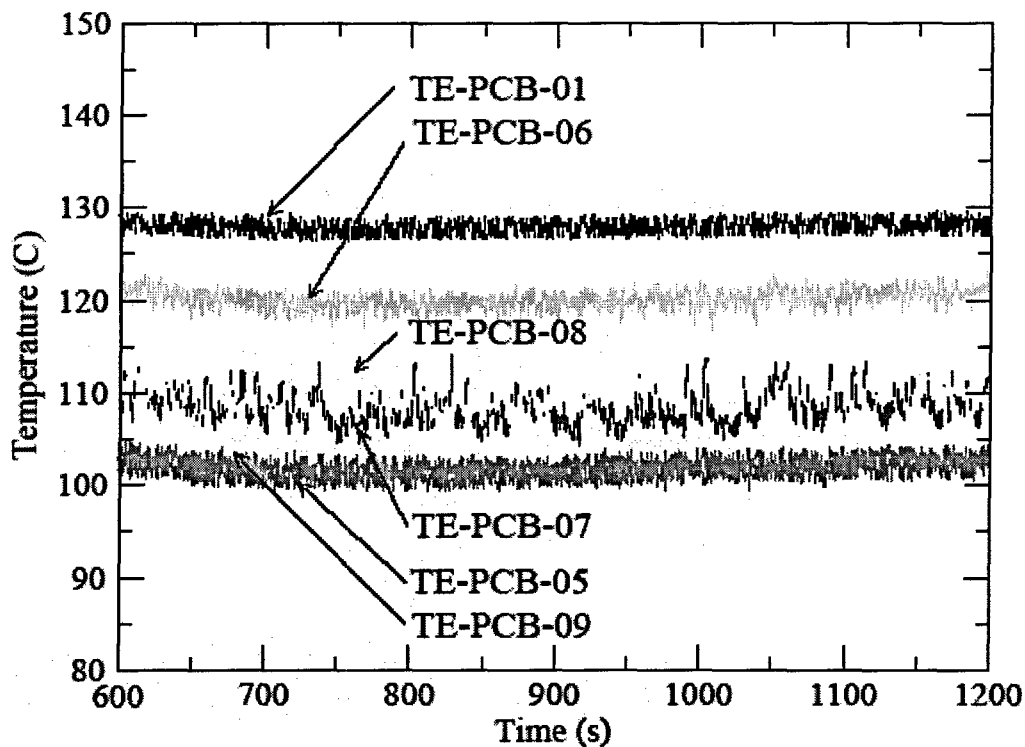Test No.:   LM807B
Mode: Long-term cooling with low pool level
Pressure Setting: 230 kPa
Noncondensable Gas Concentration: <1%

PT-DW-01: Upper drywell pressure
PT- SP -01: Wetwell pressure in gas space
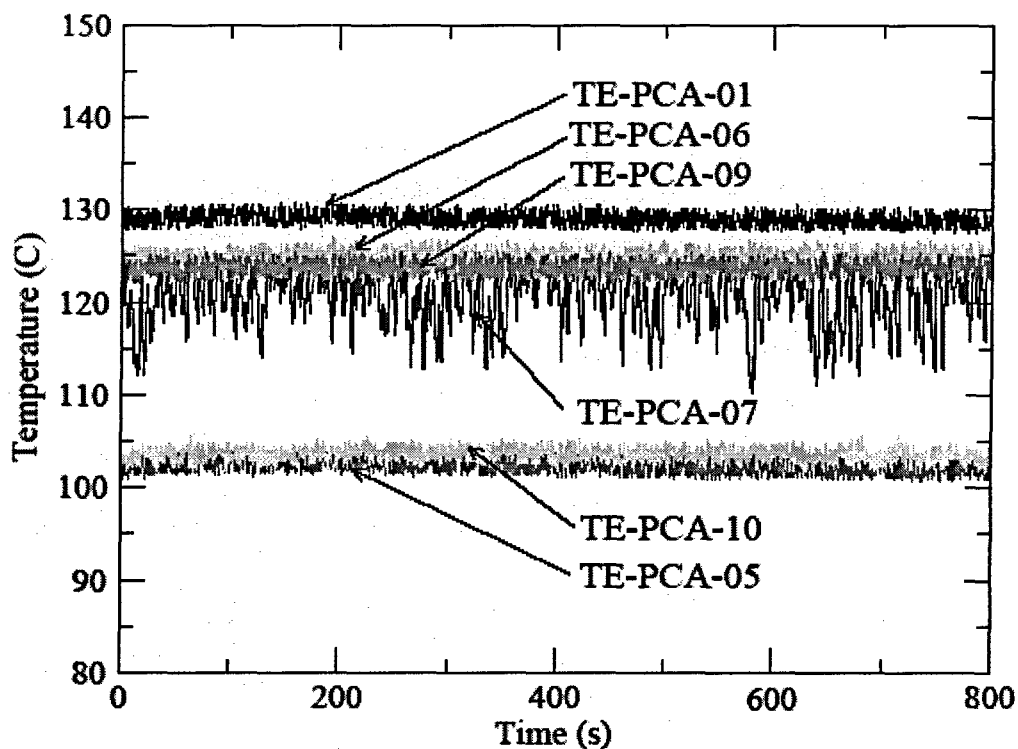
Figure 3.14 Temperatures in PCCS-A

PCCS Separate Effect Test

Test No.:	LM807B
Mode:	Long-term cooling with low pool level
Pressure Setting:	230 kPa
Noncondensable Gas Concentration:	<1%

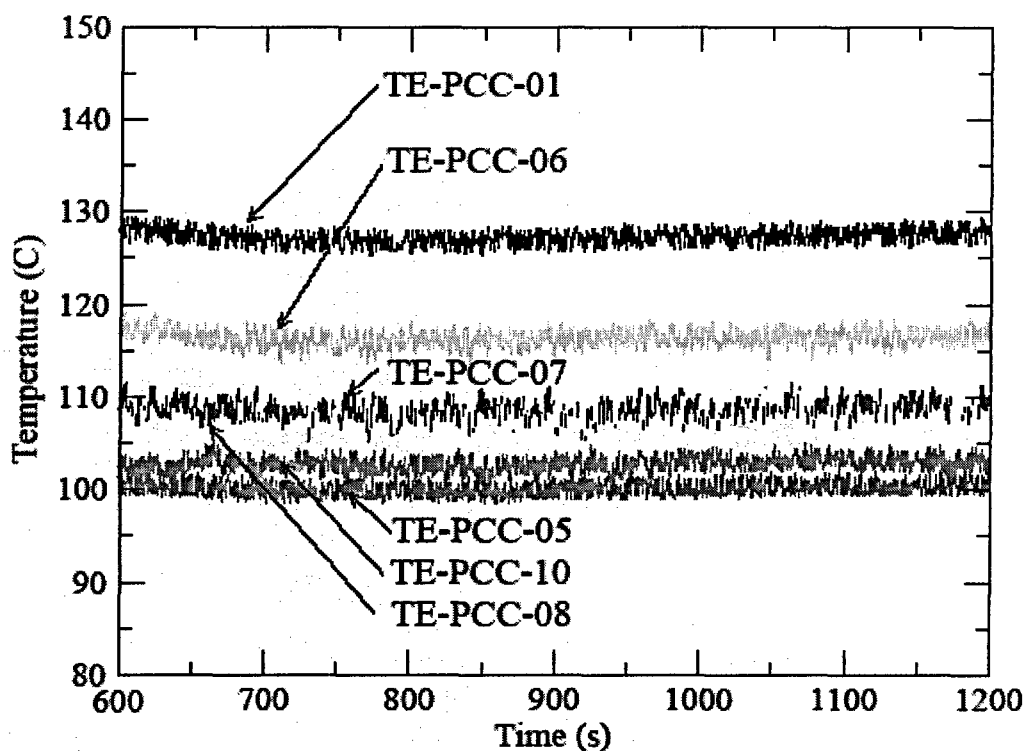|	
TE-PCA-01:	Temperature of steam in PCCS supply line A
TE-PCA-05:	Temperature of water in PCCS pool A (z=254)
TE-PCA-06:	Temperature of condenser tube centerline in PCCS-A (z=745)
TE-PCA-07:	Temperature of condenser tube centerline in PCCS-A (z=580)
TE-PCA-09:	Temperature of condenser tube surface in PCCS-A (z=745)
TE-PCA-10:	Temperature of condenser tube surface in PCCS-A (z=580)

Figure 3.15 Temperatures in PCCS-B

PCCS Separate Effect Test

Test No.:	LM807B
Mode:	Long-term cooling with low pool level
Pressure Setting:	230 kPa
Noncondensable Gas Concentration:	<1%

TE-PCB-01:   Temperature of steam in PCCS supply line B
TE-PCB-05:   Temperature of water in PCCS pool B (z=254)
TE-PCB-06:   Temperature of condenser tube centerline in PCCS-B (z=745)
TE-PCB-07:   Temperature of condenser tube centerline in PCCS-B (z=580)
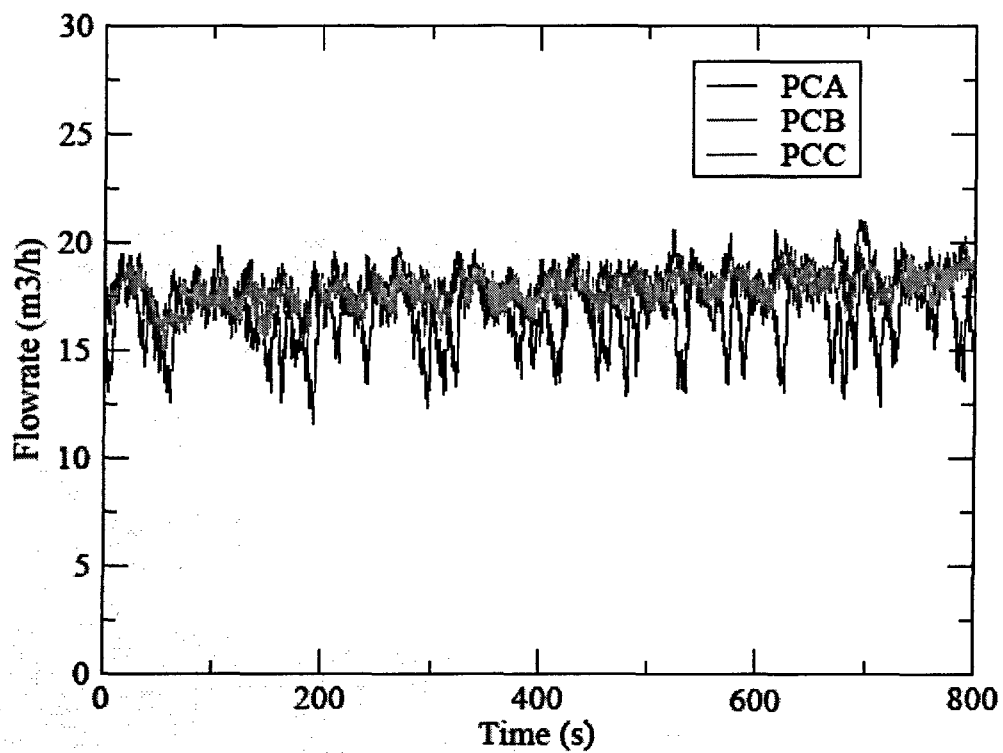TE-PCA-09:   Temperature of condenser tube surface in PCCS-A (z=745)
TE-PCA-10:   Temperature of condenser tube surface in PCCS-A (z=580)
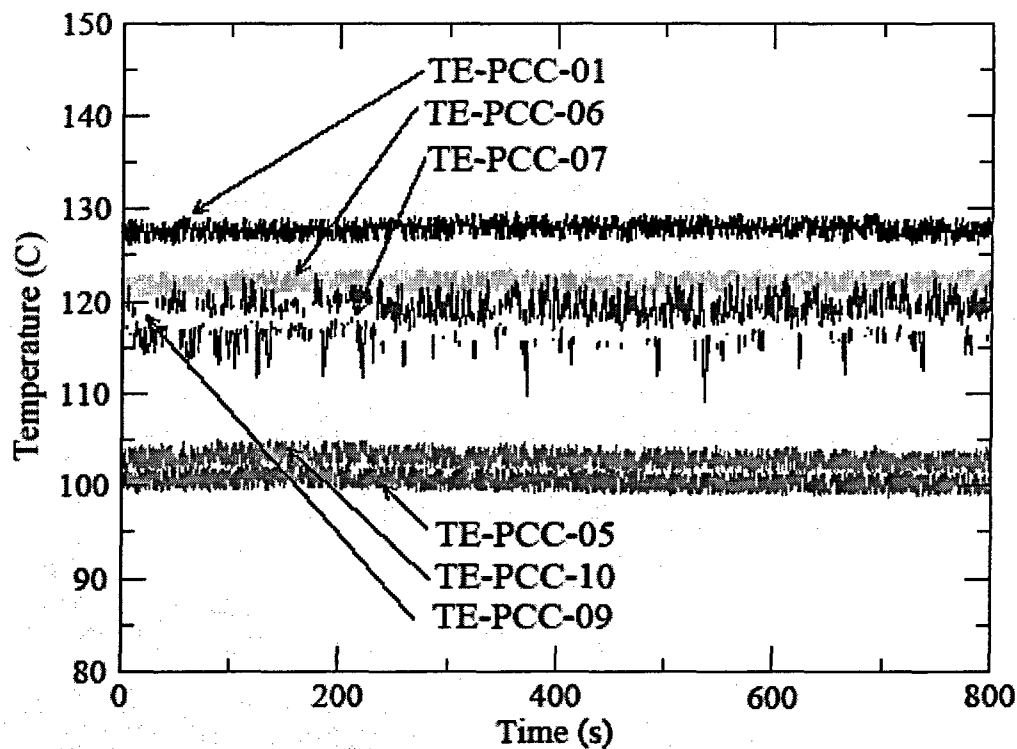
Figure 3.16 Temperatures in PCCS-C

PCCS Separate Effect Test

Test No.:	LM807B
Mode:	Long-term cooling with low pool level
Pressure Setting:	230 kPa
Noncondensable Gas Concentration:	<1%

TE-PCC-01:   Temperature of steam in PCCS supply line C
TE-PCC-05:   Temperature of water in PCCS pool C (z=254)
TE-PCC-06:   Temperature of condenser tube centerline in PCCS-C (z=745)
TE-PCC-07:   Temperature of condenser tube centerline in PCCS-C (z=580)
TE-PCA-09:   Temperature of condenser tube surface in PCCS-A (z=745)
TE-PCA-10:   Temperature of condenser tube surface in PCCS-A (z=580)
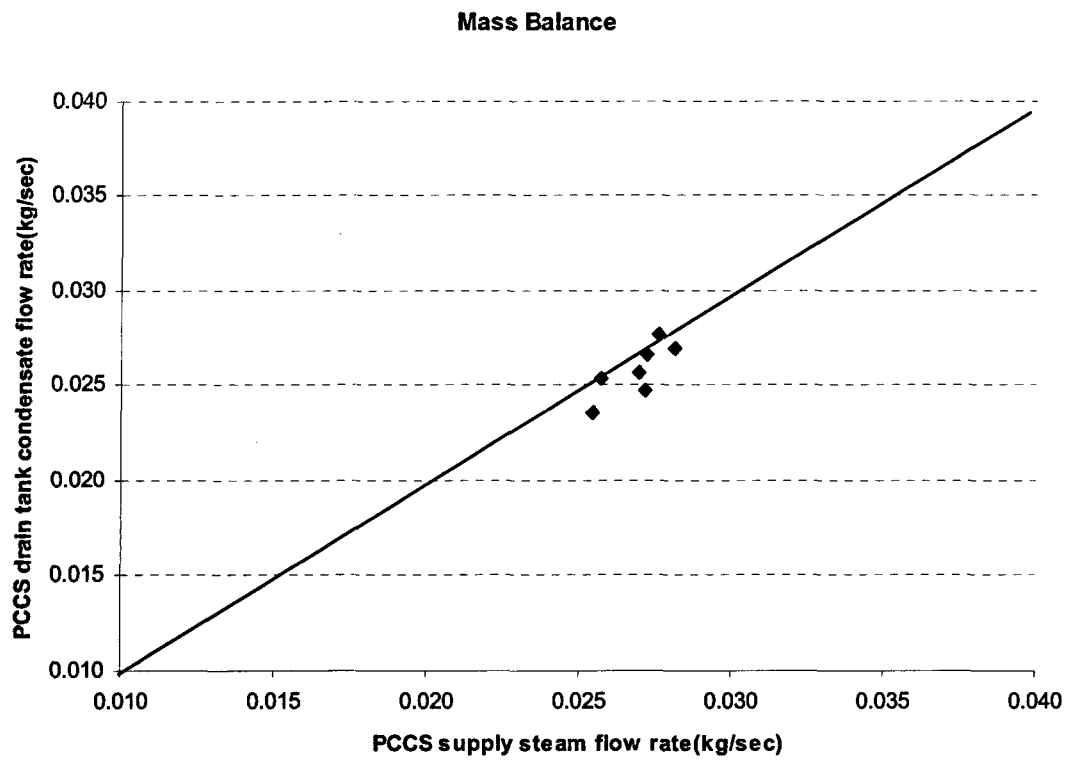
Mass Balance

Figure 3.17 Comparison of Steam Inlet Flow Rate Measured with PCCS supply line Vortex Flow Meter and Mass Flow Rate Measured by PCCS Drain Tank Water Level Change

Energy Balance
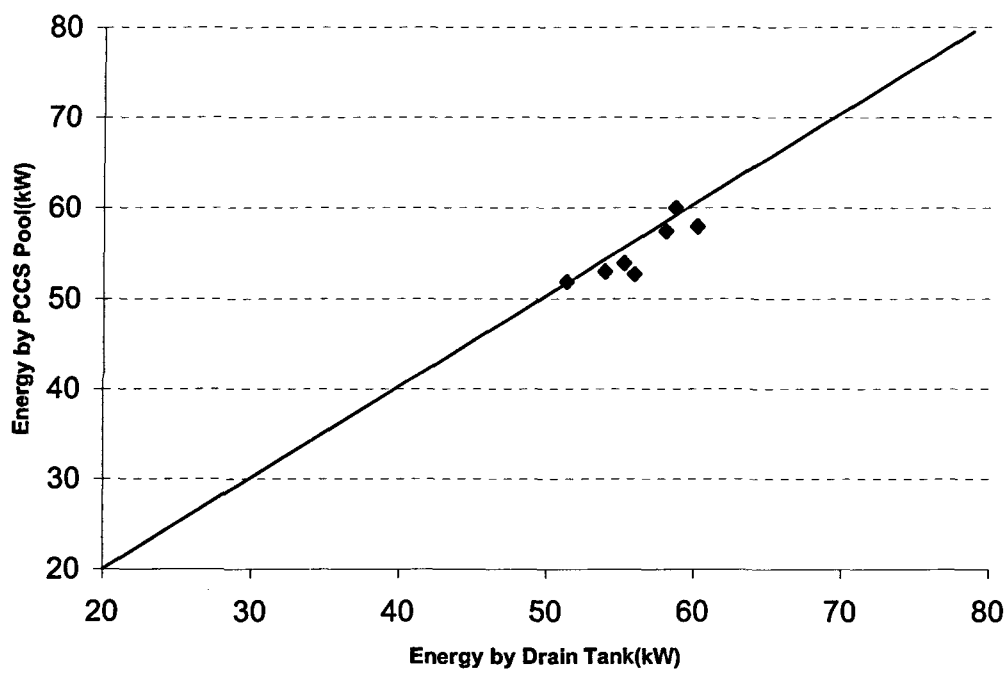
Figure 3.18 Comparison of Energy Measured with PCCS Drain Tank and Energy Measured by PCCS Pool
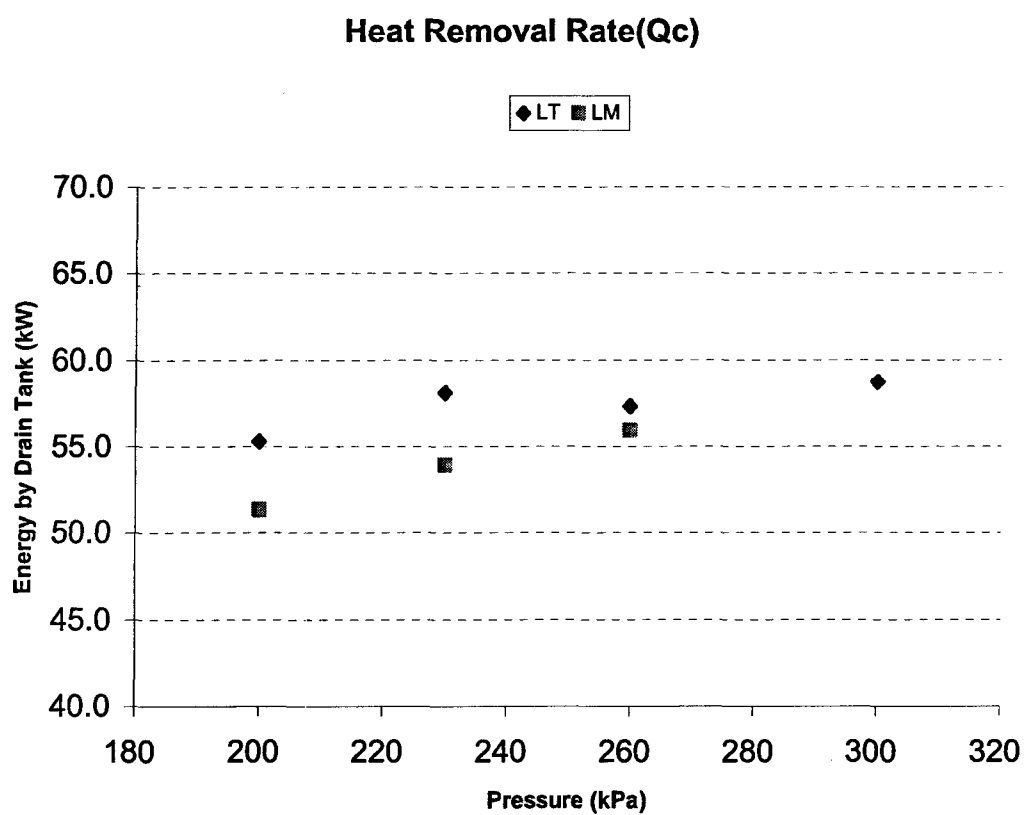
Figure 3.19 PCCS Heat Transfer Rate Dependency on the Pressure
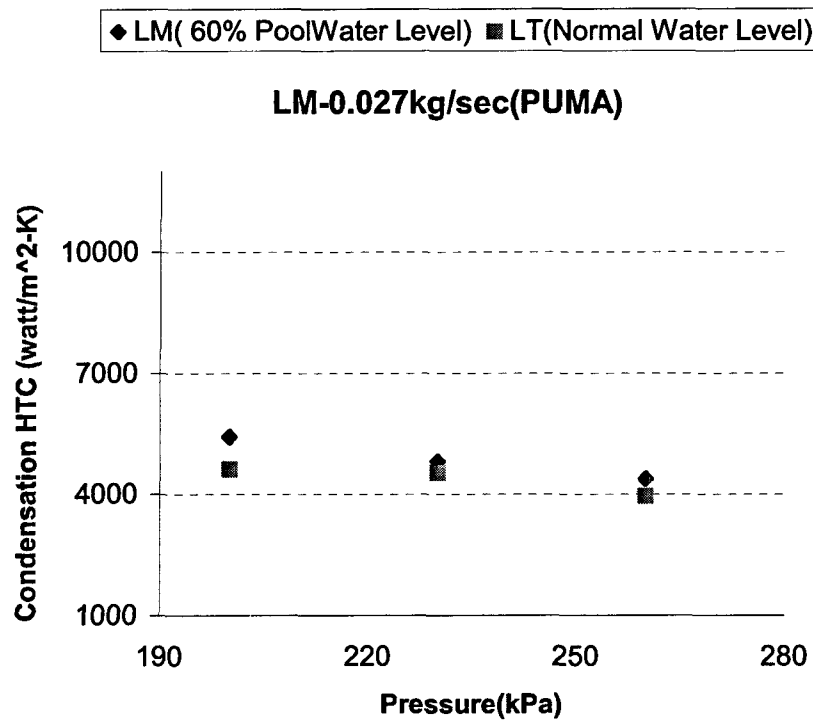
Figure 3.20 PCCS Condensation Heat Transfer Coefficient Dependency on the Pressure

LM-0.027kg/sec(UCB)
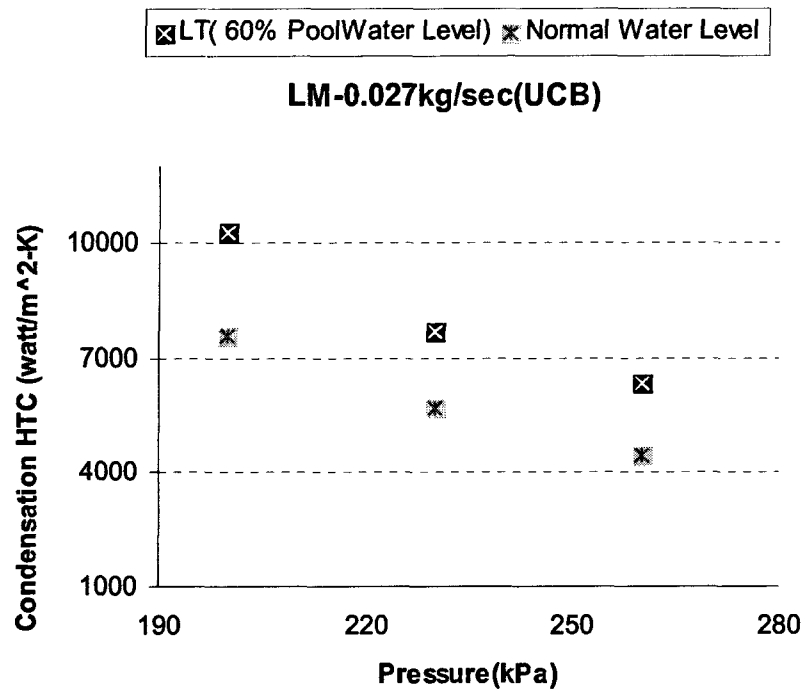
Figure 3.21 Average heat transfer coefficient calculated by UCB model
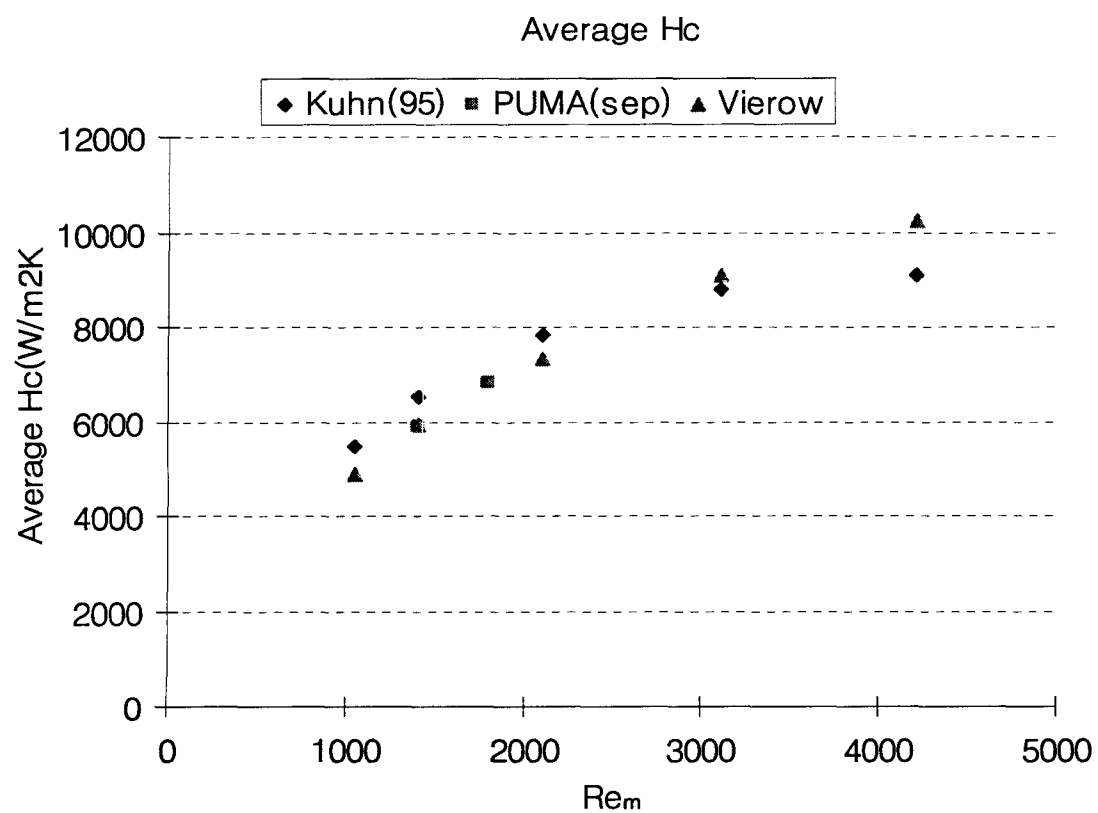
Figure 3.22 Comparison with Previous Experimental Data

4. BYPASS MODE EXPERIMENTS

4.1 Test Matrix

A total of 6 cases for the bypass mode experiments have been performed to investigate the pressure dependency and noncondensable gas effects. The inlet steam flow rate, 0.075 kg/sec from RPV to DW is large enough to have the horizontal venting flow in the wetwell. This is close to maximum inlet mixture flow condition in the PUMA separate effect tests. As shown in Table 4.1, there are three pressure conditions (220 kPa, 260 kPa and 300 kPa). For noncondensable gas effects in the condensation, pure steam and three cases of 10% noncondensable gas mixture flow and one case of 15% noncondensable gas mixture at 300 kPa experiments were conducted.

4.2 Experimental Data

In the bypass mode, the pressure difference between the drywell and wetwell is larger than 2 kPa, which is the hydrostatic head of the submerged PCCS vent line. Steam and noncondensable gas pass through the PCCS condensers with condensation and noncondensable gas and uncondensed steam are vented through the vent pipe into the wetwell.

In the bypass mode experiments, noncondensable gas concentration in the mixture flow is one of the key parameters. To see the effect of noncondensable gas in the flow, pure steam experiments were carried out. As explained in Chapter 3, to ensure a nearly pure steam experimental condition, two methods are used to obtain the initial conditions. The first method is to follow the same procedures as in the 2004 experiments which used the oxygen analyzer located at the inlet of PCCS supply line A. The second method is to monitor the temperatures of PCCS supply line and noncondensable gas venting line temperatures. For mixture flow cases, noncondensable gas fractions were set up by blowing mixture flow long enough to purge more than five times the drywell volume as the pure steam condition was obtained.

Steam Volumetric Flow rate in PCCS supply lines and condensate water flow rate PCCS drain lines are shown in Figure 4.1 and Figure 4.2, respectively. The PCCS pool water level and PCCS drain tank level are shown in Figure 4.3 and Figure 4.4, respectively. Figure 4.5 shows the

pressure condition of the drywell and wetwell. The PCCS inlet steam temperatures, tube wall temperatures, tube centerline temperatures and pool temperatures are shown in Figure 4.6, Figure 4.7 and Figure 4.8. Compared with the mixture bypass mode, tube centerline temperatures along the axial directions are uniform due to high pure steam flow in the condenser tube. The tube surface temperature (z = 745 mm) in PCCS-C is not provided due to malfunction of the thermocouple.

Table 4.2 lists the average overall heat transfer rate ($\bar{U}$), the average heat transfer coefficient in the pool ($\bar{h}_p$), and the average of the condensation heat transfer coefficient ($\bar{h}_c$) for PCCS condenser. Here $\bar{T}_g$, $\bar{T}_w$ and $\bar{T}_p$ are the averages of the temperatures taken at the discrete vertical locations for all PCCS. Condensate water flow rates are obtained by measuring the PCCS drain line flow rate and crosschecked against PCCS drain tank water level changes.

Test BL723E has somewhat quasi steady state condition in terms of drain line flow rate because the steady boundary conditions were difficult to maintain during down blowdown tests due to large energy transfer from RPV to the DW and WW. This data can be used as reference to see the parameter effects.

4.3 Data Discussion

The temperature profiles in Figure 4.8, PCCS-C are different from other PCCS units. This can be explained by referring to the previous PUMA integral test data report (NUREG/CR-6727). Figure 4.13 shows the centerline temperature profile (z=745) of each PCCS in the blowdown phase. PCCS-C always shows a lower temperature compared with other PCCS units. This may be due to the slightly different inlet flow condition or the noncondensable gas trapped in PCCS-C tubes and PUMA system characteristics. Thus it appears that the behaviors of the three PCCS units are not identical. The reported data can be used to evaluate the total PCCS cooling capacity but not a local data analysis. The PUMA facility is designed to carry out the integral test. There are some limitations for the separate effect test to simulate the same boundary condition of each PCCS pool.

The experimental data conditions which demonstrate the effect of drywell pressure and noncondensable gas effects are shown in Figure 4.11 and Figure 4.12.

4-2

As shown in Figure 4.9, 3 data sets with mixture flow conditions show a large discrepancy because there is a bypass flow from drywell to wetwell through not only PCCS noncondensable gas venting line but also the horizontal venting line. On the other hand, pure steam condition has much closer mass balance between inlet steam flow rate and condensate water flow rate.

The total average heat removal rates over the PCCS units, Q_{con}, were calculated by using the condensate water flow rate obtained by PCCS drain tank water level change with time. As shown in the energy balance figure, these values are well matched with the heat removal rate by PCCS pool water evaporation rate. Other data reduction methods are the same with those of the long-term cooling mode.

As we can expect, the heat transfer coefficient decreases when noncondensable gases present. In general, it has been acknowledged that the noncondensable gases act to reduce the heat transfer capability in the condensation process. It was further shown that as the inlet mixture Reynolds number decreases, the local heat transfer coefficient decreases.

The current experimental data show the similar trends as other researcher's results. The total average heat removal rate increases as the drywell pressure increases. As the inlet pressure increases, the tube-average heat transfer coefficient decreases. However, the degradation effect of heat removal rate comparing 10% with 15% NC gas concentration is not significant comparing the pure steam condition with the 10% results. Finally, it is observed that high inlet steam flow condition has a bypass flow at the horizontal venting line, which reduces the PCCS inlet steam flow rate and imposes a limit of maximum inlet mixture flow condition.

The venting frequency in the bypass mode is very high. It was observed and recorded for the PCCS venting line C through the side view window on the wetwell. The venting period between one venting and the next by high speed camera image processing is difficult to quantify. We think that continuous venting conditions were present.

Table 4.1 Test Matrix for the Bypass Mode

Test No.	$\dot{m}_{msl}$ (kg/Sec)	Pressure kPa (psia)	PCCS inlet noncondensable gas mass fraction (%)	PCCS Pool water level (m)
BL721AR	0.070	220 (32)	0.0	0.92
BL723D	0.062		10.8	
BL731BR	0.077	260 (38)	0.0	
BL723E	0.062		10.8	
BL723C	0.071	300 (43)	0.0	
BL723G	0.055		16.3	

Table 4.2 Summary of the Bypass Mode Data

Test No.	$\dot{m}_{msl}$ (kg/Sec)	Pressure (kPa)	NC Gas (%)	Q_{con} (Kw)	$\bar{U}$ (W/m^{2}K)	$\bar{h}_p$ (W/m^{2}K)	$\bar{h}_c$ (W/m^{2}K)	$\bar{T}_s$ (°C)	$\bar{T}_w$ (°C)	$\bar{T}_p$ (°C)
BL721AR	0.0699	220	0.0	105.10	2959	23265	5021	119.8	103.5	101.3
BL723D	0.0620	220	10.8	52.00	2037	7670	3695	115.7	104.8	101.2
BL731BR	0.0772	260	0.0	121.07	2506	14818	4209	126.7	105.4	101.4
BL723E	0.0620	260	10.8	71.30	2029	12265	3144	119.9	104.6	101.8
BL723C	0.0710	300	0.0	131.34	2411	14366	3980	125.4	105.8	101.5
BL723G	0.0554	300	16.3	64.28	1779	14349	2511	122.3	103.3	101.9
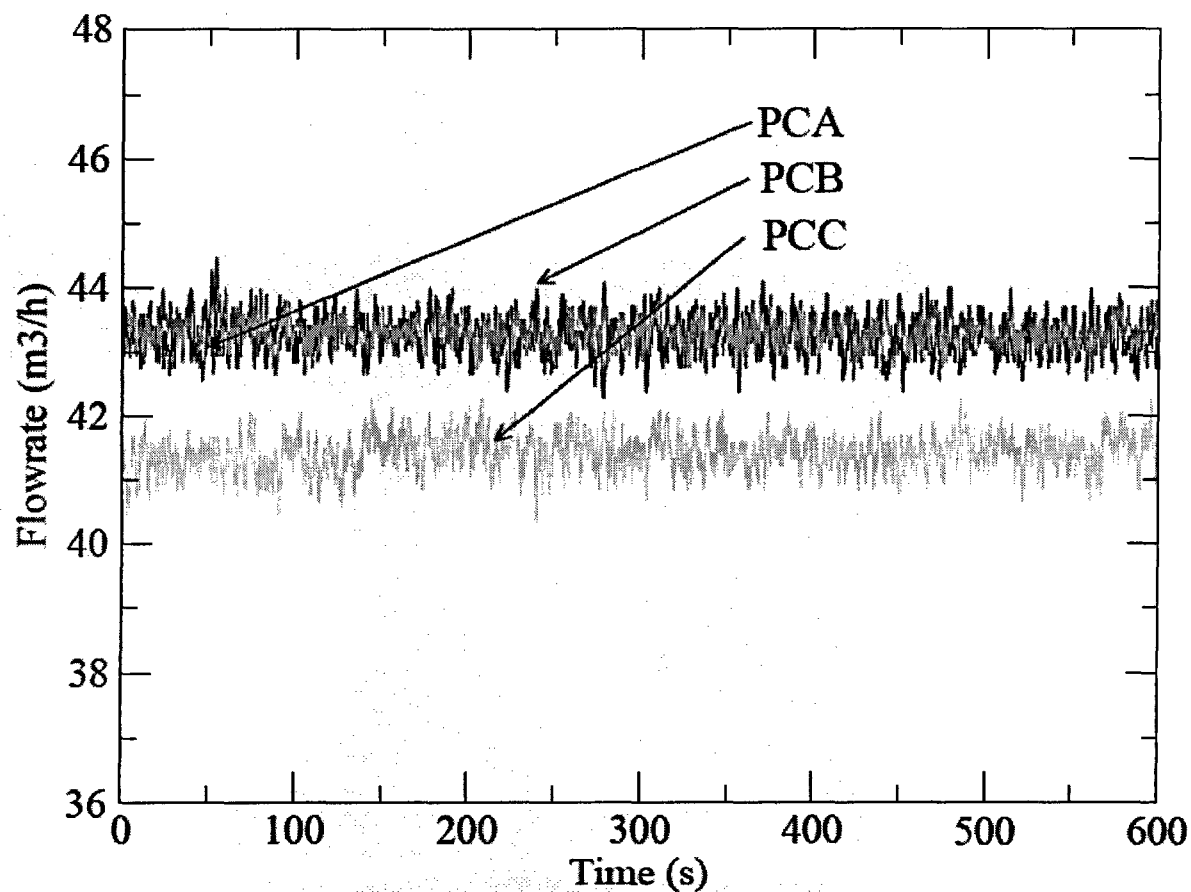
Figure 4.1 Steam Volumetric Flow Rates in PCCS Supply Lines from Vortex Flow Meter

PCCS Separate Effect Test

Test No.:	BL723D
Mode:	Bypass
Pressure Setting:	220 kPa
Noncondensable Gas Concentration:	10 %
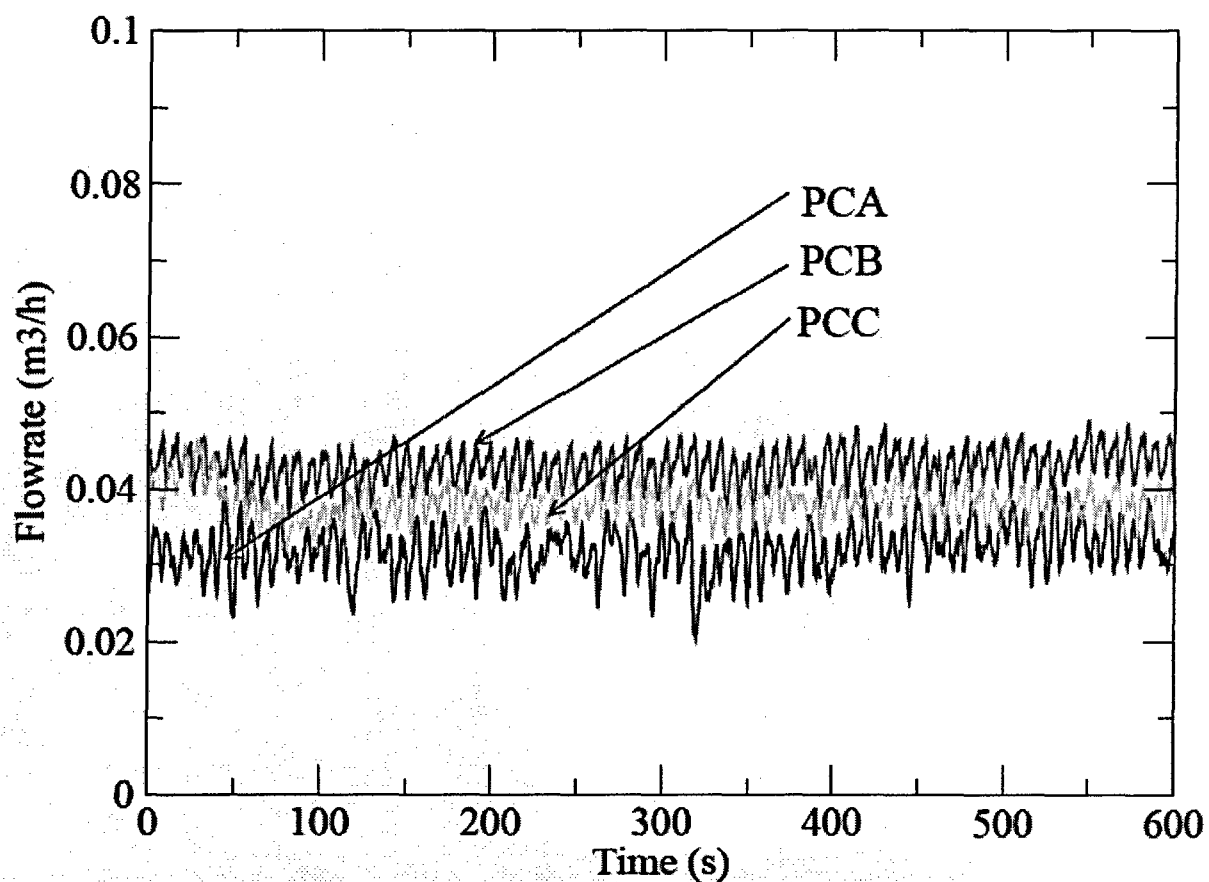
Figure 4.2 Water Volumetric Flow Rates in PCCS Drain Lines

PCCS Separate Effect Test

Test No.:	BL723D
Mode:	Bypass
Pressure Setting:	220 kPa
Noncondensable Gas Concentration:	10 %
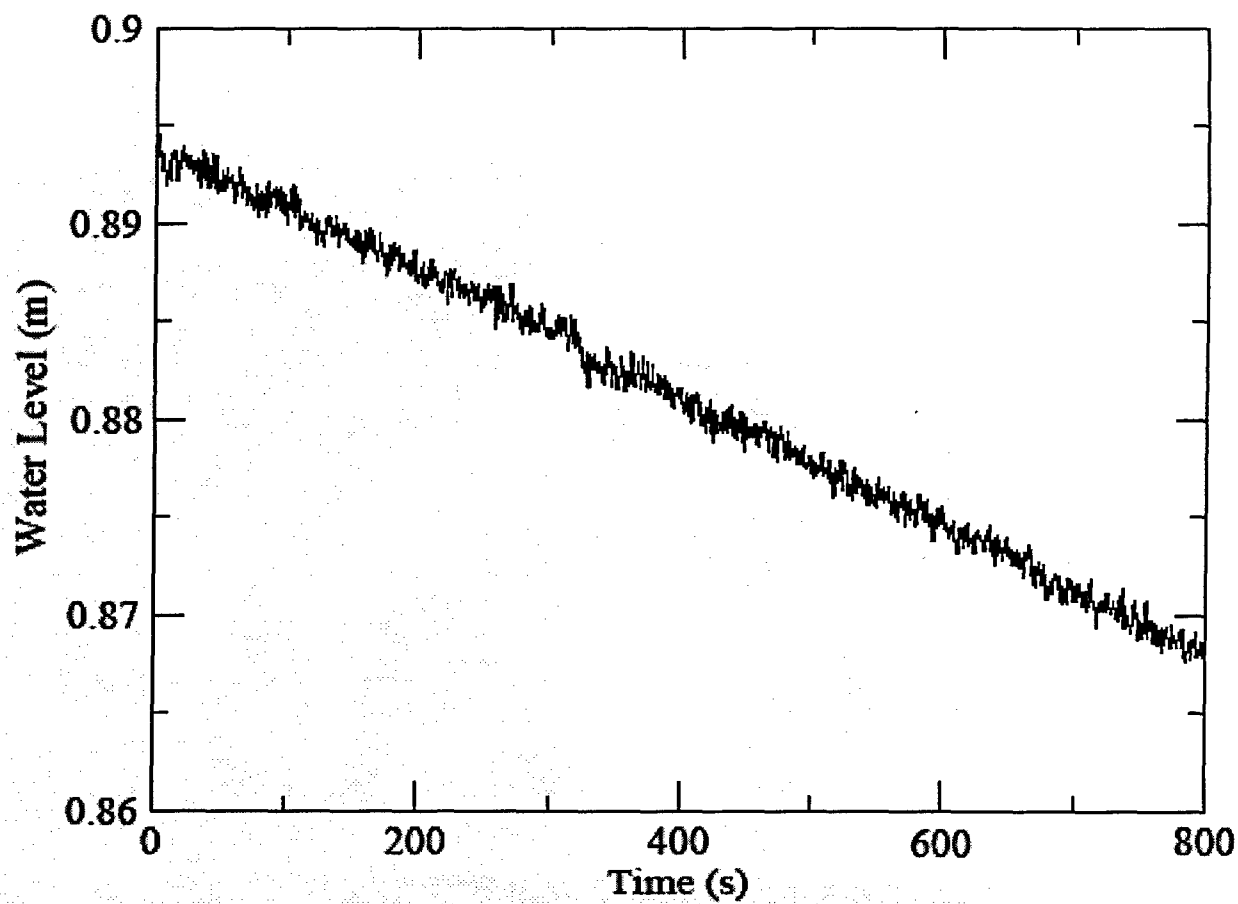
Figure 4.3 Water Level in the PCCS Pool

PCCS Separate Effect Test

Test No.:	BL723D
Mode:	Bypass
Pressure Setting:	220 kPa
Noncondensable Gas Concentration:	10 %
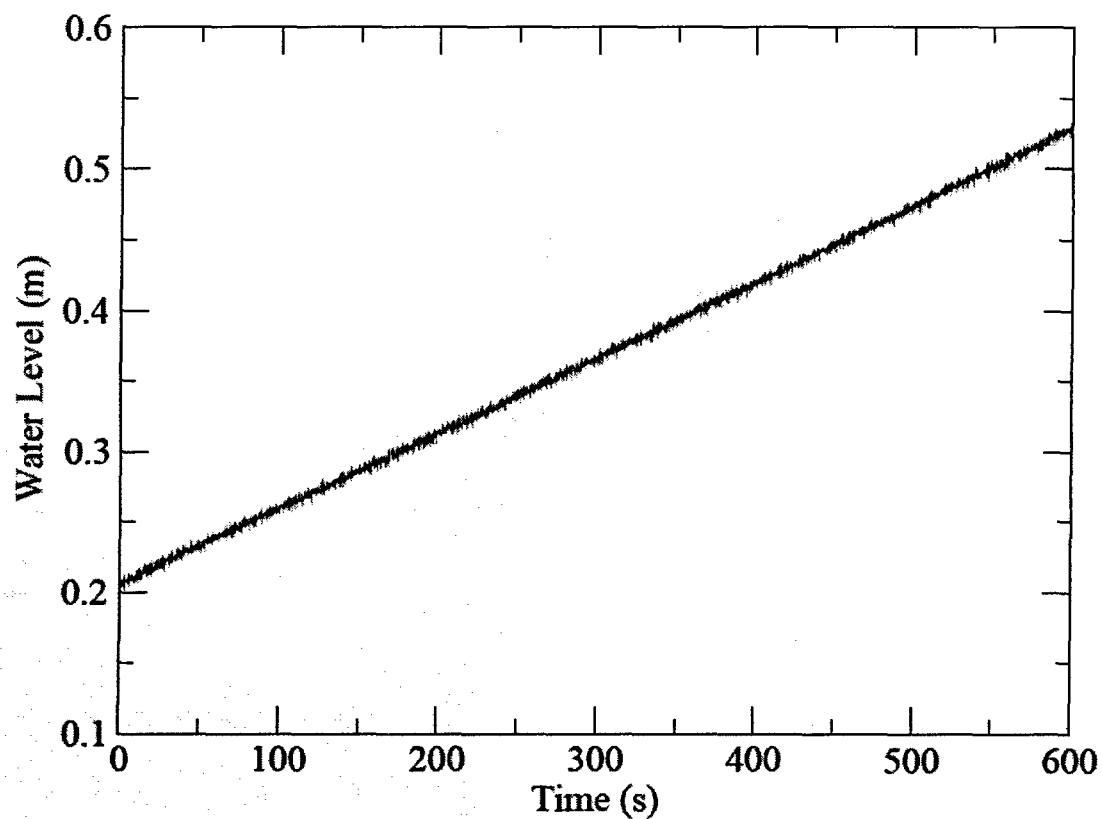
Figure 4.4 Water Level in the PCCS Drain Tank

PCCS Separate Effect Test

Test No.:	BL723D
Mode:	Bypass
Pressure Setting:	220 kPa
Noncondensable Gas Concentration:	10 %

PT-DW-01:   Upper drywell pressure
PT- SP -01:   Wetwell pressure in gas space
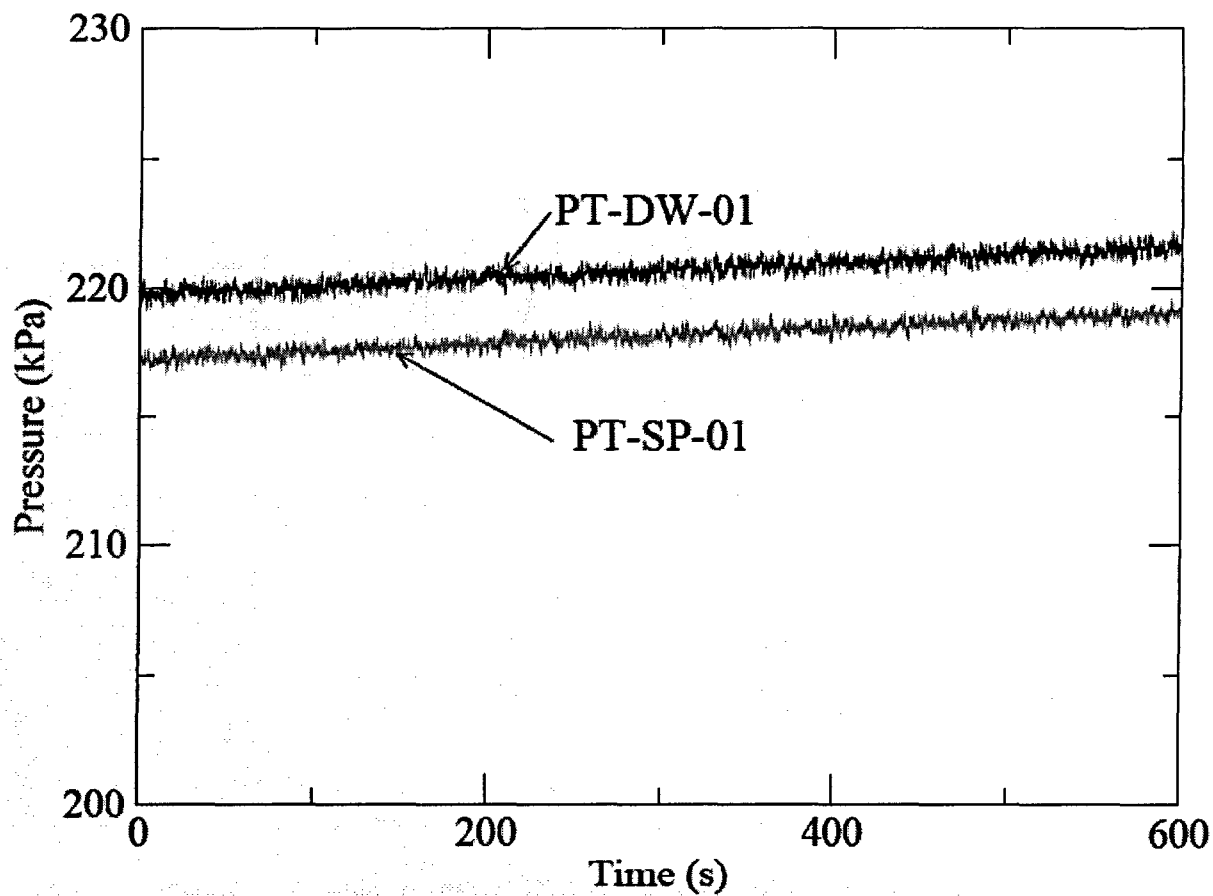
Figure 4.5 Upper Drywell and Wetwell Gas Space Pressures

PCCS Separate Effect Test

Test No.:	BL723D
Mode:	Bypass
Pressure Setting:	220 kPa
Noncondensable Gas Concentration:	10 %

PT-DW-01: Upper drywell pressure
PT- SP -01: Wetwell pressure in gas space
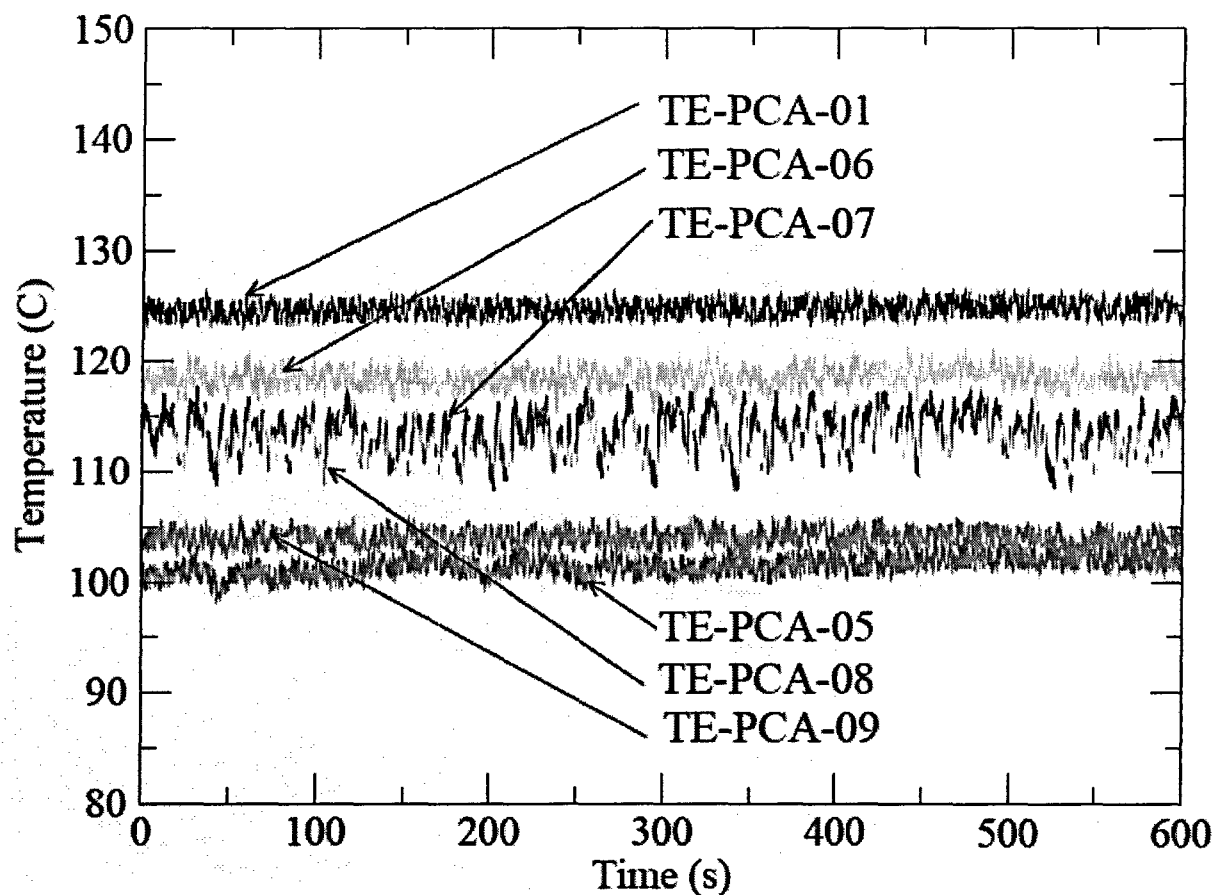
Figure 4.6 Temperatures in PCCS-A

PCCS Separate Effect Test

Test No.:	BL723D
Mode:	Bypass
Pressure Setting:	220 kPa
Noncondensable Gas Concentration:	10 %

TE-PCA-01:   Temperature of steam in PCCS supply line A
TE-PCA-05:   Temperature of water in PCCS pool A (z=254)
TE-PCA-06:   Temperature of condenser tube centerline in PCCS-A (z=745)
TE-PCA-07:   Temperature of condenser tube centerline in PCCS-A (z=580)
TE-PCA-08:   Temperature of condenser tube centerline in PCCS-A (z=415)
TE-PCA-09:   Temperature of condenser tube surface in PCCS-A (z=745)
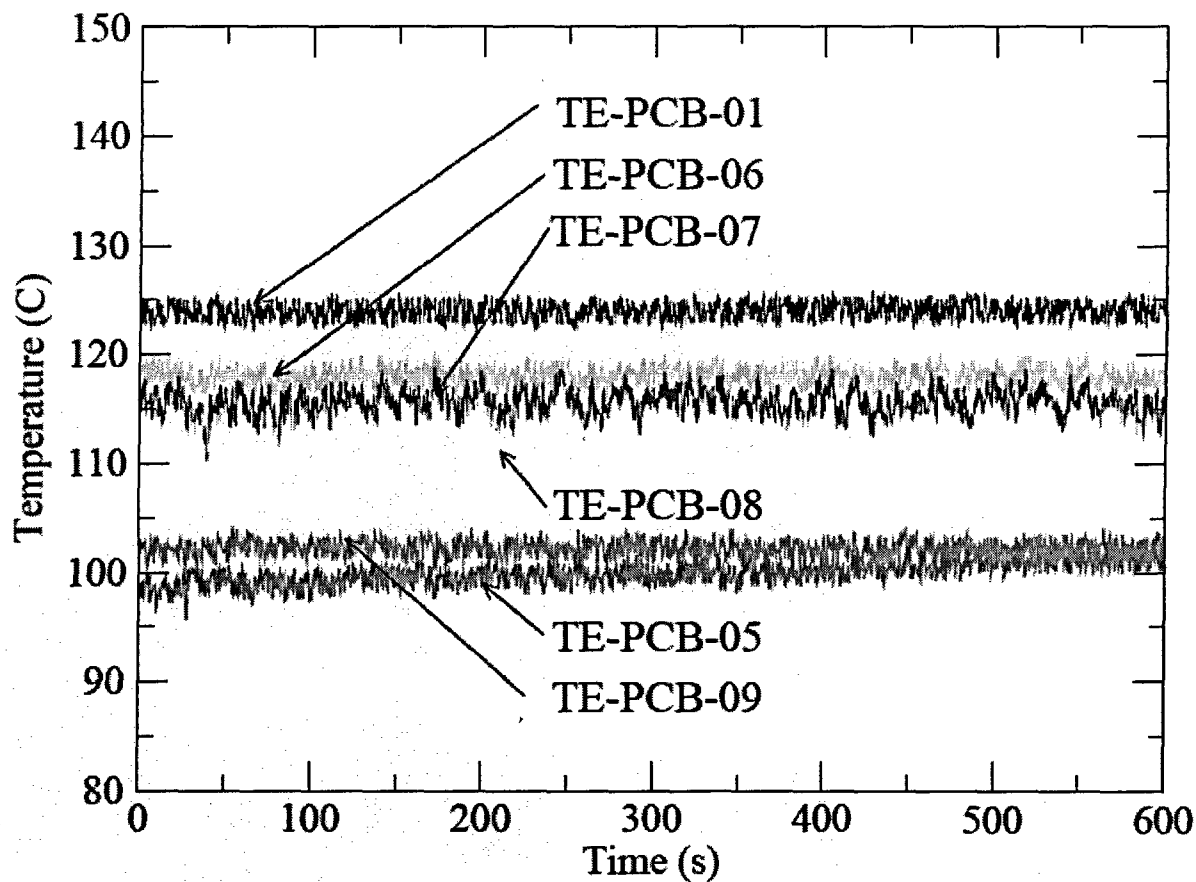
Figure 4.7 Temperatures in PCCS-B

PCCS Separate Effect Test

Test No.:	BL723D
Mode:	Bypass
Pressure Setting:	220 kPa
Noncondensable Gas Concentration:	10 %

TE-PCB-01:	Temperature of steam in PCCS supply line B
TE-PCB-05:	Temperature of water in PCCS pool B (z=254)
TE-PCB-06:	Temperature of condenser tube centerline in PCCS-B (z=745)
TE-PCB-07:	Temperature of condenser tube centerline in PCCS-B (z=580)
TE-PCB-08:	Temperature of condenser tube centerline in PCCS-B (z=415)
TE-PCB-09:	Temperature of condenser tube surface in PCCS-B (z=745)
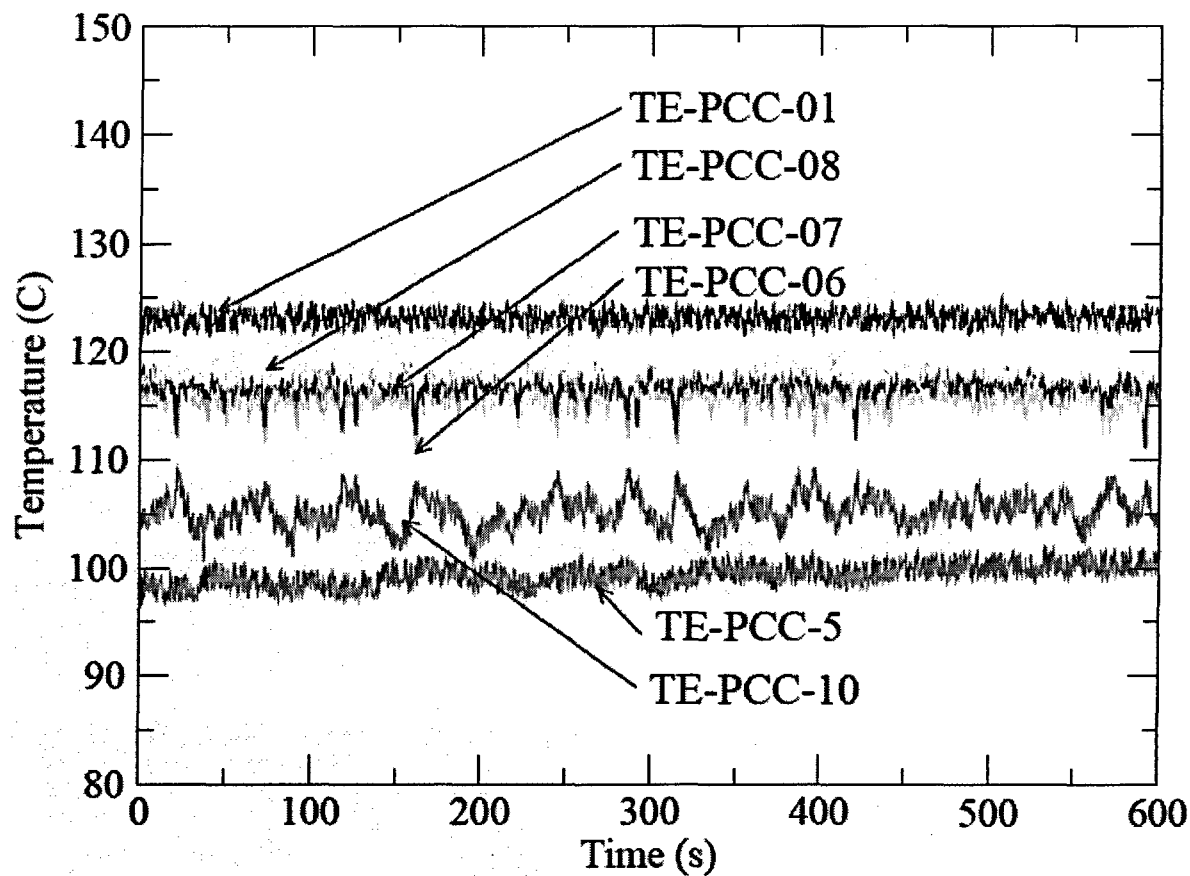
Figure 4.8 Temperatures in PCCS-C

PCCS Separate Effect Test

Test No.:	BL723D
Mode:	Bypass
Pressure Setting:	220 kPa
Noncondensable Gas Concentration:	10 %

TE-PCC-01: Temperature of steam in PCCS supply line C
TE-PCC-05: Temperature of water in PCCS pool C (z=254)
TE-PCC-06: Temperature of condenser tube centerline in PCCS-C (z=745)
TE-PCC-07: Temperature of condenser tube centerline in PCCS-C (z=580)
TE-PCC-08: Temperature of condenser tube centerline in PCCS-C (z=415)
TE-PCC-10: Temperature of condenser tube surface in PCCS-B (z=580)

Mass Balance of Blow Down Mode
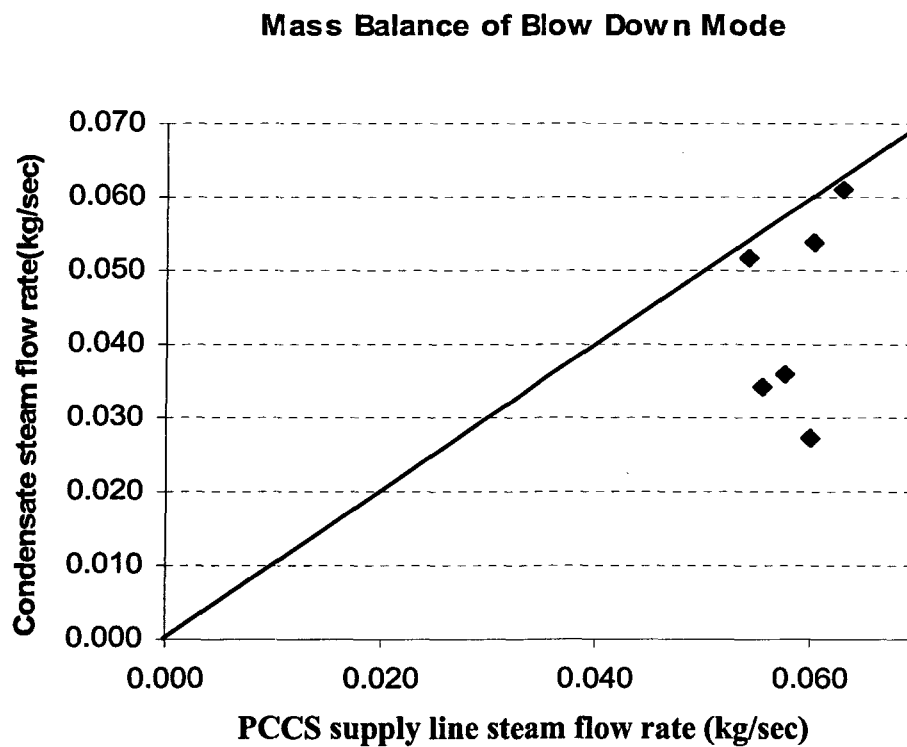
Figure 4.9 Comparison of Steam Inlet Flow Rate Measured with PCCS supply line Vortex Flow Meter and Mass Flow Rate Measured by PCCS Drain Tank Water Level Change

Energy Balance of Blow Down Mode

X-axis: Energy by Drain Tank(kW)
Y-axis: Energy by PCCS Pool(kW)
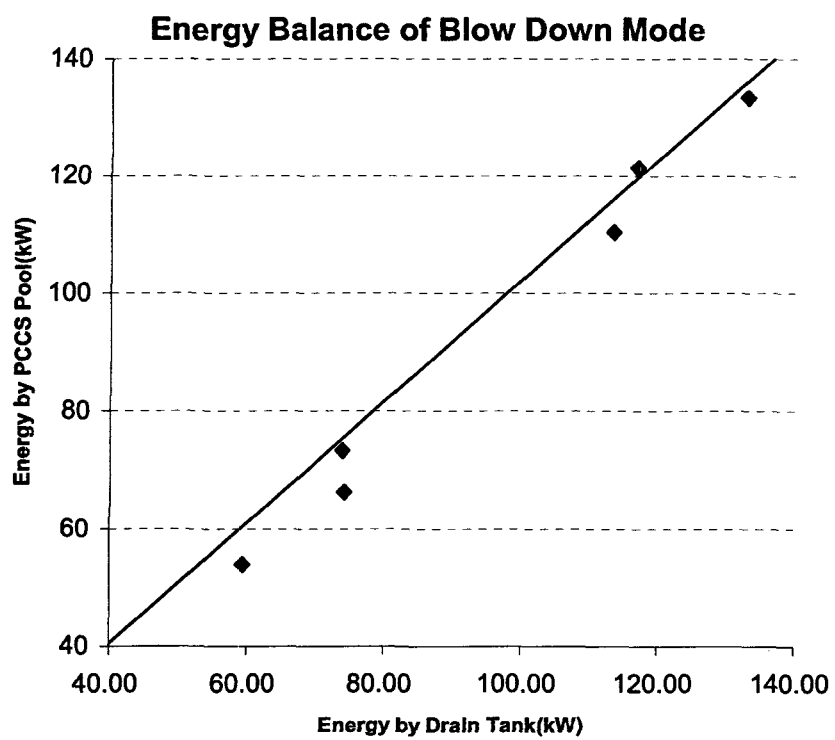
Figure 4.10 Comparison of Energy Measured with PCCS Drain Tank and Energy Measured with

PCCS pool
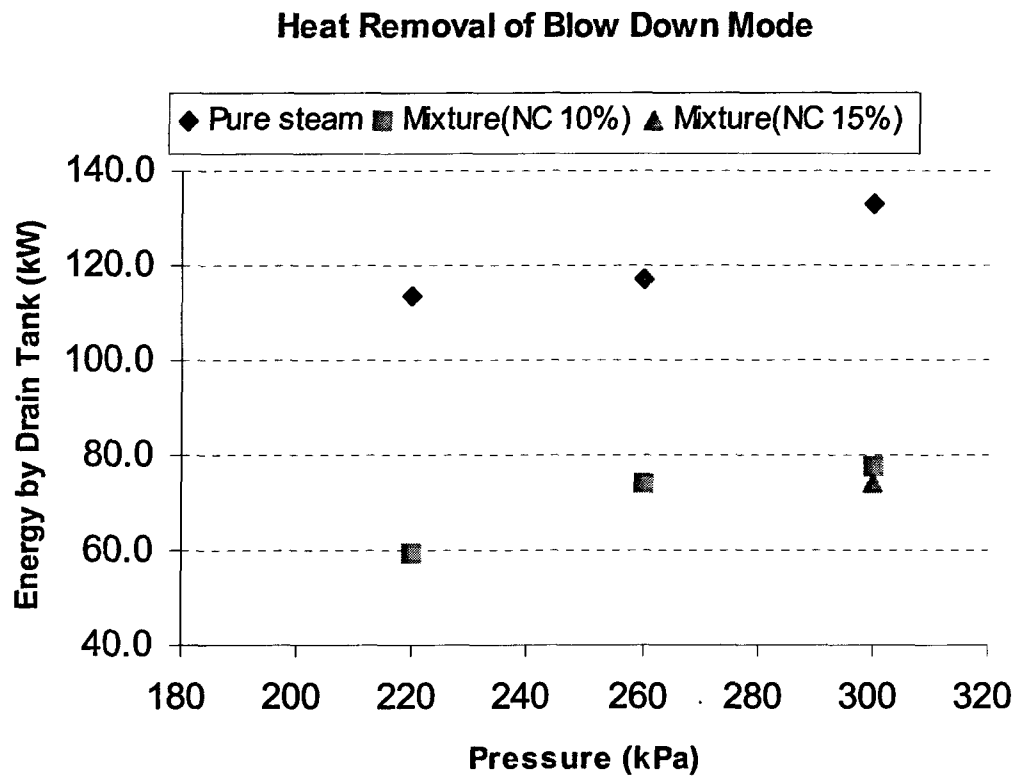
Figure 4.11 PCCS Heat Transfer Rate Dependency on the Pressure

Blowdown-0.07kg/sec

◆ Blowdown (pure steam)   ■ NC gas 10%   ▲ NC gas 15%
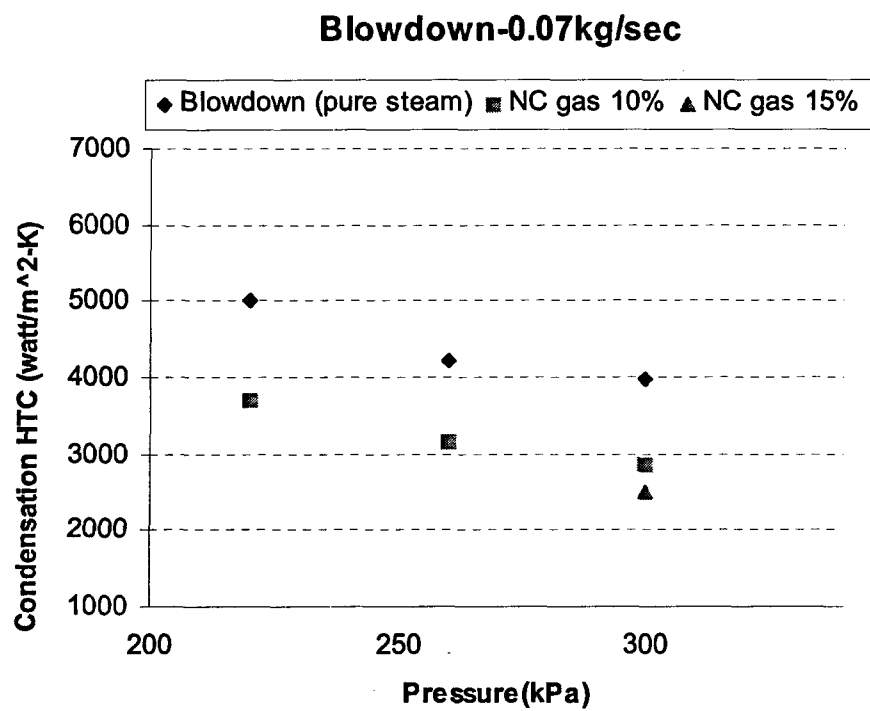
Figure 4.12 PCCS Condensation Heat Transfer Coefficient Dependency on the Pressure
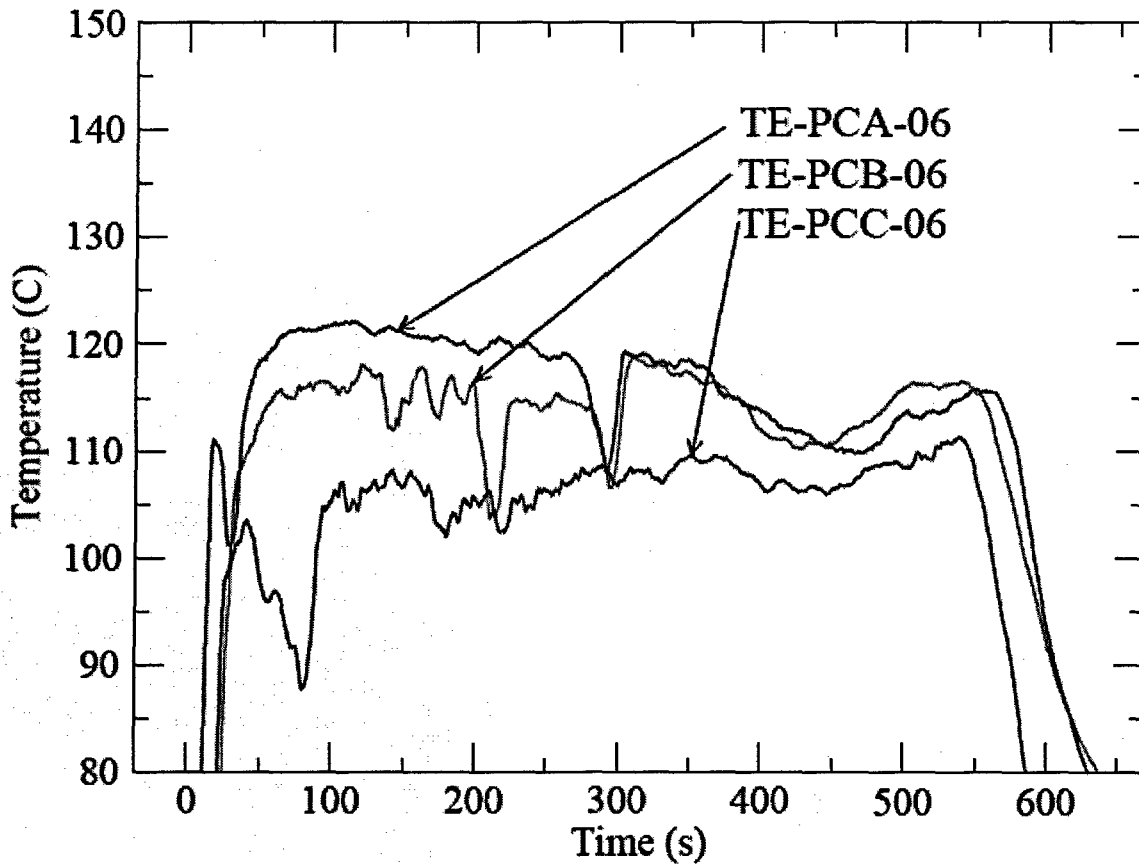
Figure 4.13 Centerline Temperatures of Tubes in PCCS (A, B and C)

MSL Break Test for SBWR (03/21/98) (NUREG/CR-6727)

5. CYCLIC VENTING MODE EXPERIMENTS

5.1 Test Matrix

A total of twenty eight cases for the cyclic venting mode experiments (CY,CH and CM) have been done to see the pressure dependency and noncondensable gas effects. As shown in Table 5.1-a for CY experiments, there are three pressure conditions (220 kPa, 240 kPa and 260 kPa). For noncondensable gas effects in the condensation, pure steam and three cases of noncondensable gas mixture flow were conducted. To see the inlet steam flow rate effect, cyclic venting mode with high steam flow rate (CH) experiments with 0.04 kg/sec from RPV to DW has been done with other test parameters similar to those in CY. Test conditions and data are summarized in Table 5.2-a. To see the PCCS pool inventory effects, CM experiments with similar test conditions as CY except the PCCS pool inventory(50%) were carried out as shown in Table 5.3-a.

5.2 Experimental Data

In the cyclic venting mode, the pressure difference between the drywell and wetwell is larger than the hydrostatic head of the submerged PCCS vent line when the noncondensable gas is accumulated in the PCCS condenser tube. Venting frequency is influenced by inlet NC gas fraction. In the experiment, the pressure difference between the drywell and wetwell has a fluctuation nearby 2 kPa, the hydrostatic head on submerged PCCS vent line. It's difficult to get the exact venting frequency by using pressure difference between DW and WW because after venting happens, the pressure decrease is within the uncertainty of the DP gauge and there are large fluctuations of differential pressure due to unstable the surface condition between gas phase and water phase inside the venting tube. Therefore, cyclic venting period was measured by observing the exit of PCCS NC gas venting line C through the WW pool side view window. For high venting frequency case like high NC gas concentration conditions or high steam flow rate, high speed camera was used with 1/60 to 1/125 frames per sec conditions. Because high speed camera images can't be recorded for more than 5 seconds, data was recorded more than five times during the experiment and average for the total venting period images was taken. For low

venting frequency such as long term cooling mode, digital video camcorder was used to record the venting images. Venting frequency was obtained by time averaging processing like the total number of bubbles divided by measuring time.

There are limitations in the cyclic venting frequency measurement. The venting frequency of vent line C can't be assumed to be the same as in the vent lines A and B because each PCCS unit does not function as identically in PUMA. Therefore, only the trend of venting frequency according to the noncondensable gas fraction can be used as reference.

In the cyclic venting mode experiments, noncondensable gas concentration in the mixture flow is one of the key parameters. To see the effect of noncondensable gas in the flow, pure steam experiments were carried out. As explained in Chapter 3, long term cooling mode, to ensure a nearly pure steam experimental condition, two methods are used. The first method is to follow the same procedures as in previous experiments (Quick Look Report,2004) which used the oxygen analyzer located at the inlet of PCCS supply line A. The second method is to monitor the temperatures of PCCS supply line and noncondensable gas venting line temperatures. For mixture flow cases, noncondensable gas fractions were set up by blowing mixture flow long enough to purge more than five times the drywell volume as the pure steam condition was obtained.

Steam Volumetric Flow rates in PCCS supply lines and condensate water flow rates in PCCS drain lines are shown in Figure 5.1 and Figure 5.2, respectively. The PCCS pool and drain tank water level changes are shown in Figure 5.3 and Figure 5.4, respectively. Figure 5.5 shows the pressure condition of the drywell and wetwell. PCCS inlet steam temperatures, tube wall temperatures, tube centerline temperatures and pool temperatures are shown in Figure 5.6, Figure 5.7 and Figure 5.8.

Due to measurement range limitation of the vortex flow meters installed on the PCCS supply lines for low steam flow rates, especially for the CY and CM test, steam flow rates measured on the main steam line B ($ms = 0.03$ kg/sec) are used as the total inlet steam flow rate into the PCCS units and compared with the total condensate flow rate in the drain line. An accurate average PCCS supply steam flow rate can be also obtained by subtracting the drywell and system heat loss (3.38 kW) from the RPV power and converting this to an RPV steam flow rate. Steam flow rates from the RPV to the drywell are cross-checked by calculating the

evaporation rate from RPV water level changes. In Figures 5.1 and 5.9 show the PCCS supply flow rate measured by vortex flow meters on each of PCCS supply line during experiments. This reading can be used as steady inlet flow conditions, not a real flow rate reading due to limitation of reading for low flow rate.

For cyclic venting mode with 50% of PCCS pool inventory experiment (CM), same kinds of instrument measurement figures for normal PCCS pool level case are shown from Figure 5.9 to Figure 5.16. As shown from Figure 5.14 to Figure 5.16 the temperature profiles are plotted for PCCS supply line, tube centerline and tube surface temperature with elevation z=745 and z=580 respectively. As explained in the long term experiment, the tube surface temperature is close to the tube centerline temperature due to condenser tube uncoverage in the z=745 elevation, Two phase water level can be estimated by two phase water level calibration using the tube surface temperature. The tube surface temperature (z = 745mm) in PCCS-C is not provided due to malfunction of the thermocouple.

It is important to estimate the two phase water level for PCCS pool water inventory effect experiment. Simple hand calculations for two phase water level would require assumptions that induce large error. As an empirical approach, two phase water level calibration was conducted using the condenser tube middle surface temperature. As shown in Figure 5.17, when the two phase water level becomes lower than the middle of condenser tube elevation, temperature shows large fluctuations close to the PCCS inlet temperature. The time information and collapsed water level measured by LT-PC-03 as shown Figure 5.18 for that time. There is an elevation difference between collapsed water level in the pool and thermocouple (z=580mm) elevation of about 5 cm. Therefore, to estimate the submerged heat transfer area, the two phase water level can be obtained by adding the 5.5 cm to the collapsed water level.

Table 5.1-b, 5.2-b and 5.3-b list the average overall heat transfer rate ($\overline{U}$), the average heat transfer coefficient in the pool ($\overline{h}_p$), and the average of the condensation heat transfer coefficient ($\overline{h}_c$) for PCCS test condition CY, CH and CM respectively. Here $\overline{T}_g$, $\overline{T}_w$ and $\overline{T}_p$ are the averages of the temperatures taken at the discrete vertical locations for all PCCS. Condensate water flow rates are obtained by measuring the PCCS drain line flow rate.

5.3 Data Discussion

To confirm the test data quality, the mass and energy balance are checked as shown in Figure 5.19 and 5.20 respectively. The experimental data conditions demonstrate the effect of drywell pressure and noncondensable gas effects as shown from Figure 5.21 to Figure 5.25. The general trend follows the same as the long term and bypass mode.

The total average heat removal rates, Q_{con} over the PCCS units were calculated by using the condensate water flow rate obtained by PCCS drain tank water level change with time and as shown in the energy balance figure, these values are well matched with the heat removal rate by PCCS pool water evaporation rate. Figure 5.21.shows the effect of pressure condition to the heat removal rate for CY experiment. In order to see the pool inventory effect and steam inlet flow rate from the CY data, comparison of heat removal rate is shown in Figure 5.22. As expected, high inlet steam flow rate had a higher heat removal rate and low PCCS pool water level had a lower heat removal rate compared to the CY experiment.

As shown in Figure 5.23, the current experimental data show the similar trend as other research results. As the inlet pressure increases, the tube-average heat transfer coefficient decreases. However, the change of degradation effect of heat removal rate is not significant on high NC gas concentration condition and Khun's model had a higher heat transfer coefficients compared with PUMA data. That can be explained by the different outlet condition of noncondensable gas in the experiment. Khun's experiment couldn't simulate the noncondensable gas accumulation in the condenser tube due to the cyclic venting of NC venting line. Figure 5.24 and 5.25 shows the pressure condition effect for the heat transfer coefficient respectively. Other parametric effect such as pressure, steam flow rate and PCCS pool inventory follows the same trend as long term and bypass mode.

To further validate the experimental data, combined correlated date results are compared with experimental data. The data are plotted as $\frac{Nu}{(1-\chi)^c}$, to isolate the flow rate (Re) dependence. The constants were determined to be $c = 2.5 \pm 0.05$. The comparison data sets are composed of data of Vierow (1990), Siddique et al.(1992), Park(1999), Leonard (2000) and PANTHERS data. As shown in Figure 5.26, cyclic venting mode data and bypass mode data with continuous

venting both follow the same trends as other research results. This is clearly seen showing that the PUMA separate effect test and PANTHERS data fall on the same trend line.

As shown in Figure 5.27, the venting period changes according to the pressure is negligible for very low noncondensable gas fraction test which is less than 1% but the low inlet steam flow rates had longer venting periods than high flow rate. One of Oh's cyclic venting frequencys is compared with PUMA data. Oh (2004) obtained the venting frequency by manually controlling the venting line valve according to the DP reading value between PCCS inlet and outlet. It would induce the large error in a venting frequency measurement. Figure 5.28.shows the effect of noncondensable gas to the venting period. As the noncondensable gas fraction increases, the venting frequency also increases while venting period decreases because it takes less time for NC gas to accumulate inside condenser tube.

Based on the results for heat removal rate and HTC according to pressure, the condensation performance with longer venting period showed better performance. It can be also explained by the relation of NC gas fraction and cyclic venting period in terms of heat removal capability in the PCCS.

Table 5.1-a Test matrix for the cyclic venting mode

Test No.	$\dot{m}_{msl}$ (kg/Sec)	Pressure kPa (psia)	PCCS inlet noncondensable gas mass fraction (%)	PCCS Pool water level (m)
CY602A	0.031	220(32)	0.0	0.92
CY602D	0.032		0.3	
CY903D2	0.032		2.0	
CY903D4	0.033		3.8	
CY602B	0.033	240(35)	0.0	
CY602E	0.033		0.3	
CY604E2	0.034		1.9	
CY903C	0.033	260(38)	0.0	
CY604F	0.034		0.3	
CY602F2	0.034		1.9	
CY903F4	0.033		3.8	

Table 5.1-b Summary of the cyclic venting mode tests data

Test No.	$\dot{m}_{msl}$ (kg/Sec)	Pressure (kPa)	NC Gas (%)	Q_{con} (W)	$\overline{U}$ (W/m²K)	$\overline{h}_p$ (W/m²K)	$\overline{h}_c$ (W/m²K)	$\overline{T}_s$ (°C)	$\overline{T}_w$ (°C)	$\overline{T}_p$ (°C)
CY602A	0.031	220	0.0	66860	2825	16145	5066	112.9	103.5	101.6
CY602D	0.032	220	0.3	65580	2650	12379	4918	115.0	104.6	102.0
CY903D2	0.032	220	2.0	52200	3018	32290	4907	113.4	104.5	102.3
CY903D4	0.033	220	3.8	51000	1994	15788	2910	115.1	103.9	102.4
CY602B	0.033	240	0.0	71550	2680	15868	4634	116.1	104.7	101.9
CY602E	0.033	240	0.3	65800	2665	24728	4189	114.6	103.1	102.2
CY604E2	0.034	240	1.9	62370	2715	61326	3931	114.0	104.1	102.0
CY903C	0.033	260	0.0	69280	2039	14969	3037	115.8	104.6	102.1
CY604F	0.034	260	0.3	69921	2117	8545	3782	117.8	105.2	101.4
CY602F2	0.034	260	1.9	67248	2435	26937	3605	116.2	103.4	101.9
CY903F4	0.033	260	3.8	61700	2527	59077	3557	115.5	104.7	102.5

Table 5.2-a Test matrix for the cyclic venting mode ($\dot{m}_{msl} = 0.04$ kg/Sec)

Test No.	$\dot{m}_{msl}$ (kg/Sec)	Pressure kPa (psia)	PCCS inlet noncondensable gas mass fraction (%)	PCCS Pool water level (m)
CH830A	0.0415	220(32)	0.0	
CH826D2	0.0404	220(32)	1.6	
CH826D4	0.0396	220(32)	3.2	
CH826E4	0.0413	240(35)	3.0	0.92
CH621C	0.0391	260(38)	0.0	
CH828F4	0.0424	260(38)	3.0	

Table 5.2-b Summary of the cyclic venting mode tests data ($\dot{m}_{msl}$ = 0.04 kg/Sec)

Test No.	$\dot{m}_{msl}$ (kg/Sec)	Pressure (kPa)	NC Gas (%)	Q_{con} (W)	$\overline{U}$ (W/m²K)	$\overline{h}_p$ (W/m²K)	$\overline{h}_c$ (W/m²K)	$\overline{T}_s$ (°C)	$\overline{T}_w$ (°C)	$\overline{T}_p$ (°C)
CH830A	0.0415	220	0.0	75759	2594	9772	5228	116.1	101.6	105.2
CH826D2	0.0404	220	1.6	73689	2456	14258	4115	116.5	104.0	102.1
CH826D4	0.0396	220	3.2	67210	2319	14186	3745	116.4	104.2	102.0
CH826E4	0.0413	240	3.0	74182	2302	16403	3587	118.2	104.3	102.2
CH621C	0.0391	240	0.0	84307	3012	27965	5001	116.1	103.6	102.2
CH826F4	0.0424	260	3.0	76771	2491	29708	3500	117.3	103.8	102.4

Table 5.3-a Test matrix for the cyclic venting mode with low PCCS pool level

Test No.	$\dot{m}_{msl}$ (kg/Sec)	Pressure kPa (psia)	PCCS inlet noncondensable gas mass fraction (%)	PCCS Pool water level (m)
CM701D	0.0309	220(32)	0.5	0.60
CM701D1	0.031	220(32)	1.1	
CM701D2	0.0296	220(32)	2.1	
CM810D4	0.0269	220(32)	4.6	
CM616E	0.0337	240(35)	0.3	
CM822E2	0.0299	240(35)	2.2	
CM707E4	0.0293	240(35)	4.2	
CM810E6	0.0269	240(35)	6.7	
CM616C	0.0310	260(38)	0.0	
CM822F2	0.0305	260(38)	2.1	

Table 5.3-b Summary of the cyclic venting mode tests data with low PCCS pool level

Test No.	$\dot{m}_{msl}$ (kg/Sec)	Pressure (kPa)	NC Gas (%)	Q_{con} (W)	$\overline{U}$ (W/m²K)	$\overline{h}_p$ (W/m²K)	$\overline{h}_c$ (W/m²K)	$\overline{T}_s$ (°C)	$\overline{T}_w$ (°C)	$\overline{T}_p$ (°C)
CM701D	0.0309	220	0.5	60255	3685	28946	7123	114.0	102.9	101.4
CM701D1	0.030	220	1.1	58011	3604	26065	6999	113.0	102.9	101.5
CM701D2	0.0296	220	2.1	54477	3028	19972	5413	114.8	103.3	101.4
CM810D4	0.0269	220	4.6	43274	2599	23187	4071	113.8	102.7	101.6
CM616E	0.0337	240	0.3	65508	3536	32593	6434	115.2	102.8	101.3
CM822E2	0.0299	240	2.2	53058	3136	28425	5340	114.2	102.9	101.6
CM707E4	0.0293	240	4.2	51800	2796	24054	4543	115.2	102.9	101.4
CM810E6	0.0269	240	6.7	44510	2005	36008	2712	114.6	102.2	101.4
CM616C	0.0310	260	0.0	64011	3612	26227	7015	114.8	103.3	101.6
CM822F2	0.0305	260	2.1	56305	3084	23070	5403	115.2	103.4	102.1
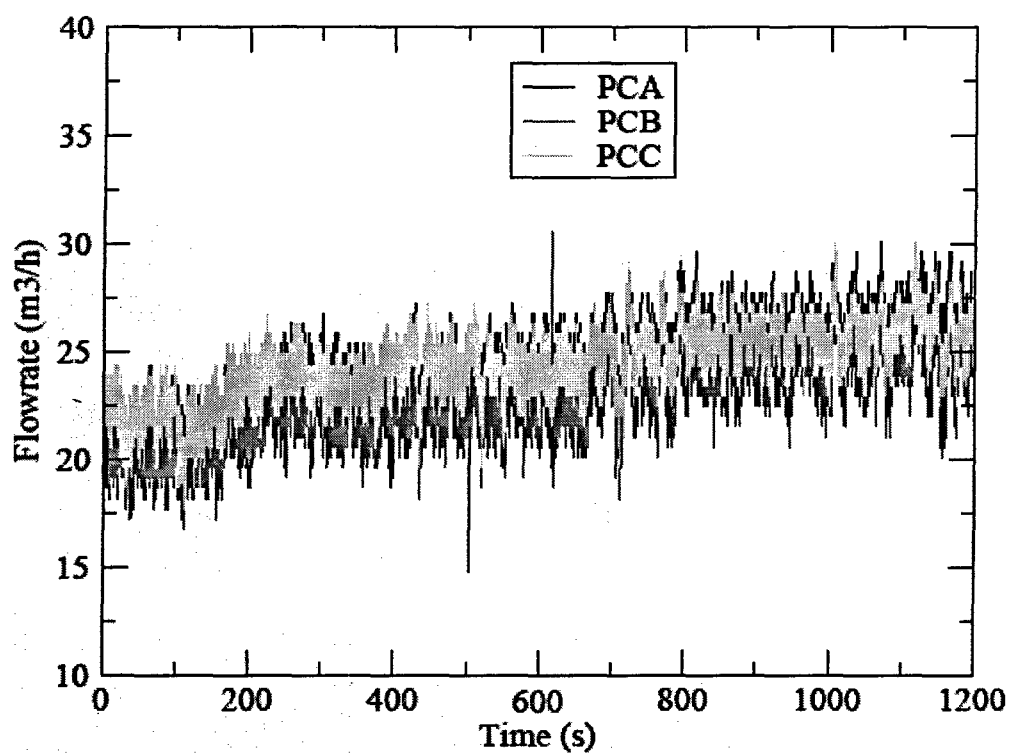
Figure 5.1 Steam Volumetric Flow Rates in PCCS Supply Lines from Vortex Flow Meter

PCCS Separate Effect Test

Test No.:	CY604E2
Mode:	Cyclic Venting
Pressure Setting:	240 kPa
Noncondensable Gas Concentration:	2%

Figure 5.2 Water Volumetric Flow Rates in PCCS Drain Lines

PCCS Separate Effect Test

Test No.:	CY604E2
Mode:	Cyclic Venting
Pressure Setting:	240 kPa
Noncondensable Gas Concentration:	2%

Figure 5.3 Water Level in the PCCS Pool

PCCS Separate Effect Test

Test No.:   CY604E2
Mode: Cyclic Venting
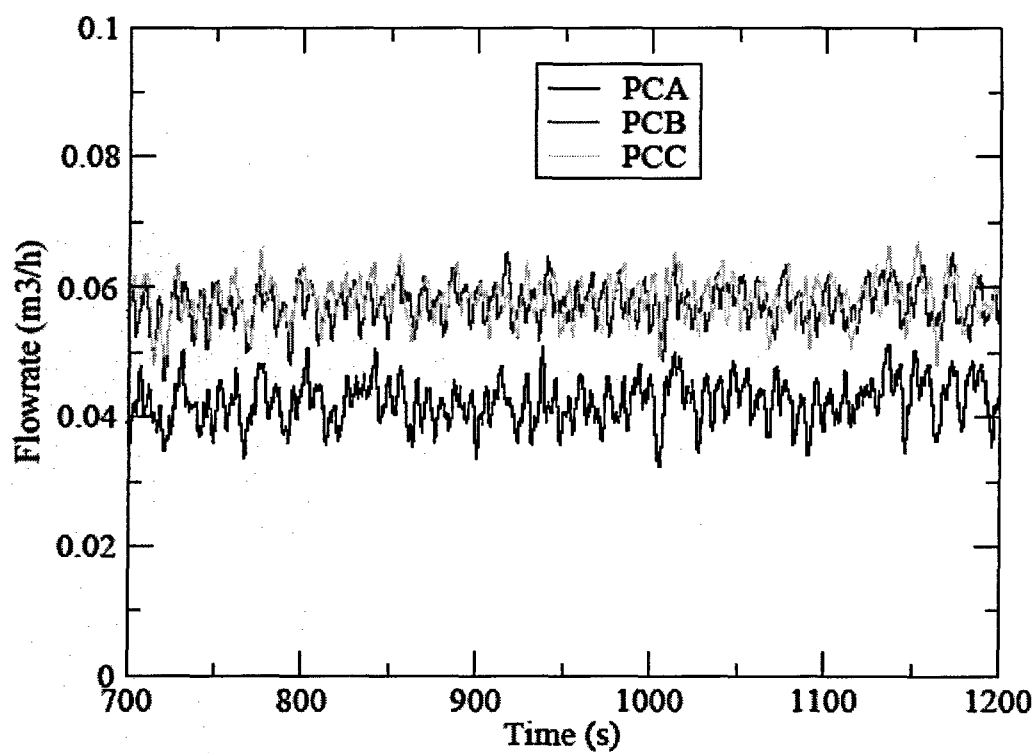Pressure Setting: 240 kPa
Noncondensable Gas Concentration: 2%

Figure 5.4 Water Level in the PCCS Drain Tank

PCCS Separate Effect Test

Test No.:	CY604E2
Mode:	Cyclic Venting
Pressure Setting:	240 kPa
Noncondensable Gas Concentration:	2%

Figure 5.5 Upper Drywell and Wetwell Gas Space Pressures

PCCS Separate Effect Test

Test No.:   CY604E2
Mode: Cyclic Venting
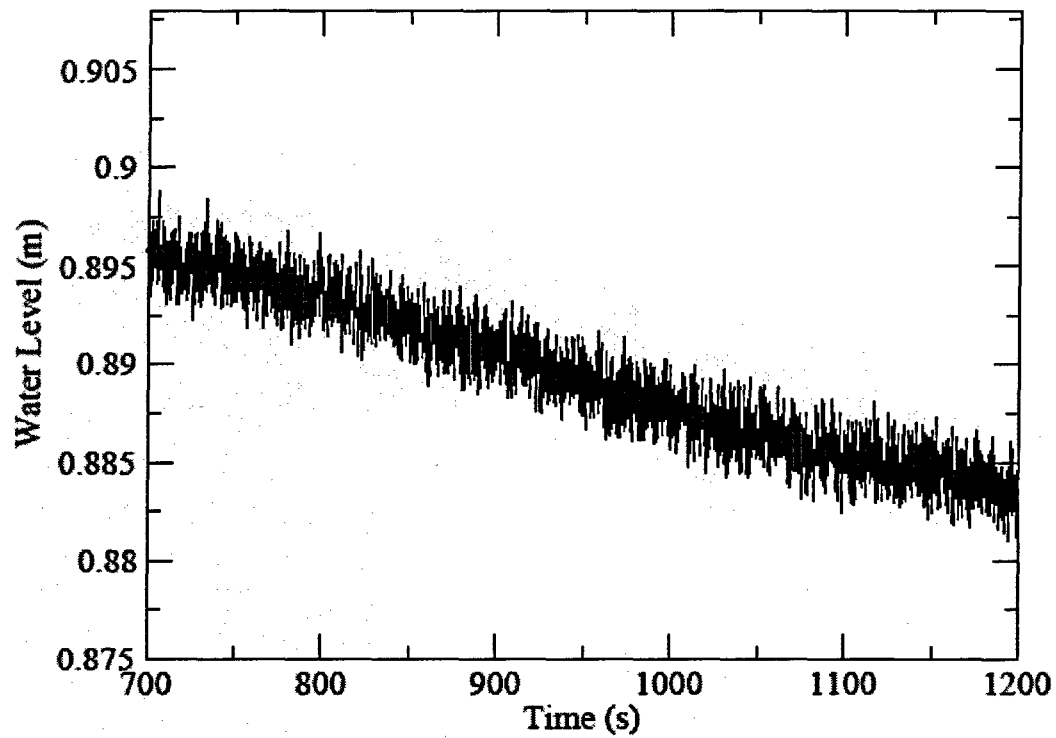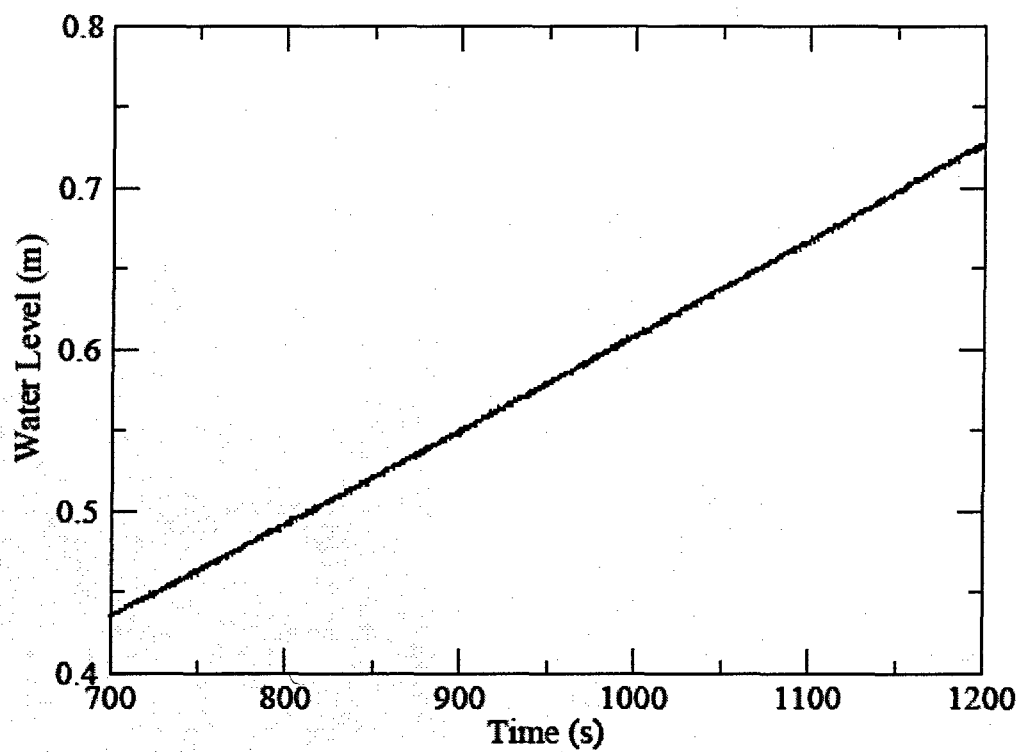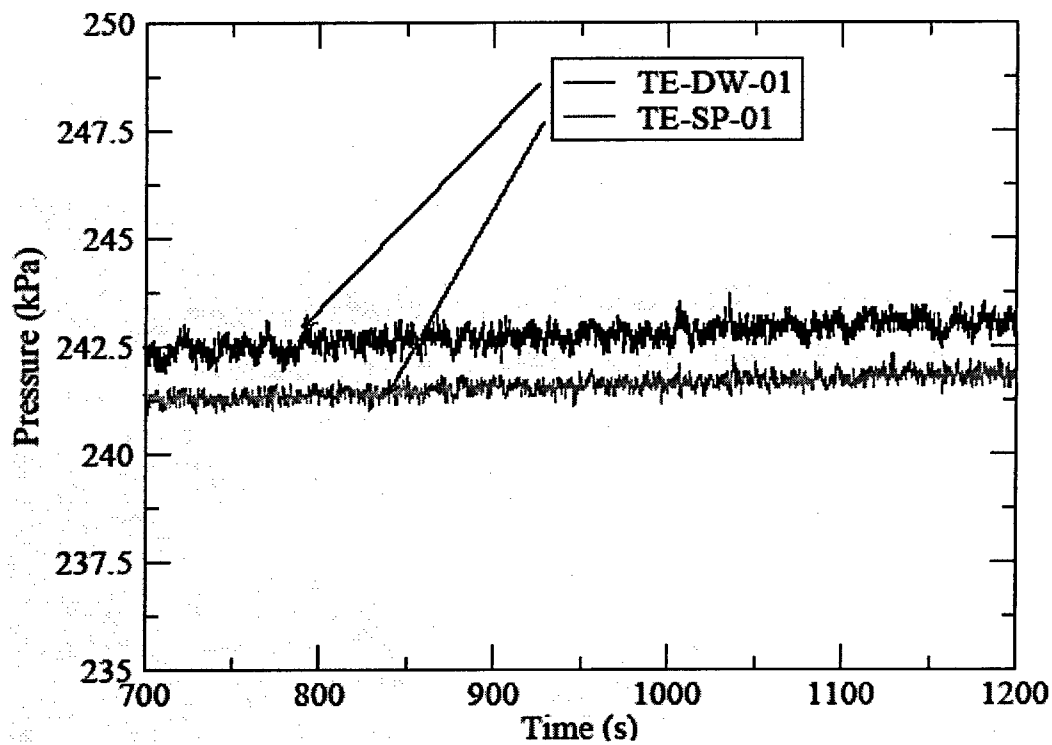Pressure Setting: 240 kPa
Noncondensable Gas Concentration: 2%

PT-DW-01: Upper drywell pressure
PT- SP -01: Wetwell pressure in gas space
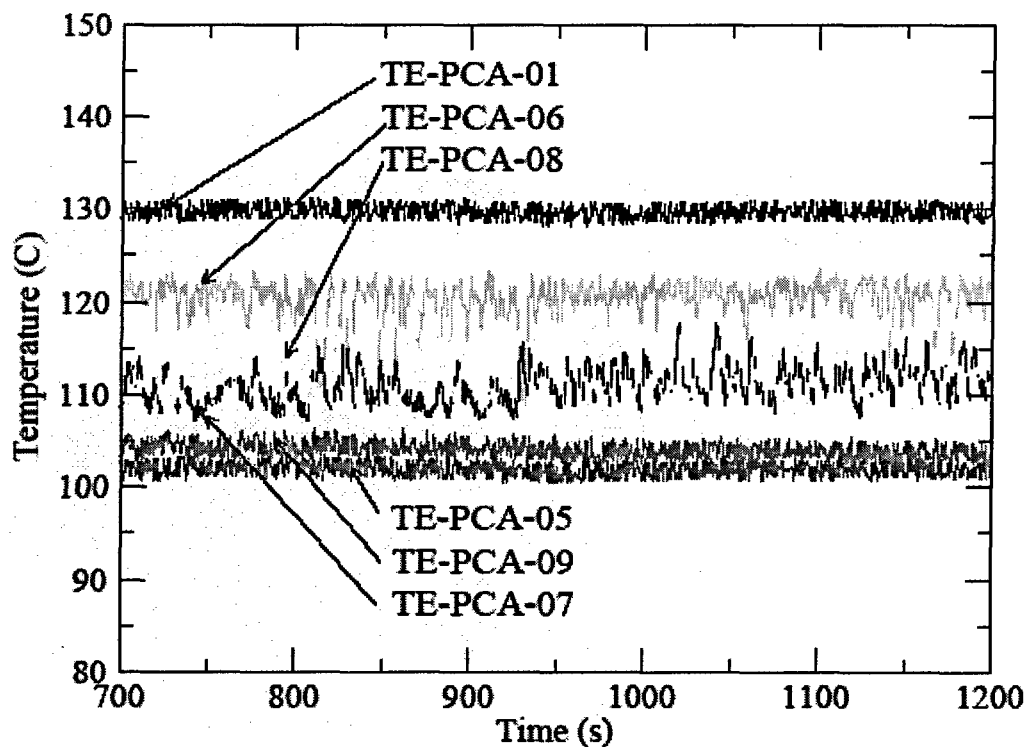
Figure 5.6 Temperatures in PCCS-A

PCCS Separate Effect Test

Test No.:	CY604E2
Mode:	Cyclic Venting
Pressure Setting:	240 kPa
Noncondensable Gas Concentration:	2%

TE-PCA-01:	Temperature of steam in PCCS supply line A
TE-PCA-05:	Temperature of water in PCCS pool A (z=254)
TE-PCA-06:	Temperature of condenser tube centerline in PCCS-A (z=745)
TE-PCA-07:	Temperature of condenser tube centerline in PCCS-A (z=580)
TE-PCA-08:	Temperature of condenser tube centerline in PCCS-A (z=415)
TE-PCA-09:	Temperature of condenser tube surface in PCCS-A (z=745)

Figure 5.7 Temperatures in PCCS-B

PCCS Separate Effect Test

Test No.:	CY604E2
Mode:	Cyclic Venting
Pressure Setting:	240 kPa
Noncondensable Gas Concentration:	2%

TE-PCB-01:   Temperature of steam in PCCS supply line B
TE-PCB-05:   Temperature of water in PCCS pool B (z=254)
TE-PCB-06:   Temperature of condenser tube centerline in PCCS-B (z=745)
TE-PCB-07:   Temperature of condenser tube centerline in PCCS-B (z=580)
TE-PCB-08:   Temperature of condenser tube centerline in PCCS-B (z=415)
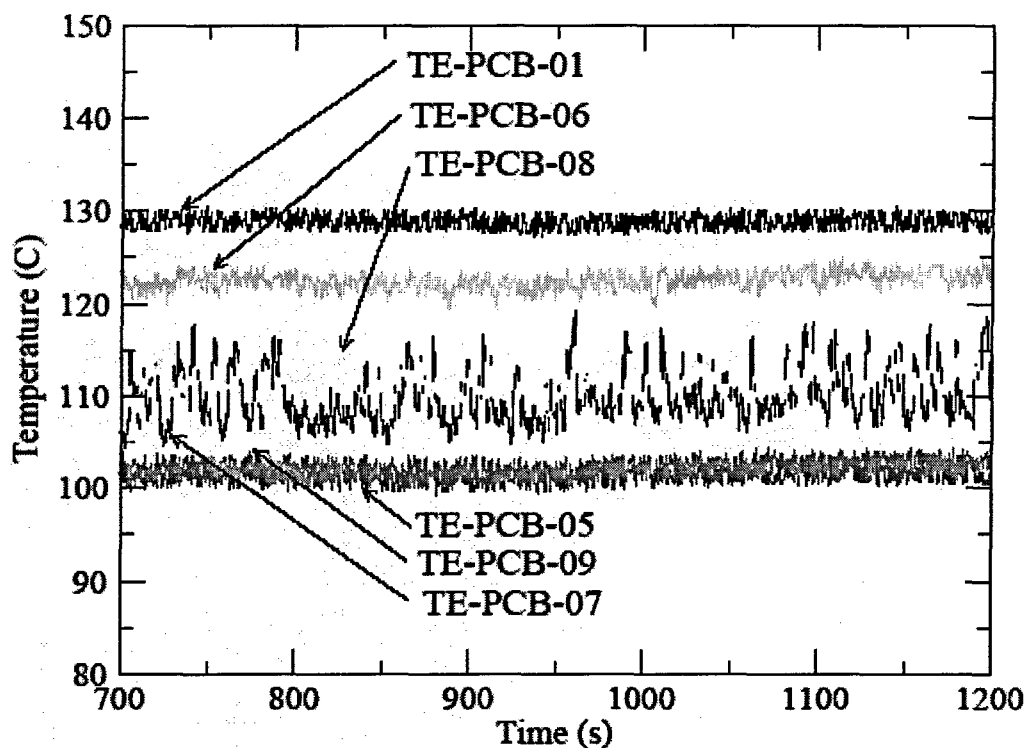TE-PCB-09:   Temperature of condenser tube surface in PCCS-B (z=745)
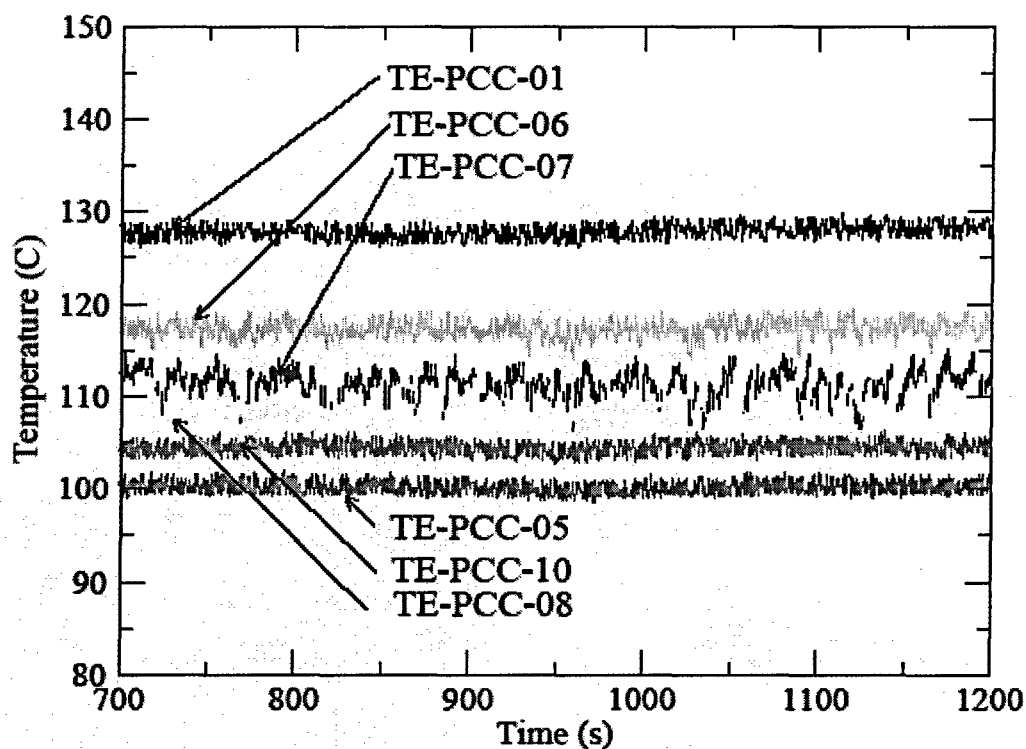
Figure 5.8 Temperatures in PCCS-C

PCCS Separate Effect Test

Test No.:	CY604E2
Mode:	Cyclic Venting
Pressure Setting:	240 kPa
Noncondensable Gas Concentration:	2%

TE-PCC-01:	Temperature of steam in PCCS supply line C
TE-PCC-05:	Temperature of water in PCCS pool C (z=254)
TE-PCC-06:	Temperature of condenser tube centerline in PCCS-C (z=745)
TE-PCC-07:	Temperature of condenser tube centerline in PCCS-C (z=580)
TE-PCC-08:	Temperature of condenser tube centerline in PCCS-C (z=415)
TE-PCC-10:	Temperature of condenser tube surface in PCCS-B (z=580)

5-19
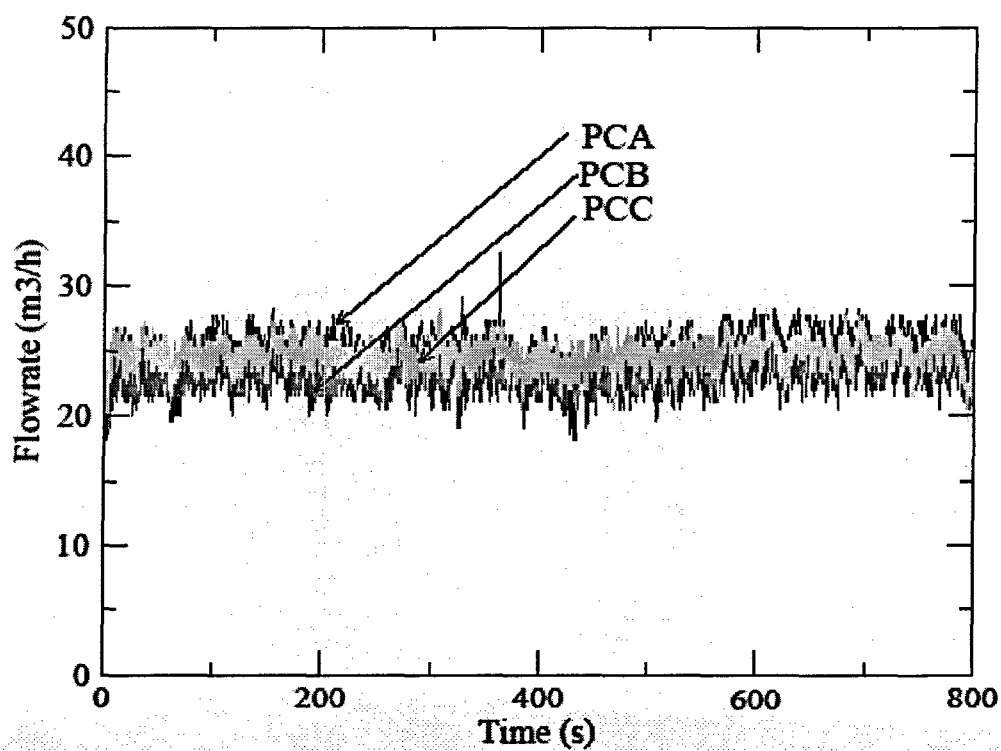
Figure 5.9 Steam Volumetric Flow Rates in PCCS Supply Lines from Vortex Flow Meter

PCCS Separate Effect Test

Test No.:	CM701D
Mode:	Cyclic venting with low pool level
Pressure Setting:	220 kPa
Noncondensable Gas Concentration:	0.3 %

5-20

Figure 5.10 Water Volumetric Flow Rates in PCCS Drain Lines

PCCS Separate Effect Test

Test No.:   CM701D
Mode: Cyclic venting with low pool level
Pressure Setting: 220 kPa
Noncondensable Gas Concentration: 0.3 %

Figure 5.11 Water Level in the PCCS Pool

PCCS Separate Effect Test

Test No.:	CM701D
Mode:	Cyclic venting with low pool level
Pressure Setting:	220 kPa
Noncondensable Gas Concentration:	0.3 %

Figure 5.12 Water Level in the PCCS Drain Tank

PCCS Separate Effect Test

Test No.:   CM701D
Mode: Cyclic venting with low pool level
Pressure Setting: 220 kPa
Noncondensable Gas Concentration: 0.3 %
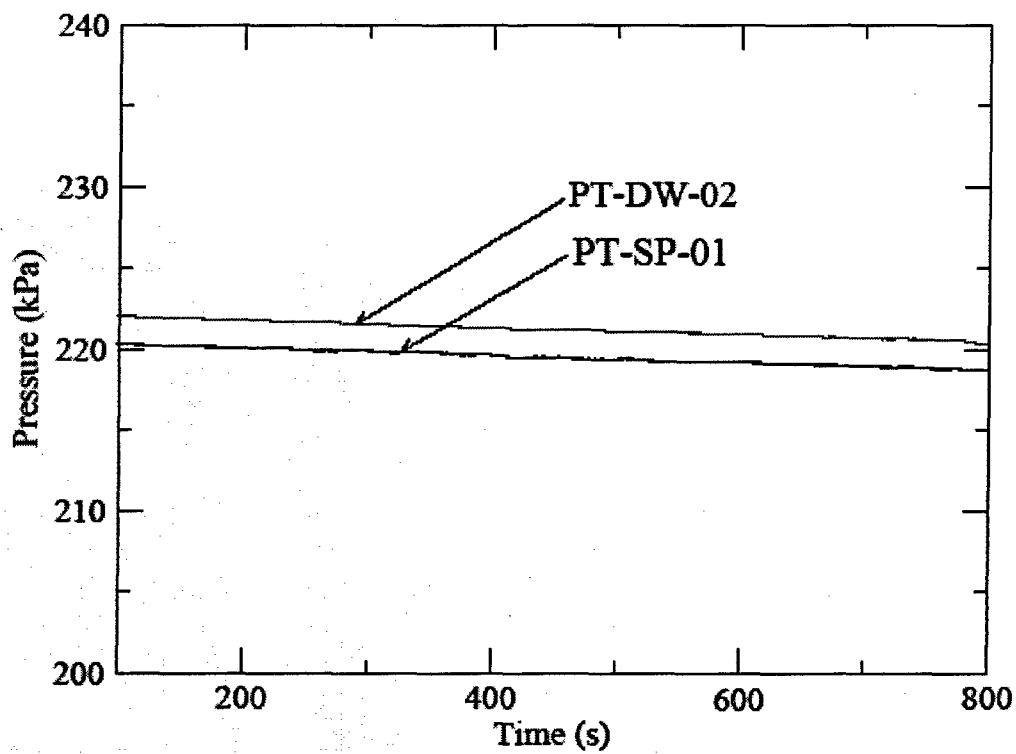
Figure 5.13 Upper Drywell and Wetwell Gas Space Pressures

PCCS Separate Effect Test

Test No.:   CM701D
Mode: Cyclic venting with low pool level
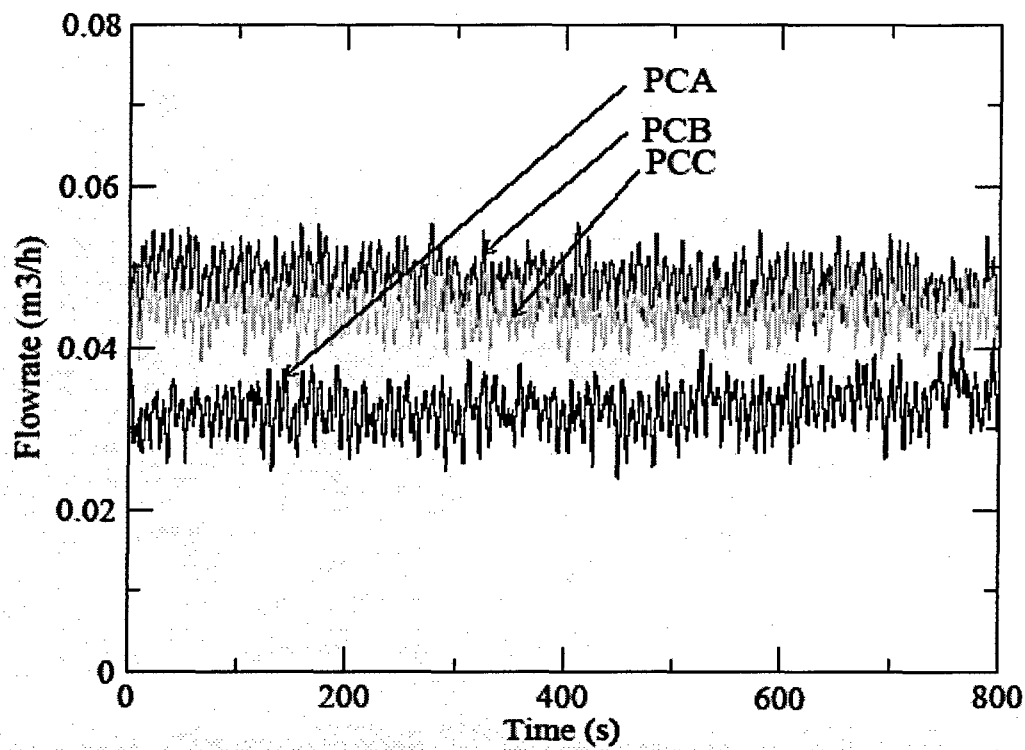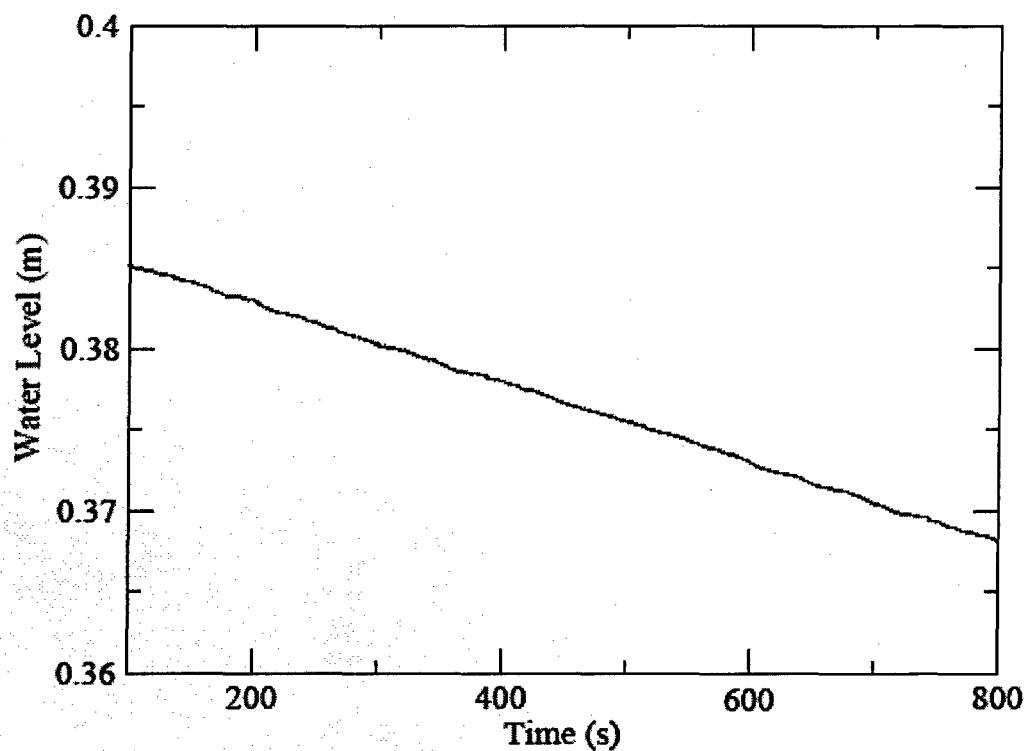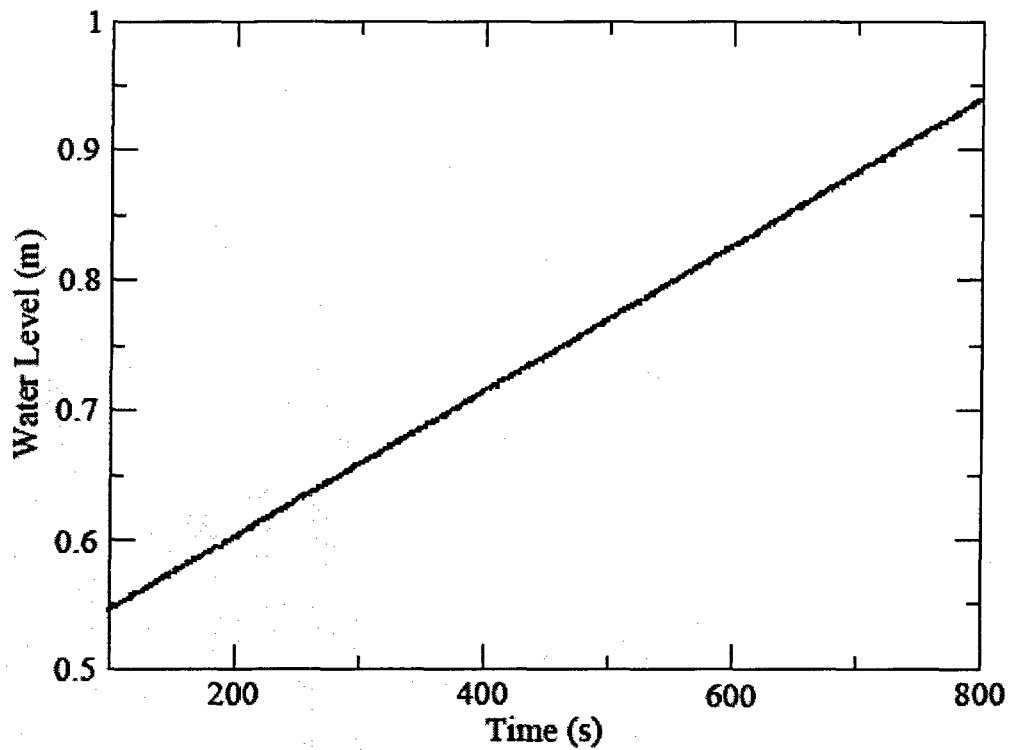Pressure Setting: 220 kPa
Noncondensable Gas Concentration: 0.3 %

PT-DW-01: Upper drywell pressure
PT- SP -01: Wetwell pressure in gas space
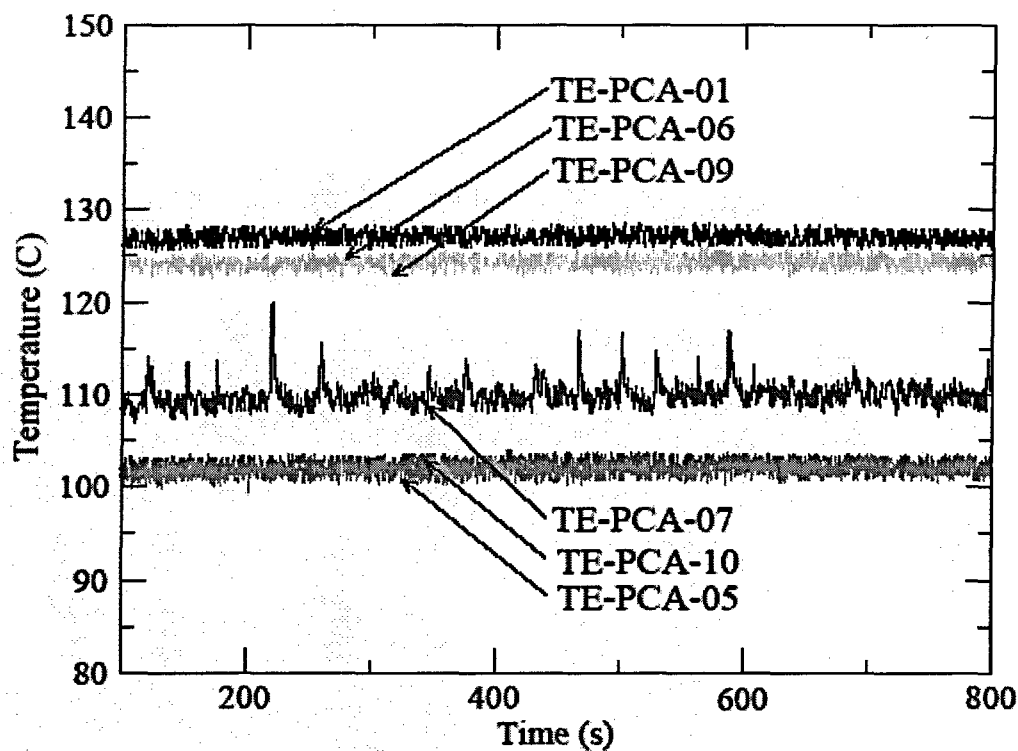
Figure 5.14 Temperatures in PCCS-A

PCCS Separate Effect Test

Test No.:	CM701D
Mode:	Cyclic venting with low pool level
Pressure Setting:	220 kPa
Noncondensable Gas Concentration:	0.3 %

TE-PCA-01:	Temperature of steam in PCCS supply line A
TE-PCA-05:	Temperature of water in PCCS pool A ($z=254$)
TE-PCA-06:	Temperature of condenser tube centerline in PCCS-A ($z=745$)
TE-PCA-07:	Temperature of condenser tube centerline in PCCS-A ($z=580$)
TE-PCA-09:	Temperature of condenser tube surface in PCCS-A ($z=745$)
TE-PCA-10:	Temperature of condenser tube surface in PCCS-A ($z=580$)

Figure 5.15 Temperatures in PCCS-B

PCCS Separate Effect Test

Test No.:	CM701D
Mode:	Cyclic venting with low pool level
Pressure Setting:	220 kPa
Noncondensable Gas Concentration:	0.3 %

TE-PCA-01:	Temperature of steam in PCCS supply line A
TE-PCA-05:	Temperature of water in PCCS pool A (z=254)
TE-PCA-06:	Temperature of condenser tube centerline in PCCS-A (z=745)
TE-PCA-07:	Temperature of condenser tube centerline in PCCS-A (z=580)
TE-PCA-09:	Temperature of condenser tube surface in PCCS-A (z=745)
TE-PCA-10:	Temperature of condenser tube surface in PCCS-A (z=580)

Figure 5.16 Temperatures in PCCS-C

PCCS Separate Effect Test

Test No.:	CM701D
Mode:	Cyclic venting with low pool level
Pressure Setting:	220 kPa
Noncondensable Gas Concentration:	0.3 %

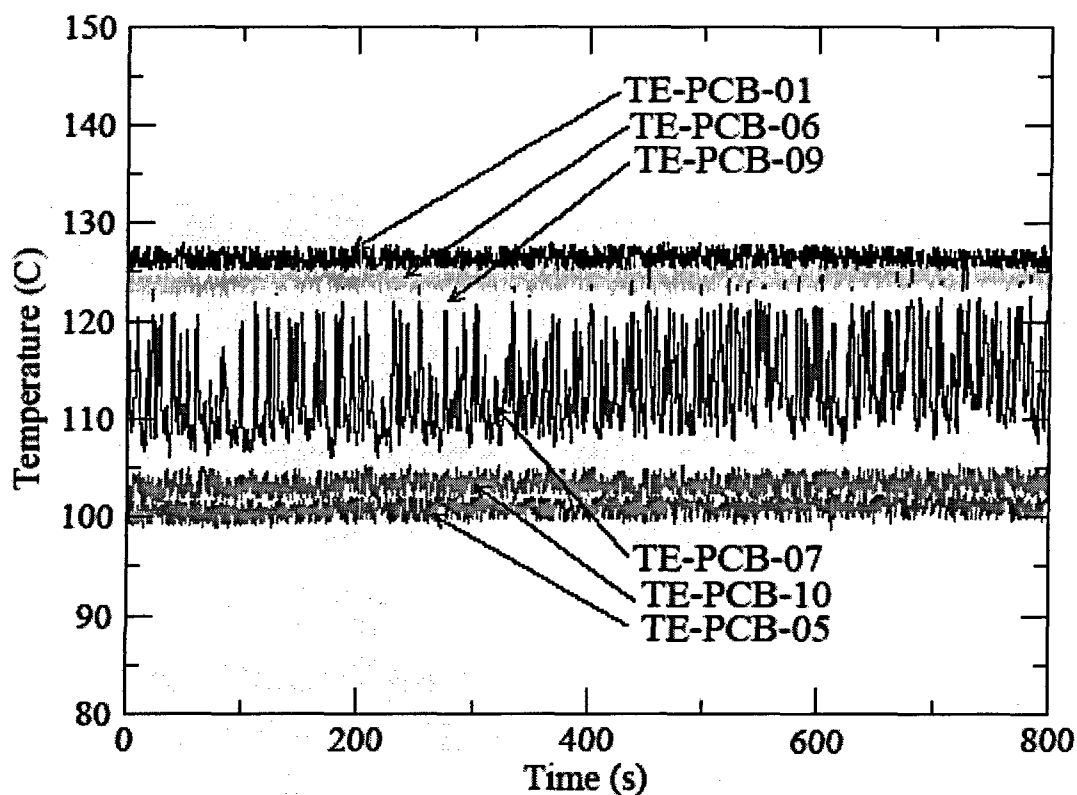|	
TE-PCA-01:	Temperature of steam in PCCS supply line A
TE-PCA-05:	Temperature of water in PCCS pool A (z=254)
TE-PCA-06:	Temperature of condenser tube centerline in PCCS-A (z=745)
TE-PCA-07:	Temperature of condenser tube centerline in PCCS-A (z=580)
TE-PCA-09:	Temperature of condenser tube surface in PCCS-A (z=745)
TE-PCA-10:	Temperature of condenser tube surface in PCCS-A (z=580)

5-27
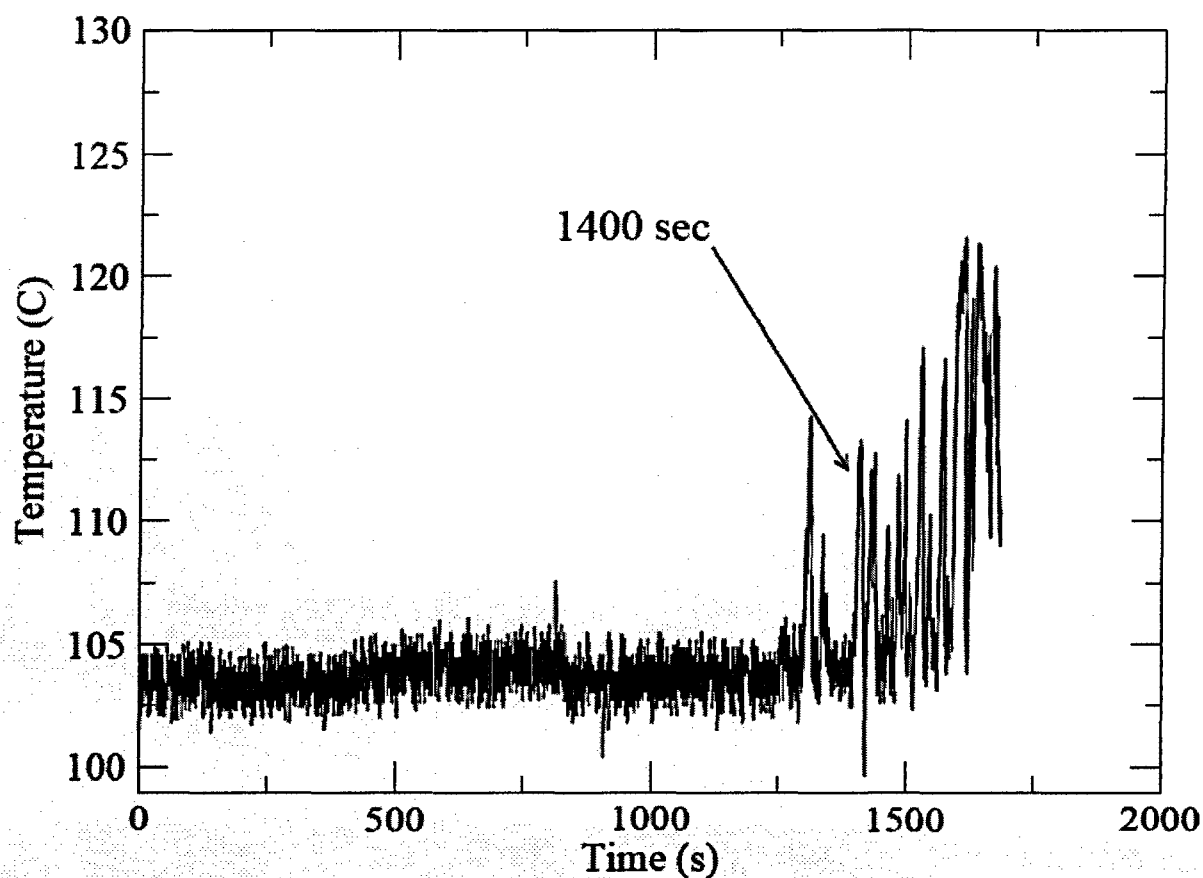
Figure 5.17 Temperatures of condenser tube surface

PCCS Separate Effect Test

Test No.:   LM918TR
Mode: Long time cooling with low pool level
Pressure Setting: 225 kPa
Noncondensable Gas Concentration: 0 %

TE-PCA-10:   Temperature of condenser tube surface in PCCS-A (z=580)
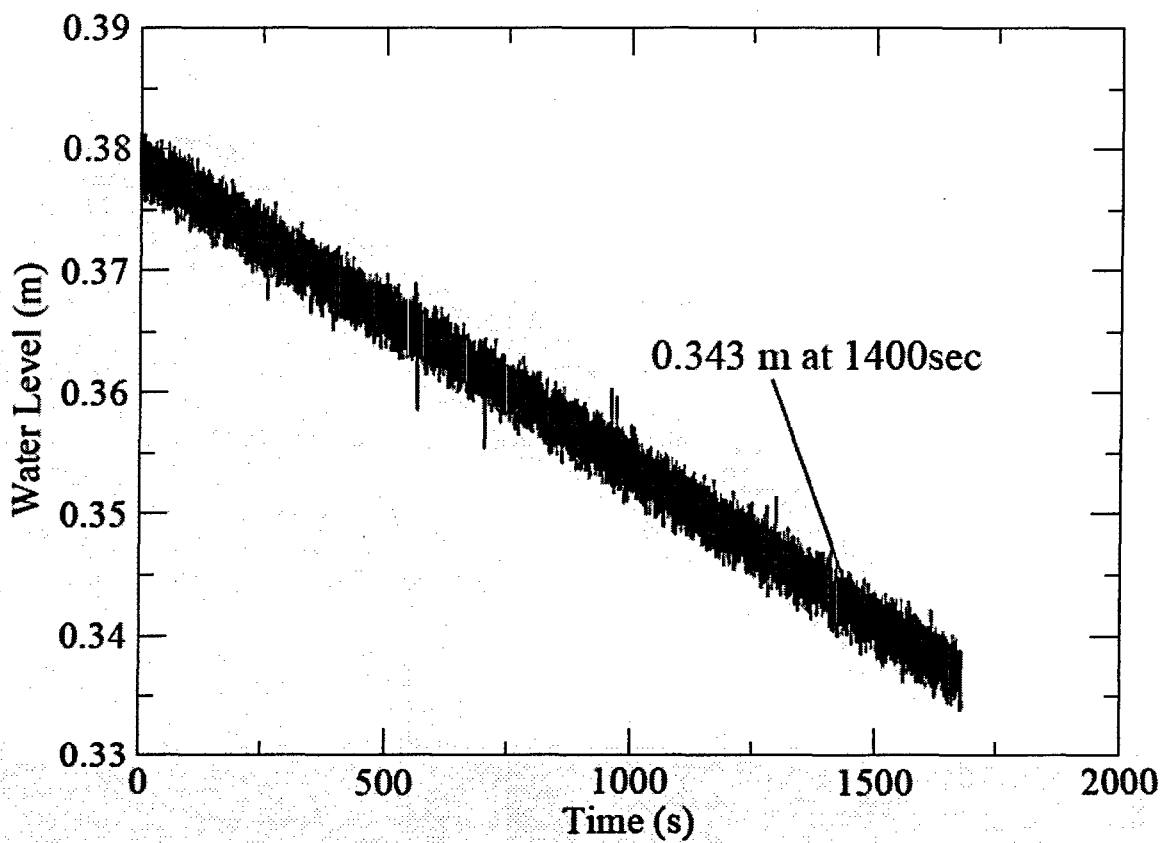
Figure 5.18 Water level in PCCS tank

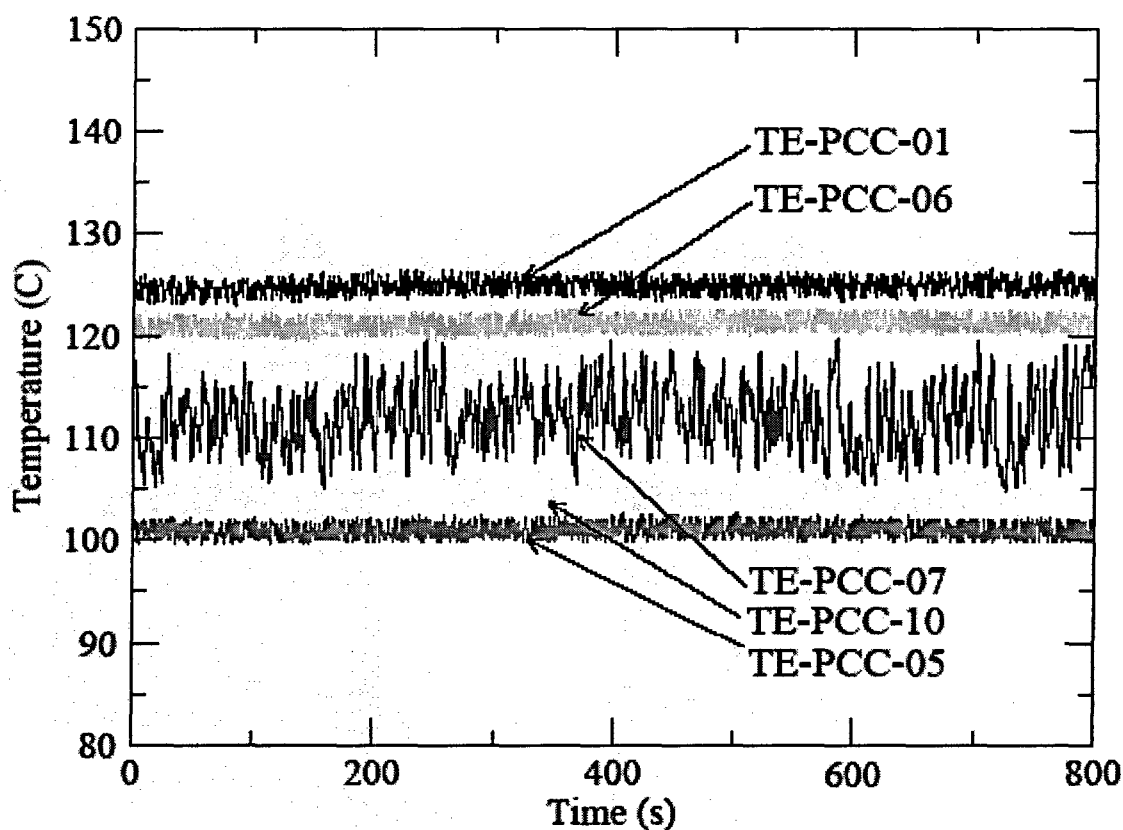PCCS Separate Effect Test

Test No.:   LM918TR
Mode: Long time cooling with low pool level
Pressure Setting: 225 kPa
Noncondensable Gas Concentration: 0 %
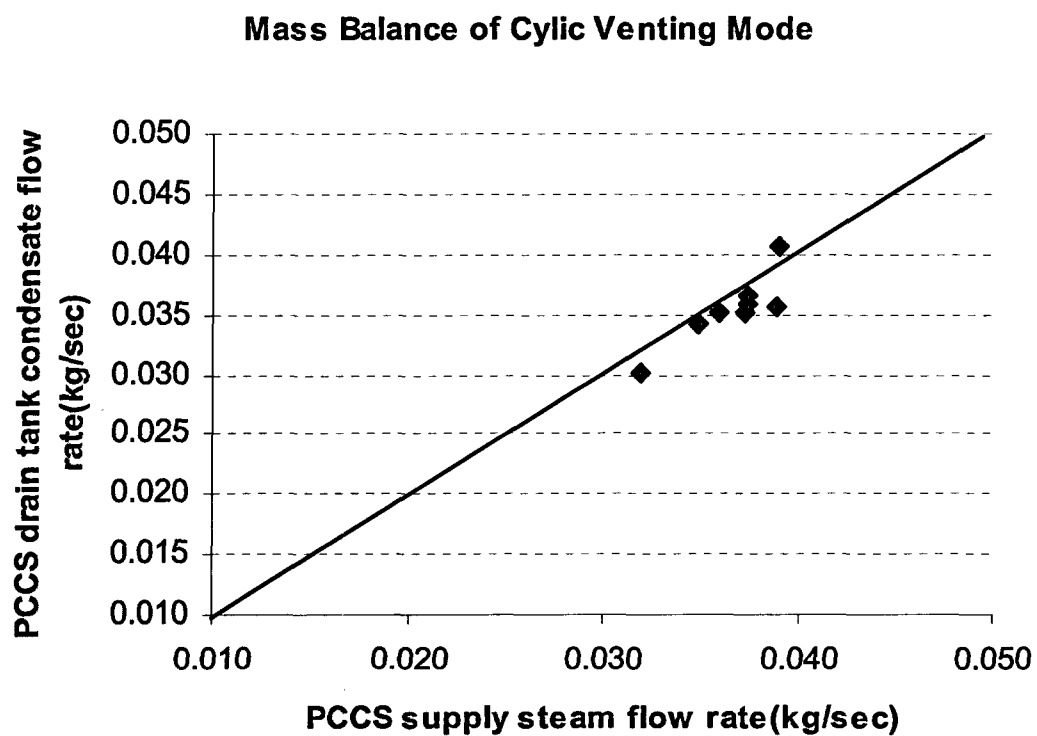
Figure 5.19 Comparison of Steam Inlet Flow Rate Measured with PCCS supply line Vortex
Flow Meter and Mass Flow Rate Measured by PCCS Drain Tank Water Level Change

Energy Balance of Cylic Venting Mode
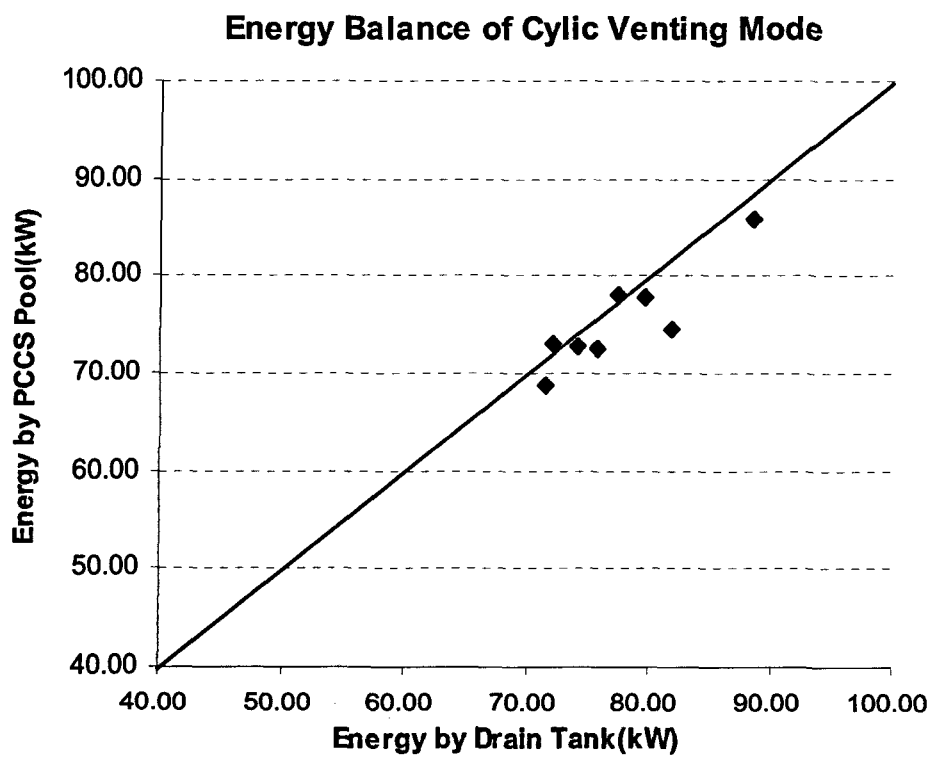
Figure 5.20 Comparison of Energy Measured with PCCS Drain Tank and Energy Measured with PCCS pool

Heat Removal Rate (kw)

◆ Pure steam ■ NC 2% ▲ NC 4%
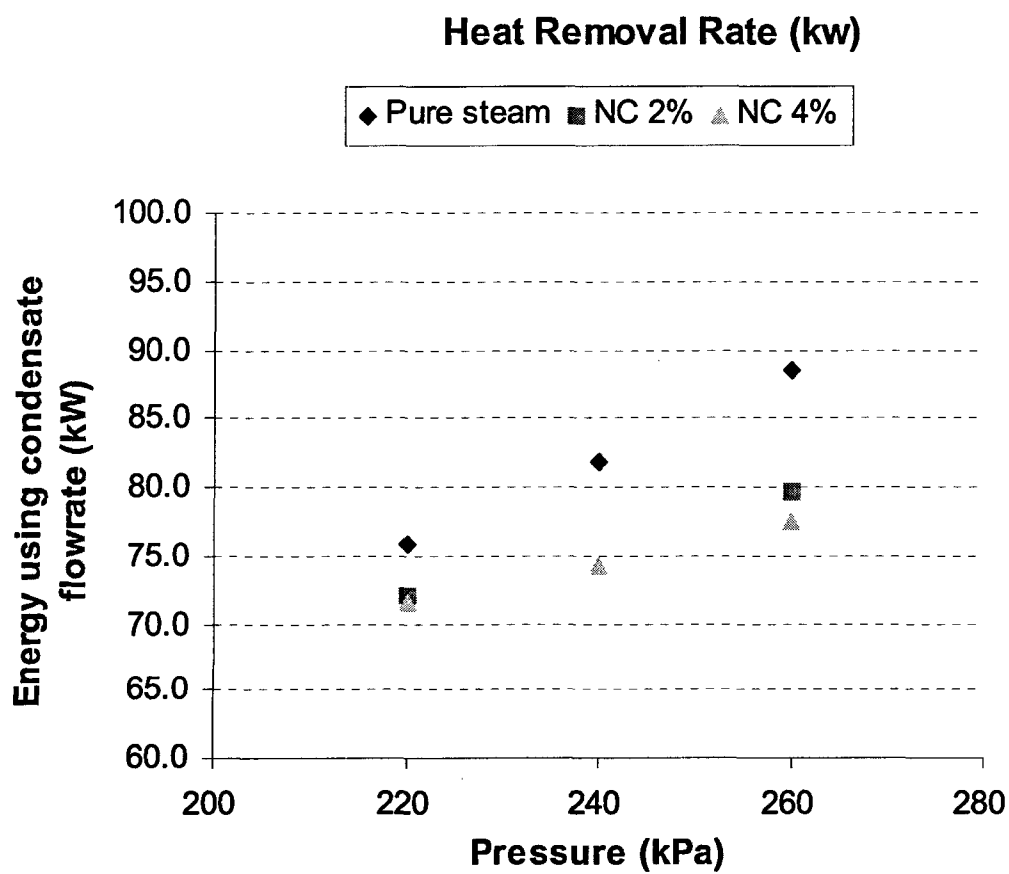
Figure 5.21 PCCS Heat Transfer Rate Dependency on the Pressure
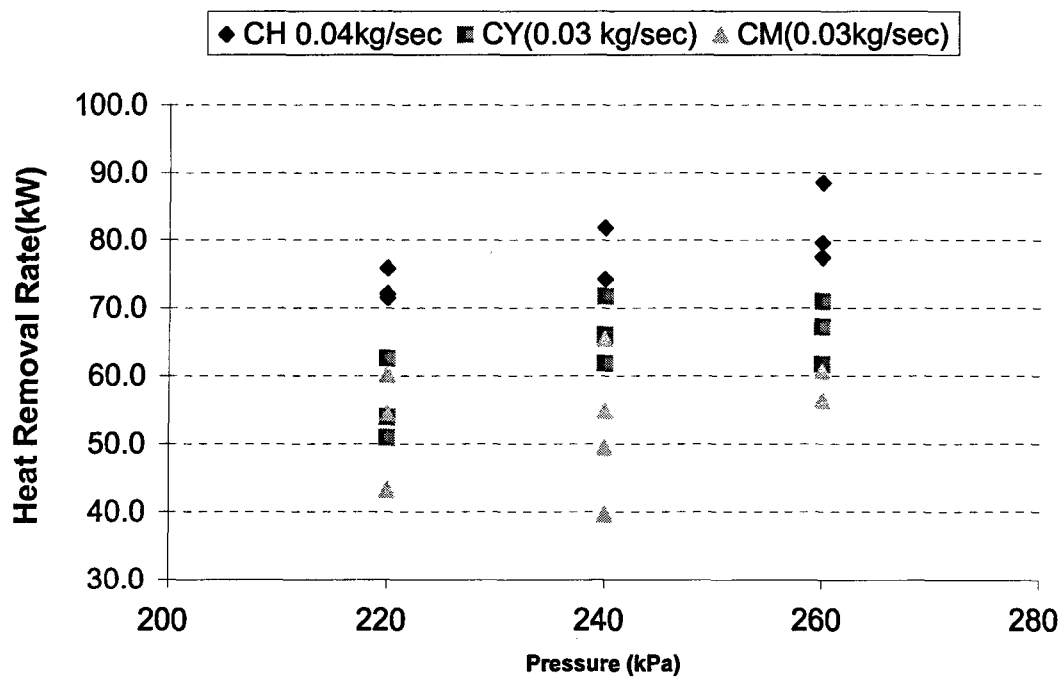
Figure 5.22 PCCS Heat Removal Rate Comparison according to the Pressure

CY-0.03kg/sec

| ◆ Long Term | ■ NC gas 0.3% | ▲ NC gas 2% |
| ✖ NC gas 4% | ✱ Khun(NC 0.3%) | ● Khun(NC 2 %) |
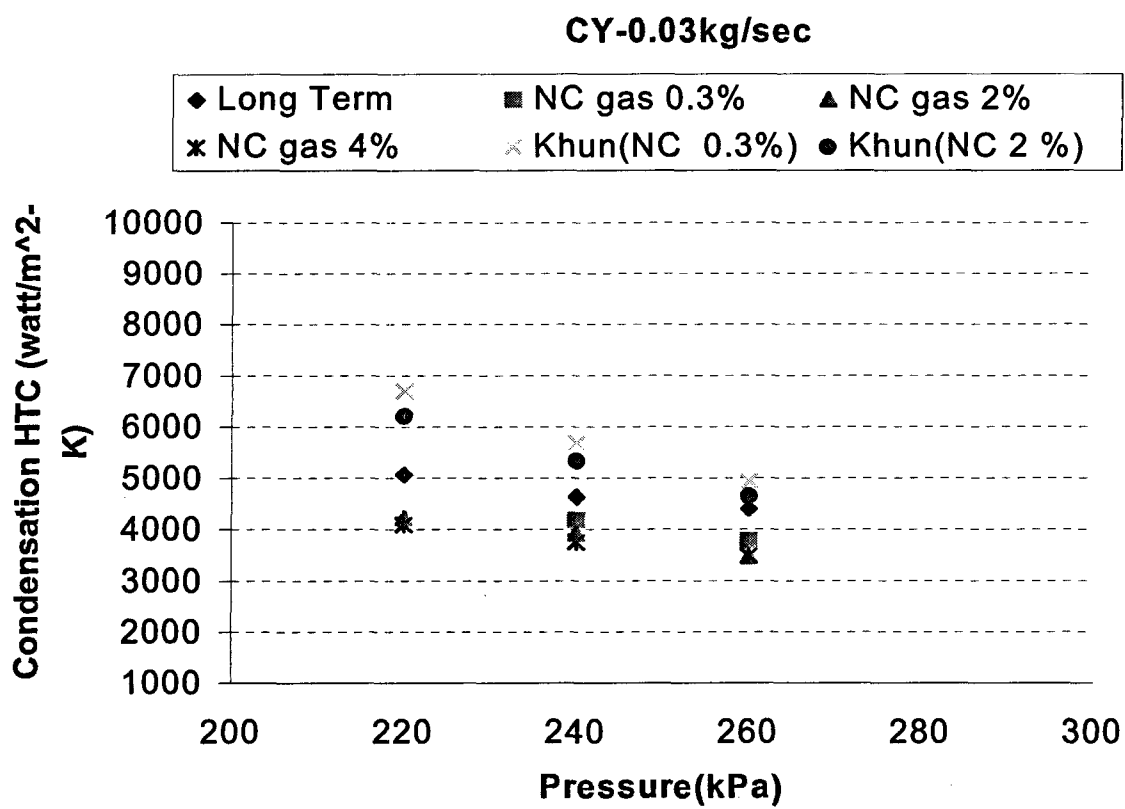
Figure 5.23 PCCS Condensation Heat Transfer Coefficient Dependency on the Pressure
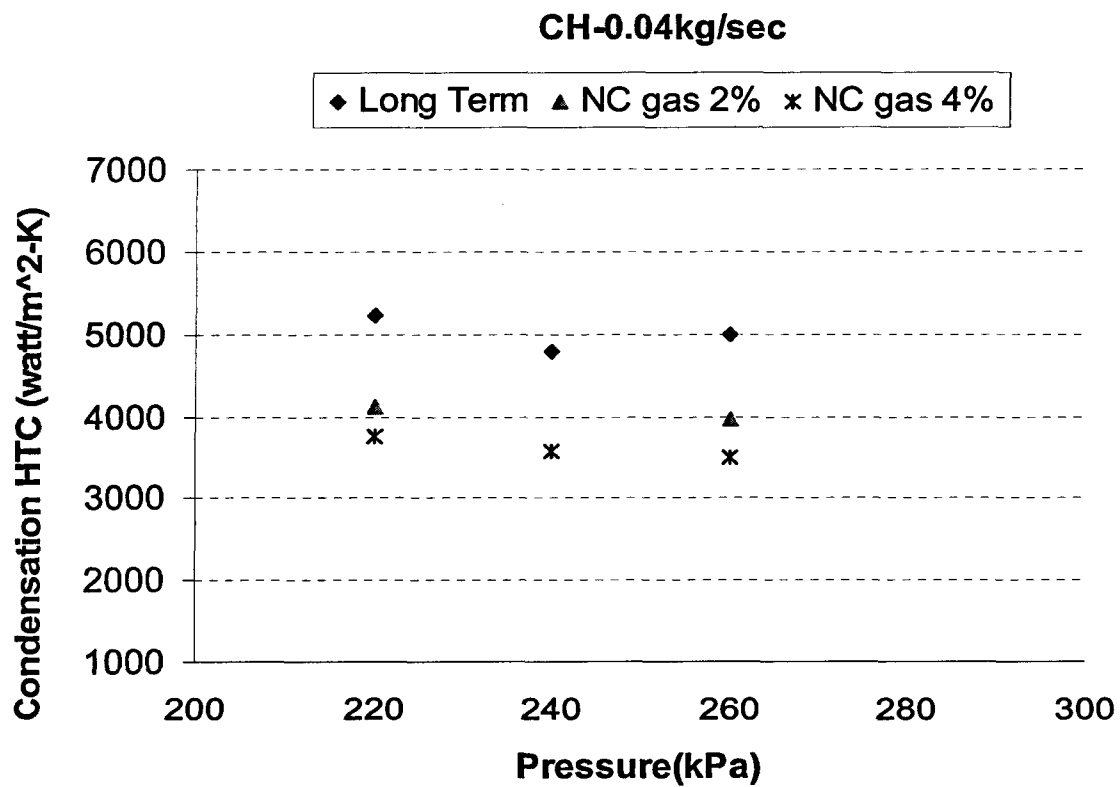
Figure 5.24 PCCS Condensation Heat Transfer Coefficient Dependency on the Pressure

CM(0.033kg/sec)

◆ NC 0.3% ■ NC 2% ▲ NC 4% ● NC 6%
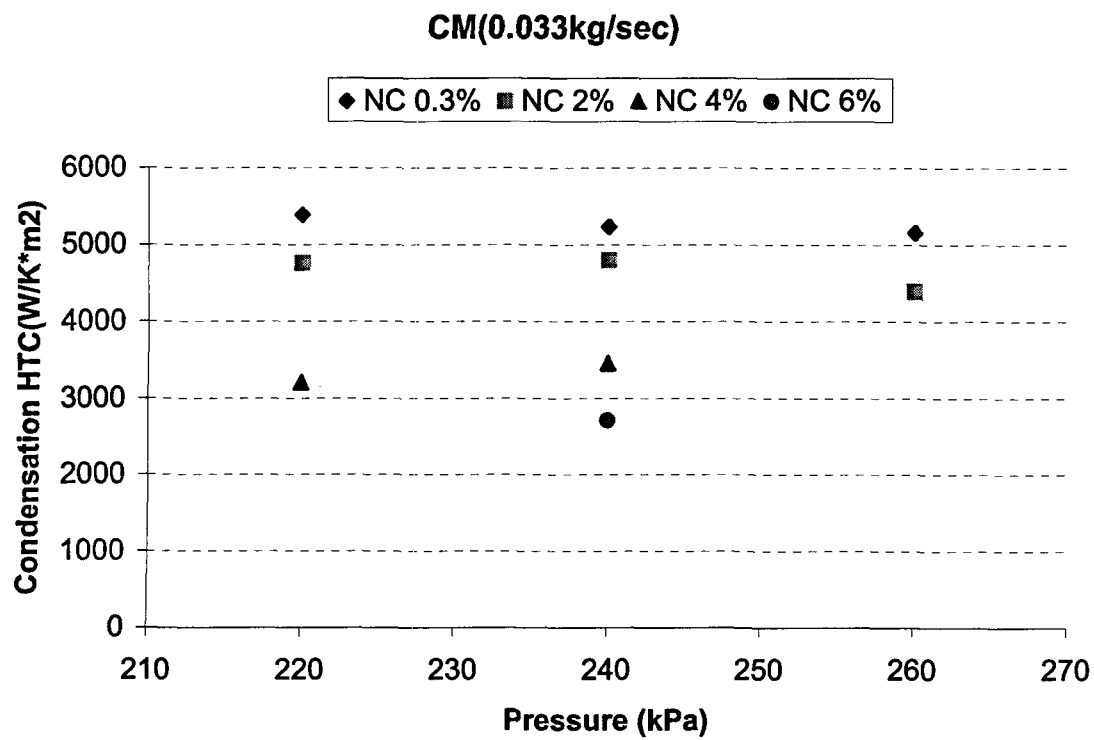
Figure 5.25 PCCS Condensation Heat Transfer Coefficient Dependency on the Pressure

5-36
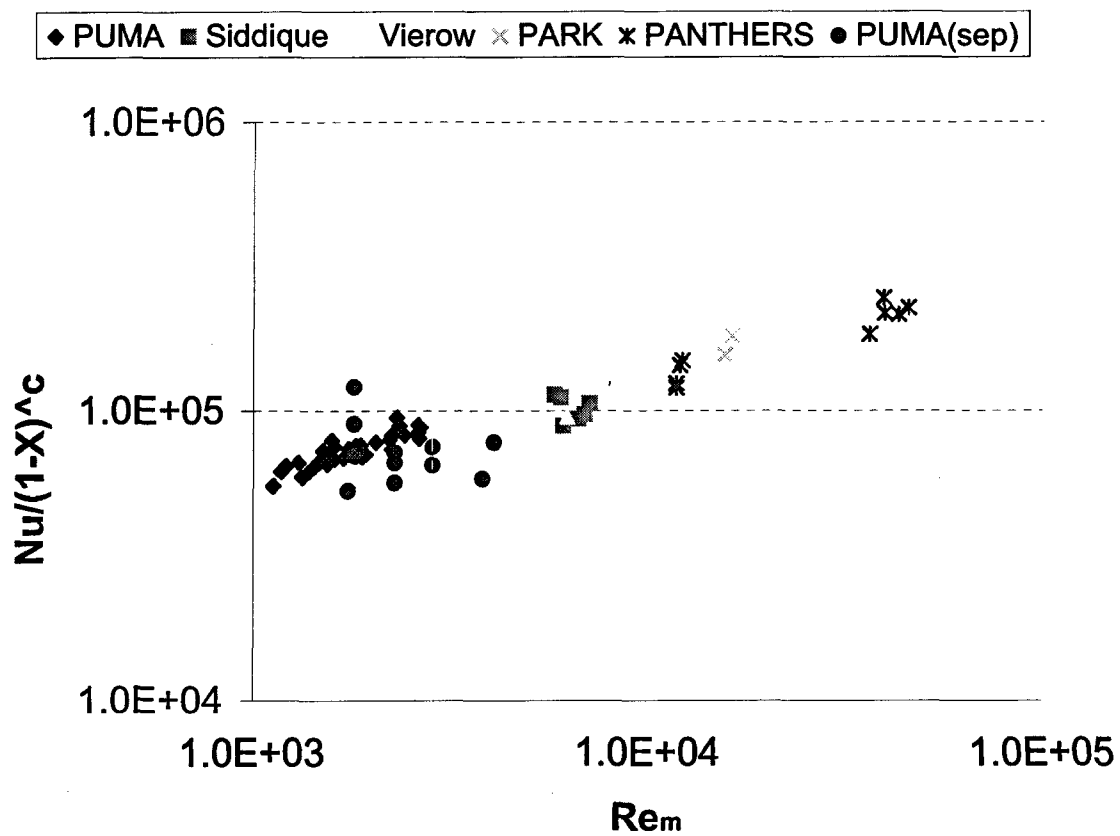
Figure 5.26 Data Comparison

Venting Period according to pure steam flow rate
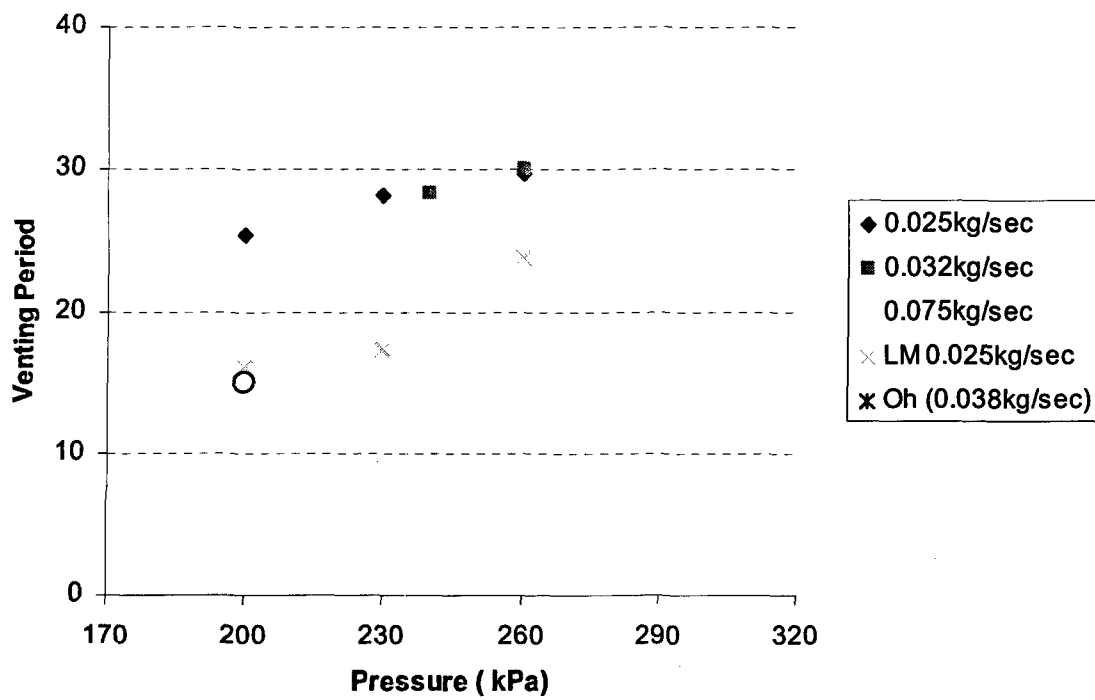
Figure 5.27 Venting Period for long term cooling mode
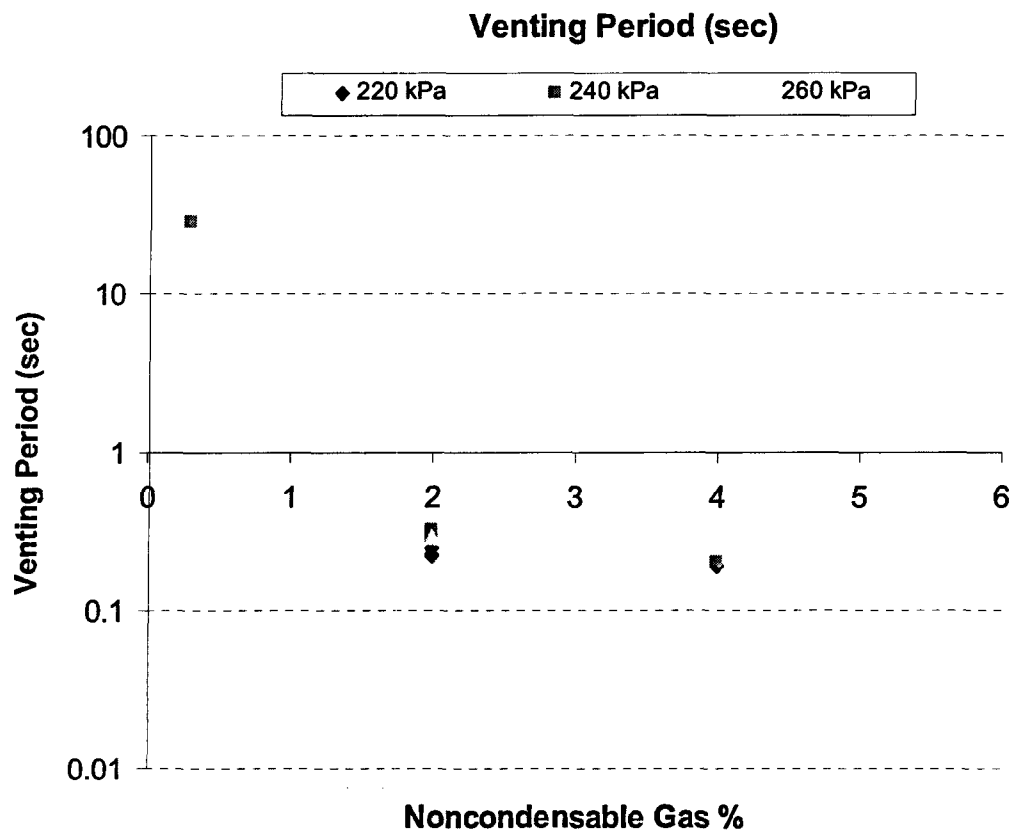
Figure 5.28 Venting Period with Respect to NC Gas

6. SUMMARY AND CONCLUSIONS

A total of 42 experiments have been conducted on the PCCS to study the heat exchanger capabilities. These tests were carried out to confirm the performance in the bypass modes, cyclic venting modes and long-term cooling modes. Three parallel PCCS loops were used in the test. To check the data quality, mass and energy conservation of the system was evaluated by using the inlet steam flow rates from the RPV to the drywell measured by vortex flow meters and the condensation water flow rate measured by magnetic flow meter and water level changes in the PCCS drain tank.

For the long-term cooling mode, the test control parameters are the drywell pressure and the PCCS pool water level. The experiments were conducted with less than 1% noncondensable gas concentration. The experimental data show the effects of the drywell pressure and the water level of the PCCS pool. As the pressure increases, the average condensate heat removal rates also increase while the tube average condensation heat transfer coefficients decrease. To confirm the experimental data, comparisons with the PUMA data of Leonardi (2000) were carried out and similar results were seen.

For the bypass mode, the experimental results demonstrate the effects of the drywell pressure and noncondensable gas concentration. The average heat removal rate increases as the drywell pressure increases while condensate heat transfer coefficients decrease as the pressure increases. Results show the reduction of the average heat transfer coefficient as the noncondensable gas concentrations increase in the PCCS.

For cyclic venting mode, a wide range of tests was performed with the parameters of pressure, steam flow rate, PCCS pool inventory and noncondensable gas concentrations. In addition to that, the venting frequency was measured using a high speed camera and digital camcorder by recording the exit of the PCCS venting line C. The parameter effect on the heat transfer rate and heat transfer coefficients are same as the long term and bypass mode.

To further validate the experimental data, combined correlated data results were compared with experimental data. The comparison data sets are composed of data of Vierow (1990), Siddique et al. (1992), Khun(1995), Park (1999), Leonardi (2000), and PANTHERS data. The comparison results showed that cyclic venting mode data and bypass mode data with continuous

venting both follow the same trends as other research results. This is clearly seen showing that the PUMA separate effect test and PANTHERS data fall on the same heat transfer coefficient trend line.

7. REFERENCES

1. Nusselt, W. "Die Oberflachenkondensation des Wasser Dampfes," Zeitschr. Ver. Deut. Ing.,60, 541(1916)

2. Vierow, K. M. and V. E. Schrock. "Condensation in a Natural Circulation Loop with Noncondensable Gases": Part I – Heat Transfer. In Proc. Of the Int. Conf. on Multiphase Flows '91, p. 183-186. (1991)

3. Siddique, M., M. W. Golay, and M. S. Kazimi. "Local Heat Transfer Coefficients for Forced-Convection of Steam in a Vertical Tube in the Presence of a Noncondensable Gas". Nuclear technology 102, 386-402. (1993)

4. Kuhn, S. Z. "Investigation of Heat Transfer fro Condensing Steam-Gas Mixtures and Turbulent Films Flowing Downward Inside a Vertical Tube". Ph.d. thesis, U.C.B. (1995)

5. Ishii, M., Revankar, S.T., Dowlati, M.L., Bertodano, M. L., Babelli, I., Wang, W., Pokharna, H., Ransom, V.H., Viskanta, R., Wilmarth, T. "Scientific Design of Purdue University Multi-Dimensional Integral Test Assembly (PUMA) for GE SBWR" NUREG/CR-6309, PU-NE 94/1 (1996)

6. Revankar, S.T., Ishii, M., Mi, Y., Bertodano, M.L. "Instrumentation for the PUMA Integral Test Facility" NUREG/CR-5578, PU/NE-98-3 (1999)

7. Park. H.S. "Steam Condensation Heat Transfer in the Presence of Noncondensables in a Vertical Tube of Passive Containment Cooling System" Ph.D. thesis, KAIST. (1999)

8. Leonardi, T. "Condensation Heat Transfer Analysis of the Passive Containment Cooling System of the Purdue University Multi-Dimensional Integral Test Assembly" Ph.D thesis Purdue University (2000)

9. Revankar, S.T., Ishii, M,. Xu, Y. Zheng. D, Leonardi T., Bertodano, M.L., Ransom V.H., "Data Report on Puma Large Break Local Main Steam Line Break Integral Tests" NUREG/CR-6727, Vol. 3, PU/NE-00-24 (2000)

10. "ESBWR Design Description", GE proprietary information, NEDC-33084P (2002)

11. Oh, S.M. " Experimental and Analytical Study of the Effects of Noncondensable Gas in a Passive Condenser System" Ph.D thesis Purdue University (2004)

Appendix A. List of Instruments

Table A.1 Thermocouples

TAG NUMBER	COMPONENT	INSTRUMENT	RANGE	UNCERTAINTY
TE-AL-01	AIR LINE INLET	Type K TC	0-250°C	2.2°C
TE-RPV-01	VESSEL	Type K TC	0-250°C	2.2°C
TE-RPV-02	VESSEL	Type K TC	0-250°C	2.2°C
TE-RPV-33	VESSEL	Type K TC	0-250°C	2.2°C
TE-MSB-01	STEAM LINE	Type K TC	0-250°C	2.2°C
TE-DW-03	DRYWELL	Type K TC	0-250°C	2.2°C
TE-DW-04	DRYWELL	Type K TC	0-250°C	2.2°C
TE-DW-10	DRYWELL	Type K TC	0-250°C	2.2°C
TE-DW-11	DRYWELL	Type K TC	0-250°C	2.2°C
TE-SP-01	WETWELL	Type K TC	0-250°C	2.2°C
TE-SP-02	WETWELL	Type K TC	0-250°C	2.2°C
TE-SP-03	WETWELL	Type K TC	0-250°C	2.2°C
TE-SP-06	WETWELL	Type K TC	0-250°C	2.2°C
TE-SP-12	WETWELL	Type K TC	0-250°C	2.2°C
TE-SP-13	WETWELL	Type K TC	0-250°C	2.2°C
TE-SP-14	WETWELL	Type K TC	0-250°C	2.2°C
TE-PCA-01	PCCS	Type K TC	0-250°C	2.2°C
TE-PCA-02	PCCS	Type K TC	0-250°C	2.2°C
TE-PCA-04	PCCS	Type K TC	0-250°C	2.2°C
TE-PCA-05	PCCS	Type K TC	0-250°C	2.2°C
TE-PCA-06	PCCS	Type K TC	0-250°C	2.2°C
TE-PCA-07	PCCS	Type K TC	0-250°C	2.2°C
TE-PCA-08	PCCS	Type K TC	0-250°C	2.2°C
TE-PCA-09	PCCS	Type K TC	0-250°C	2.2°C
TE-PCA-10	PCCS	Type K TC	0-250°C	2.2°C
TE-PCA-11	PCCS	Type K TC	0-250°C	2.2°C
TE-PCA-12	PCCS	Type K TC	0-250°C	2.2°C
TE-PCA-13	PCCS	Type K TC	0-250°C	2.2°C
TE-PCA-14	PCCS	Type K TC	0-250°C	2.2°C
TE-PCB-01	PCCS	Type K TC	0-250°C	2.2°C
TE-PCB-02	PCCS	Type K TC	0-250°C	2.2°C
TE-PCB-03	PCCS	Type K TC	0-250°C	2.2°C
TE-PCB-04	PCCS	Type K TC	0-250°C	2.2°C

TAG NUMBER	COMPONENT	INSTRUMENT	RANGE	UNCERTAINTY
TE-PCB-05	PCCS	Type K TC	0-250°C	2.2°C
TE-PCB-06	PCCS	Type K TC	0-250°C	2.2°C
TE-PCB-07	PCCS	Type K TC	0-250°C	2.2°C
TE-PCB-08	PCCS	Type K TC	0-250°C	2.2°C
TE-PCB-09	PCCS	Type K TC	0-250°C	2.2°C
TE-PCB-10	PCCS	Type K TC	0-250°C	2.2°C
TE-PCB-11	PCCS	Type K TC	0-250°C	2.2°C
TE-PCB-12	PCCS	Type K TC	0-250°C	2.2°C
TE-PCB-13	PCCS	Type K TC	0-250°C	2.2°C
TE-PCB-14	PCCS	Type K TC	0-250°C	2.2°C
TE-PCC-01	PCCS	Type K TC	0-250°C	2.2°C
TE-PCC-02	PCCS	Type K TC	0-250°C	2.2°C
TE-PCC-03	PCCS	Type K TC	0-250°C	2.2°C
TE-PCC-04	PCCS	Type K TC	0-250°C	2.2°C
TE-PCC-05	PCCS	Type K TC	0-250°C	2.2°C
TE-PCC-06	PCCS	Type K TC	0-250°C	2.2°C
TE-PCC-07	PCCS	Type K TC	0-250°C	2.2°C
TE-PCC-08	PCCS	Type K TC	0-250°C	2.2°C
TE-PCC-10	PCCS	Type K TC	0-250°C	2.2°C
TE-PCC-11	PCCS	Type K TC	0-250°C	2.2°C
TE-PCC-12	PCCS	Type K TC	0-250°C	2.2°C
TE-PCC-13	PCCS	Type K TC	0-250°C	2.2°C
TE-PCC-14	PCCS	Type K TC	0-250°C	2.2°C

Table A.2 Level, Pressure & Flow Meters

TAG NUMBER	COMPONENT	INSTRUMENT	UNIT	UNCERTAINTY
LT-RPV-14	VESSEL	Differential Pressure Gauge	kPa	0.23
PT-RPV-01	VESSEL	Absolute Pressure Transducer	kPa	4.80
PT-RPV-02	VESSEL	Absolute Pressure Transducer	kPa	3.20
FT-MSB-02	MSL	Vortex Flow Meter	kg/h	63.22
LT-DW-01	DRYWELL	Differential Pressure Gauge	kPa	2.20
PT-DW-02	DRYWELL	Absolute Pressure Transducer	kPa	2.20
PT-DW-04	DRYWELL	Differential Pressure Gauge	kPa	0.17
LT-SP-01	WETWELL	Differential Pressure Gauge	kPa	0.10
LT-SP-03	WETWELL	Differential Pressure Gauge	kPa	0.10
PT-SP-01	WETWELL	Absolute Pressure Transducer	kPa	1.60
FT-PCA-01	PCCS	Vortex Flow Meter	m^3/h	3.40
FT-PCA-03	PCCS	Magnetic Flow Meter	m^3/h	0.01
FT-PCB-01	PCCS	Vortex Flow Meter	m^3/h	3.40
FT-PCB-02	PCCS	Magnetic Flow Meter	m^3/h	0.01
FT-PCC-01	PCCS	Vortex Flow Meter	m^3/h	3.40
FT-PCC-02	PCCS	Magnetic Flow Meter	m^3/h	0.01
LT-PCA-02	PCCS	Differential Pressure Gauge	kPa	0.46
LT-PCB-02	PCCS	Differential Pressure Gauge	kPa	0.46
LT-PCC-02	PCCS	Differential Pressure Gauge	kPa	0.46
LT-PC-03	PCCS	Differential Pressure Gauge	kPa	0.10
LT-PCR-01	PCCS DRAIN TANK	Differential Pressure Gauge	kPa	0.10

Appendix B. Instrument Locations

Table B.1 Thermocouple Locations

TAG NAME	RADIAL (mm)	HEIGHT (mm)	MEASUREMENT	DRAWING NO
TE-AL-01	-	-	AIR TEMPERATURE	Figure 2.1
TE-RPV-01	0	5525	CORE TEMP	Figure B.2
TE-RPV-02	0	5525	CORE TEMP	Figure B.2
TE-RPV-33	276	4000	CORE TEMP	Figure B.2
TE-MSB-01	-	-	TEMPERATURE	Figure 2.2
TE-DW-03	800	6170	TEMPERATURE	Figure B.6
TE-DW-04	425	4091	TEMPERATURE	Figure B.6
TE-DW-10	800	6425	TEMPERATURE	Figure B.6
TE-DW-11	800	5982	TEMPERATURE	Figure B.6
TE-SP-01	700	3004	GAS TEMP	Figure B.8
TE-SP-02	700	2800	GAS TEMP	Figure B.8
TE-SP-03	700	2597	GAS TEMP	Figure B.8
TE-SP-06	818	1199	GAS TEMP	Figure B.8
TE-SP-12	991	1603	GAS TEMP	Figure B.8
TE-SP-13	457	1603	GAS TEMP	Figure B.8
TE-SP-14	762	1603	GAS TEMP	Figure B.8
TE-PCA-01	-	-	INLET TEMP	Figure B.4
TE-PCA-02	562	1003	POOL TEMP	Figure B.4
TE-PCA-04	562	505	POOL TEMP	Figure B.4
TE-PCA-05	562	254	POOL TEMP	Figure B.4
TE-PCA-06	-	745	CONDENSER TEMP	Figure B.4
TE-PCA-07	-	580	CONDENSER TEMP	Figure B.4
TE-PCA-08	-	415	CONDENSER TEMP	Figure B.4
TE-PCA-09	-	745	COND TUBE TEMP	Figure B.4
TE-PCA-10	-	580	COND TUBE TEMP	Figure B.4
TE-PCA-11	-	415	COND TUBE TEMP	Figure B.4
TE-PCA-12	-	-	CONDENSATE TEMP	Figure B.4
TE-PCA-13	-	-	NC GAS VENT TEMP	Figure B.4
TE-PCA-14	-	-	CONDENSATE TEMP	Figure B.4
TE-PCB-01	-	-	INLET TEMP	Figure B.4
TE-PCB-02	562	1003	POOL TEMP	Figure B.4
TE-PCB-03	562	753	POOL TEMP	Figure B.4
TE-PCB-04	562	505	POOL TEMP	Figure B.4

TAG NAME	RADIAL (mm)	HEIGHT (mm)	MEASUREMENT	DRAWING NO
TE-PCB-05	562	254	POOL TEMP	Figure B.4
TE-PCB-06	-	745	CONDENSER TEMP	Figure B.4
TE-PCB-07	-	580	CONDENSER TEMP	Figure B.4
TE-PCB-08	-	415	CONDENSER TEMP	Figure B.4
TE-PCB-09	-	745	COND TUBE TEMP	Figure B.4
TE-PCB-10	-	580	COND TUBE TEMP	Figure B.4
TE-PCB-11	-	415	COND TUBE TEMP	Figure B.4
TE-PCB-12	-	-	CONDENSATE TEMP	Figure B.4
TE-PCB-13	-	-	NC GAS VENT TEMP	Figure B.4
TE-PCC-01	-	-	INLET TEMP	Figure B.4
TE-PCC-02	562	1003	POOL TEMP	Figure B.4
TE-PCC-03	562	753	POOL TEMP	Figure B.4
TE-PCC-04	562	505	POOL TEMP	Figure B.4
TE-PCC-05	562	254	POOL TEMP	Figure B.4
TE-PCC-06	-	745	CONDENSER TEMP	Figure B.4
TE-PCC-07	-	580	CONDENSER TEMP	Figure B.4
TE-PCC-08	-	415	CONDENSER TEMP	Figure B.4
TE-PCC-10	-	580	COND TUBE TEMP	Figure B.4
TE-PCC-11	-	415	COND TUBE TEMP	Figure B.4
TE-PCC-12	-	-	CONDENSATE TEMP	Figure B.4
TE-PCC-13	-	-	NC GAS VENT TEMP	Figure B.4
TE-PCC-14	-	-	CONDENSATE TEMP	Figure B.4

Table B.2 Instruments Locations

TAG NUMBER	RADIAL (mm)	HEIGHT (mm)	MEASRUEMENT	DRAWING NO
LT-RPV-14	300	108-6153	DOWNCOMER LEVEL	Figure B.1
PT-RPV-01	-	-	STEAM DOME PRESSURE	Figure B.1
PT-RPV-02	-	-	STEAM DOME PRESSURE	Figure B.1
FT-MSB-02	-	-	FLOW RATE (VORTEX)	Figure 2.2
LT-DW-01	-	-	LEVEL	Figure B.5
PT-DW-02	-	7150	PRESSURE	Figure B.5
PT-DW-04	-	-	DRYWELL-WETWELL DP	Figure B.5
LT-SP-01	-	0-3180	LEVEL	Figure B.7
LT-SP-03	-	-	VENT LEVEL	Figure B.7
PT-SP-01	868	3182	PRESSURE	Figure B.7
FT-PCA-01	-	-	FLOW RATE (VORTEX)	Figure B.10
FT-PCA-03	-	-	CONDENSATE FLOW	Figure 2.1
FT-PCB-01	-	-	FLOW RATE (VORTEX)	Figure 2.1
FT-PCB-02	-	-	CONDENSATE FLOW	Figure 2.1
FT-PCC-01	-	-	FLOW RATE (VORTEX)	Figure 2.1
FT-PCC-02	-	-	CONDENSATE FLOW	Figure 2.1
LT-PCA-02	-	-	DP between DW and WW	Figure B.3
LT-PCB-02	-	-	DP between DW and WW	Figure B.3
LT-PCC-02	-	-	DP between DW and WW	Figure B.3
LT-PC-03	-	-	TANK LEVEL	Figure B.3
LT-PCR-01	-	-	TANK LEVEL	-

Table B.3 Doubtful and failed instrumentations

TAG NUMBER	COMPONENT	Status
TE-PCB-14	PCCS B drain line	Doubtful reading
TE-PCB-12	PCCS B drain line	Malfunction in some of test data
TE-PCA-03	PCCS A Pool	Fluctuation
TE-PCC-09	PCCS C tube wall	malfunction

Table B.4 Symbols Used in Isometric Drawings

MOTORIZED BALL VALVE

MANUAL BALL VALVE

MANUAL GLOBE VALVE

NOZZLE

VENTURI

MAGNETIC FLOW METER

CAPACITANCE METER

VORTEX FLOW METER

ORIFICE PLATE

THERMOCOUPLE

RESISTANCE TEMPERATURE DEVICE (RTD)

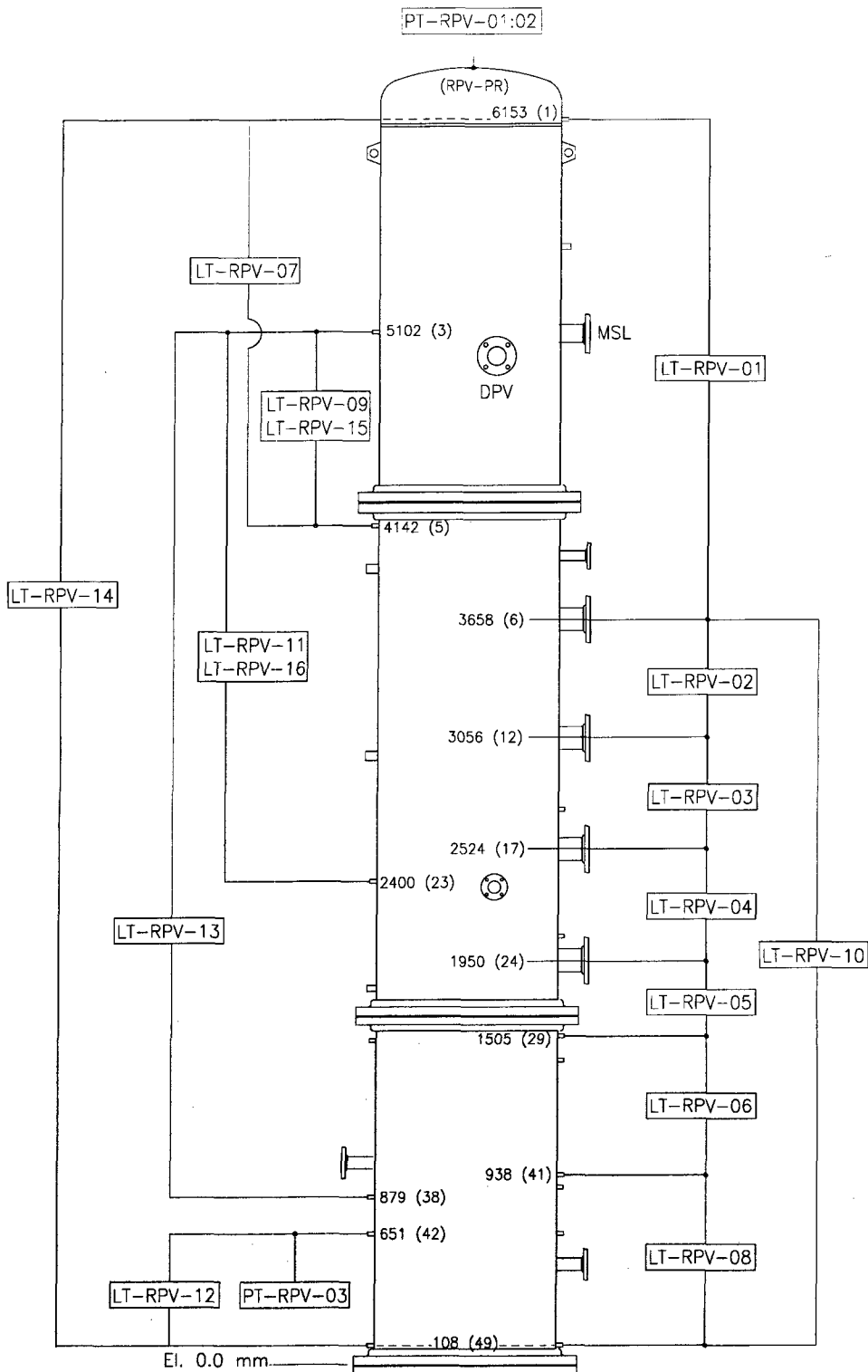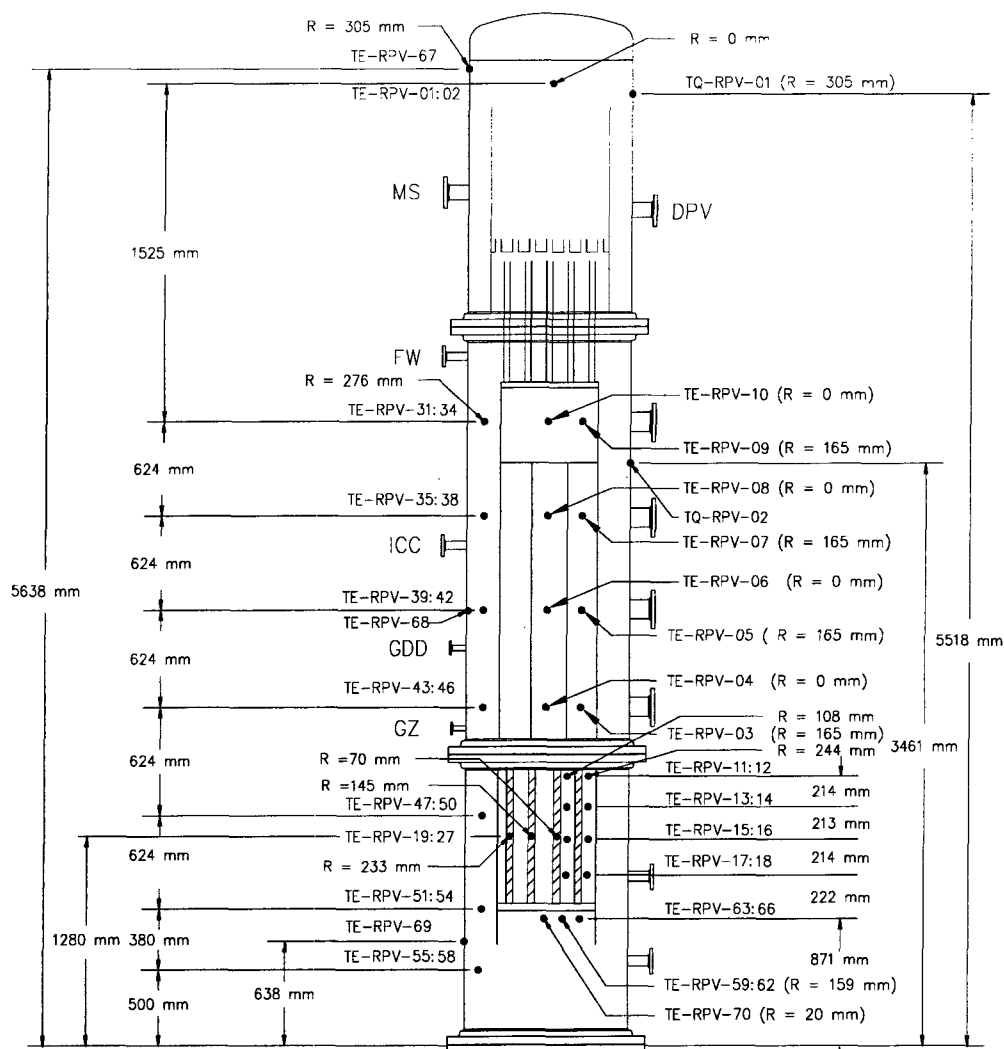CHECK VALVE

LIFT VALVE

FLEXIBLE COUPLING

Figure B.1 RPV Pressure and Level Transmitter Locations

Tag Name	Azimuthal Angle	Tag Name	Azimuthal Angle	Tag Name	Azimuthal Angle
TE-RPV-01	331	TE-RPV-25	151	TE-RPV-52	151
TE-RPV-02	331	TE-RPV-26	259	TE-RPV-53	241
TE-RPV-03	16	TE-RPV-27	97	TE-RPV-54	331
TE-RPV-04	16	TE-RPV-31	61	TE-RPV-55	61
TE-RPV-05	16	TE-RPV-32	151	TE-RPV-56	151
TE-RPV-06	16	TE-RPV-33	241	TE-RPV-57	241
TE-RPV-07	16	TE-RPV-34	331	TE-RPV-58	331
TE-RPV-08	16	TE-RPV-35	61	TE-RPV-59	106
TE-RPV-09	16	TE-RPV-36	151	TE-RPV-60	196
TE-RPV-10	16	TE-RPV-37	241	TE-RPV-61	286
TE-RPV-11	17	TE-RPV-38	331	TE-RPV-62	16
TE-RPV-12	358	TE-RPV-39	61	TE-RPV-63	106
TE-RPV-13	17	TE-RPV-40	151	TE-RPV-64	196
TE-RPV-14	358	TE-RPV-41	241	TE-RPV-65	286
TE-RPV-15	17	TE-RPV-42	331	TE-RPV-66	16
TE-RPV-16	358	TE-RPV-43	61	TE-RPV-67	-
TE-RPV-17	17	TE-RPV-44	151	TE-RPV-68	-
TE-RPV-18	358	TE-RPV-45	241	TE-RPV-69	-
TE-RPV-19	31	TE-RPV-46	331	TE-RPV-70	286
TE-RPV-20	271	TE-RPV-47	61	CQ-RPV-01	241
TE-RPV-21	151	TE-RPV-48	151	CQ-RPV-02	151
TE-RPV-22	151	TE-RPV-49	241	CQ-RPV-03	151
TE-RPV-23	31	TE-RPV-50	331	TQ-RPV-01	241
TE-RPV-24	271	TE-RPV-51	61	TQ-RPV-02	151

Figure B.2 RPV Thermocouple & Heat Flux Sensor Locations
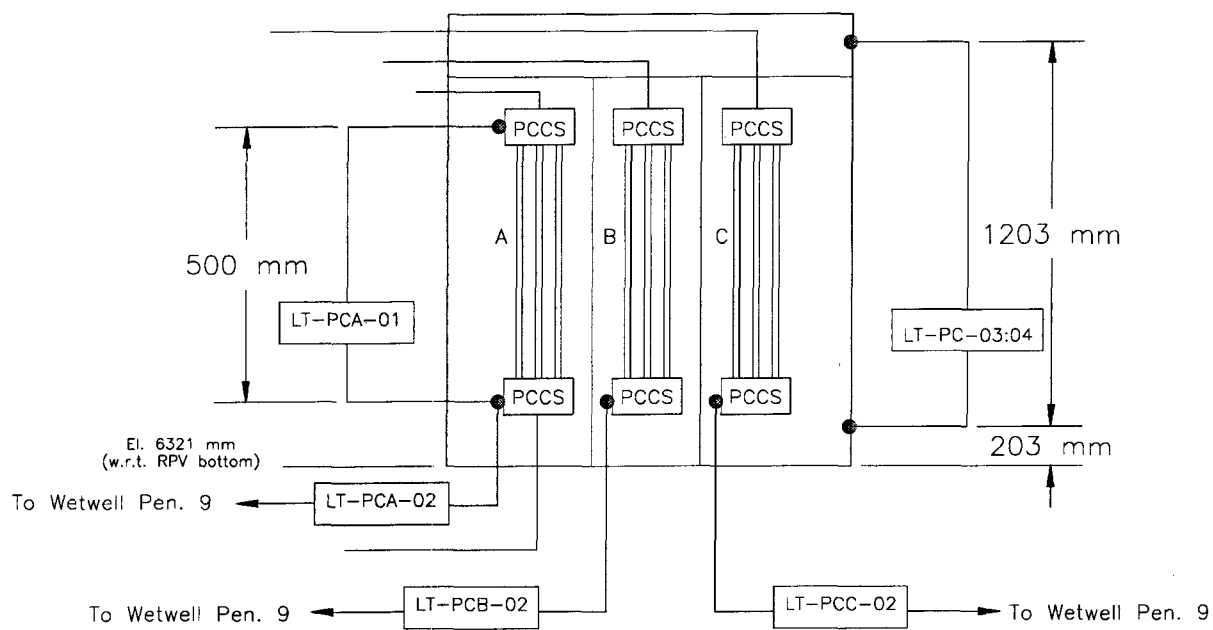
Figure B.3 PCCS Pressure and Level Transmitter Locations

TE—PCX ——> X = A, B, or C condensers
TE—PCX—02,03,04,05 ———> water temperature in pool
TE—PCX—06,07,08 ———> fliud temperature at the centerline of tube
TE—PCX—09,10,11 ———> outer surface temperature of tube

R = 562 mm

TE—PCX—01

TE—PCX—02

TE—PCX—03

TE—PCX—04

TE—PCX—05

El. 6321 mm
(w.r.t. RPV bottom)

1003 mm
753 mm
505 mm
254 mm

A   B   C

PCCS   PCCS   PCCS

PCCS   PCCS   PCCS

TE—PCX—09
TE—PCX—06
TE—PCX—10
TE—PCX—07
TE—PCX—11
TE—PCX—08

814 mm
745 mm
580 mm
415 mm
364 mm

TE—PCX—12

50.8 mm **OD**

47.5 mm **ID**

Thermocouple

Cross—sectional view of tube

Figure B.4 PCCS Thermocouple Locations

B-8
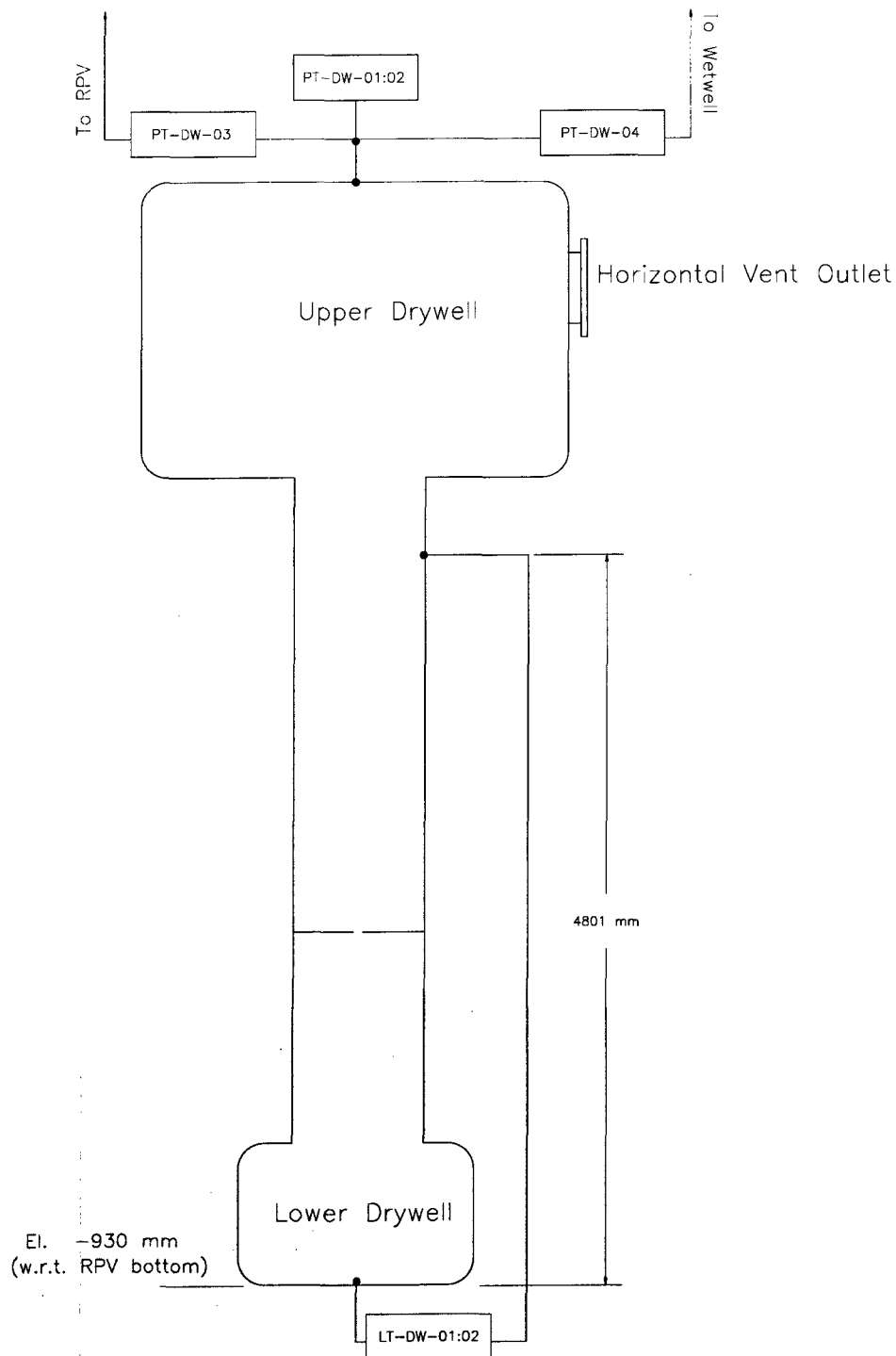
Figure B.5 Drywell Pressure and Level Transmitter Locations

Figure B.6 Drywell Thermocouple , Heat Flux Sensor Locations
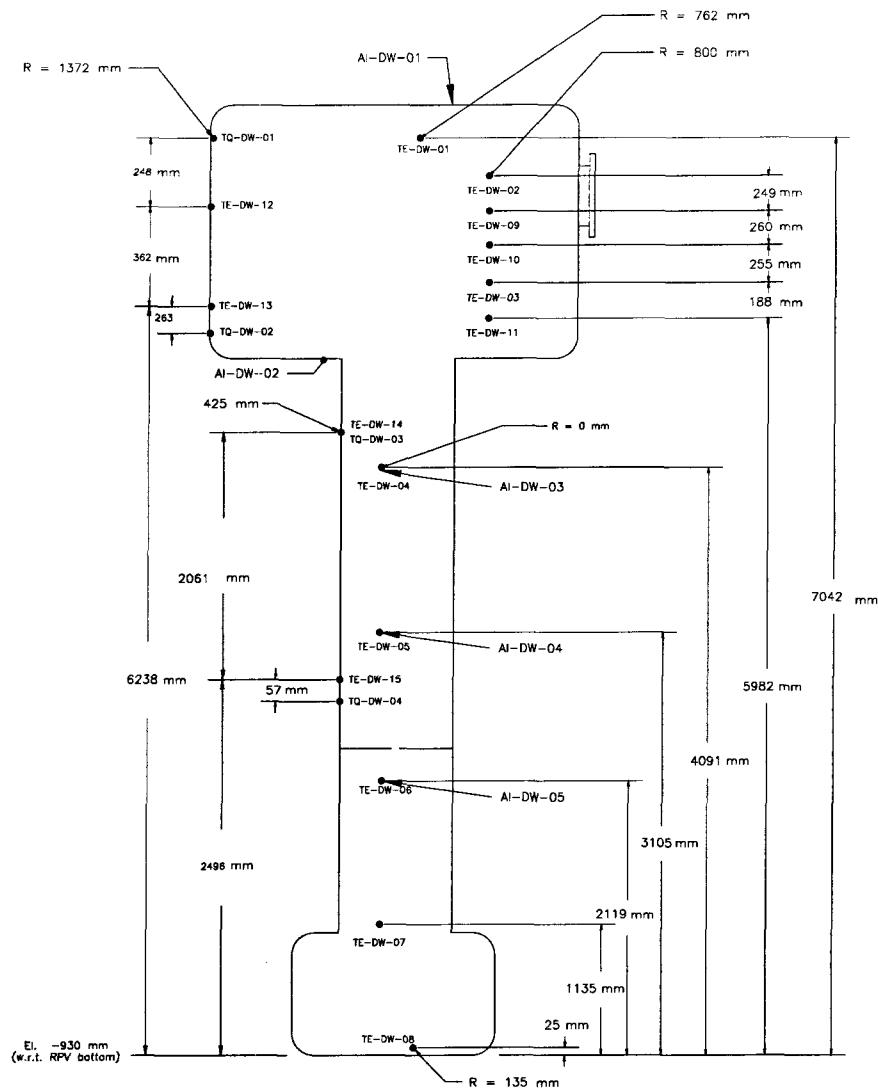
Tag Name	Azimuthal Angle	Tag Name	Azimuthal Angle
TE-DW-01	91	TE-DW-13	286
TE-DW-02	121	TE-DW-14	271
TE-DW-03	121	TE-DW-15	271
TE-DW-04	271	CQ-DW-01	286
TE-DW-05	271	CQ-DW-02	271
TE-DW-06	271	CQ-DW-03	200
TE-DW-07	271	CQ-DW-04	271
TE-DW-08	271	AI-DW-01	181
TE-DW-09	121	AI-DW-02	271
TE-DW-10	121	AI-DW-03	271
TE-DW-11	121	AI-DW-04	271
TE-DW-12	286	AI-DW-05	271
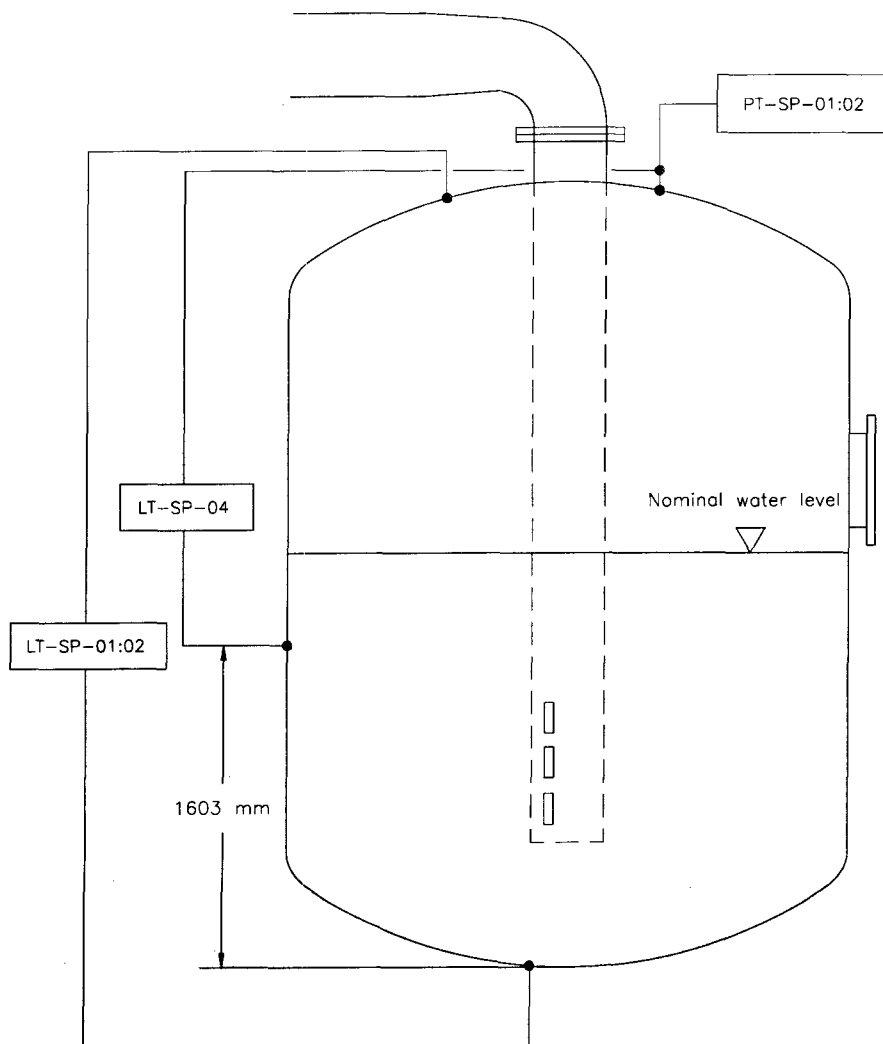
Figure B.7 Wetwell Pressure and Level Transmitter Locations

The following measurements and labels appear in the figure:

- R = 700 mm
- TE-SP-01
- 203 mm
- TE-SP-02
- 203 mm
- TE-SP-03
- 203 mm
- TE-SP-04
- TQ-SP-01
- R = 762 mm
- 261 mm
- R = 457 mm
- TQ-SP-02
- R = 991 mm
- Nominal water level
- R = 818 mm
- TE-SP-12
- TE-SP-13
- TE-SP-14
- TE-SP-05
- 203 mm
- TE-SP-06
- 203 mm
- 2394 mm
- TE-SP-07
- 203 mm
- 2633 mm
- 1603 mm
- TE-SP-08
- 203 mm
- TE-SP-09
- 203 mm
- TE-SP-10
- 387 mm
- El. 894 mm (w.r.t. RPV bottom)
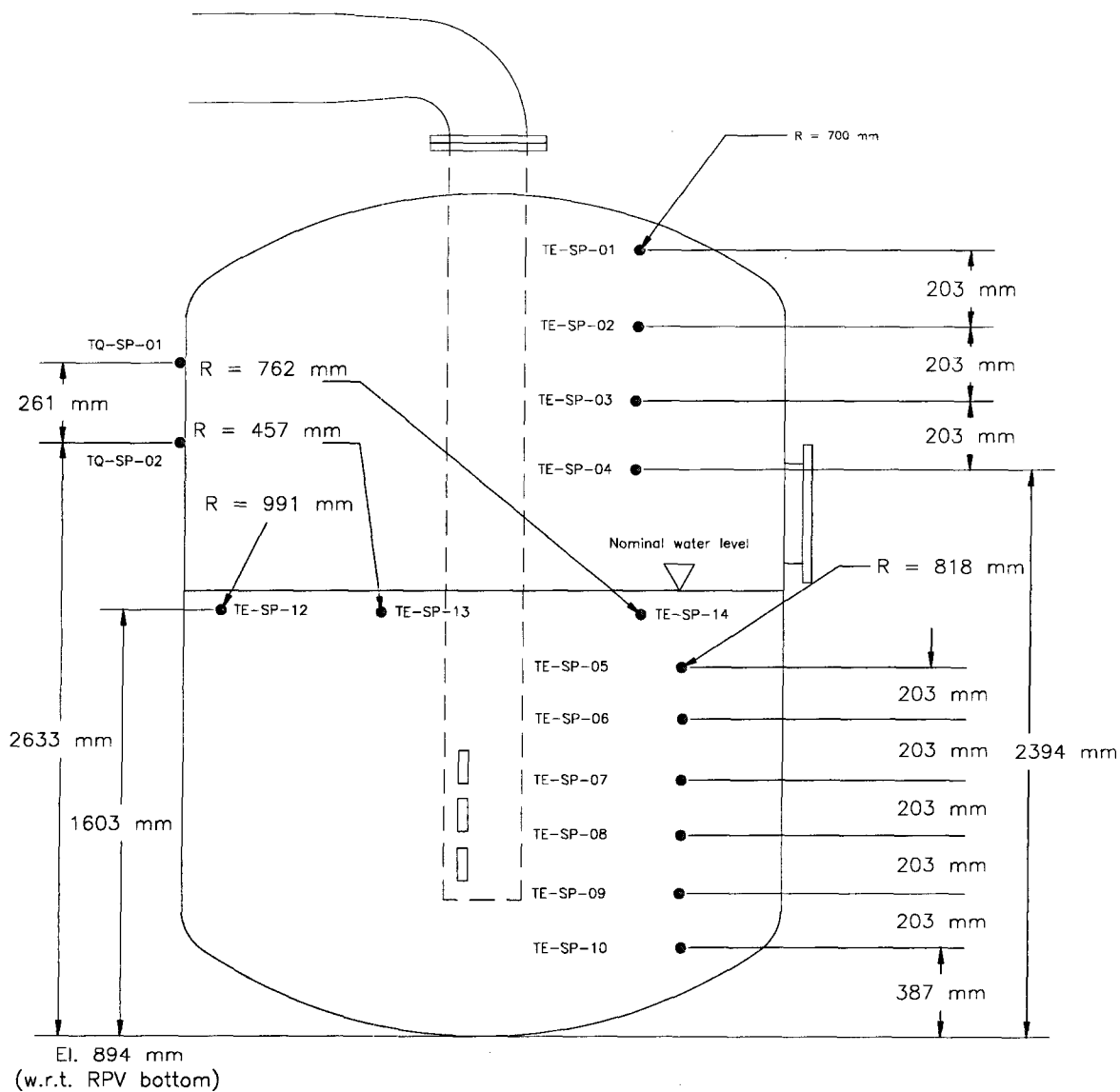
Tag Name	Azimuthal Angle	Tag Name	Azimuthal Angle
TE-SP-01	151	TE-SP-10	91
TE-SP-02	151	TE-SP-11	--
TE-SP-03	151	TE-SP-12	191
TE-SP-04	151	TE-SP-13	316
TE-SP-05	91	TE-SP-14	76
TE-SP-06	91	CQ-SP-01	191
TE-SP-07	91	CQ-SP-02	106
TE-SP-08	91	TQ-SP-01	191
TE-SP-09	91	TQ-SP-02	106

Figure B.8 Wetwell Thermocouple & Heat Flux Sensor Locations

DIMENSIONS IN mm
ALL VALVES 1.5"
PIPE SCHEDULE IS 40
INSULATION — FIBERGLASS
2.25" THICK

PCCS TANK

EL 6321

457

EL 5864

318

45°

45°

0   EL 5639

597

TE-PCA-13   902

ORIFICE PLATE
ID =22.86 MM

1283   V-PCVA-01

1369

1511
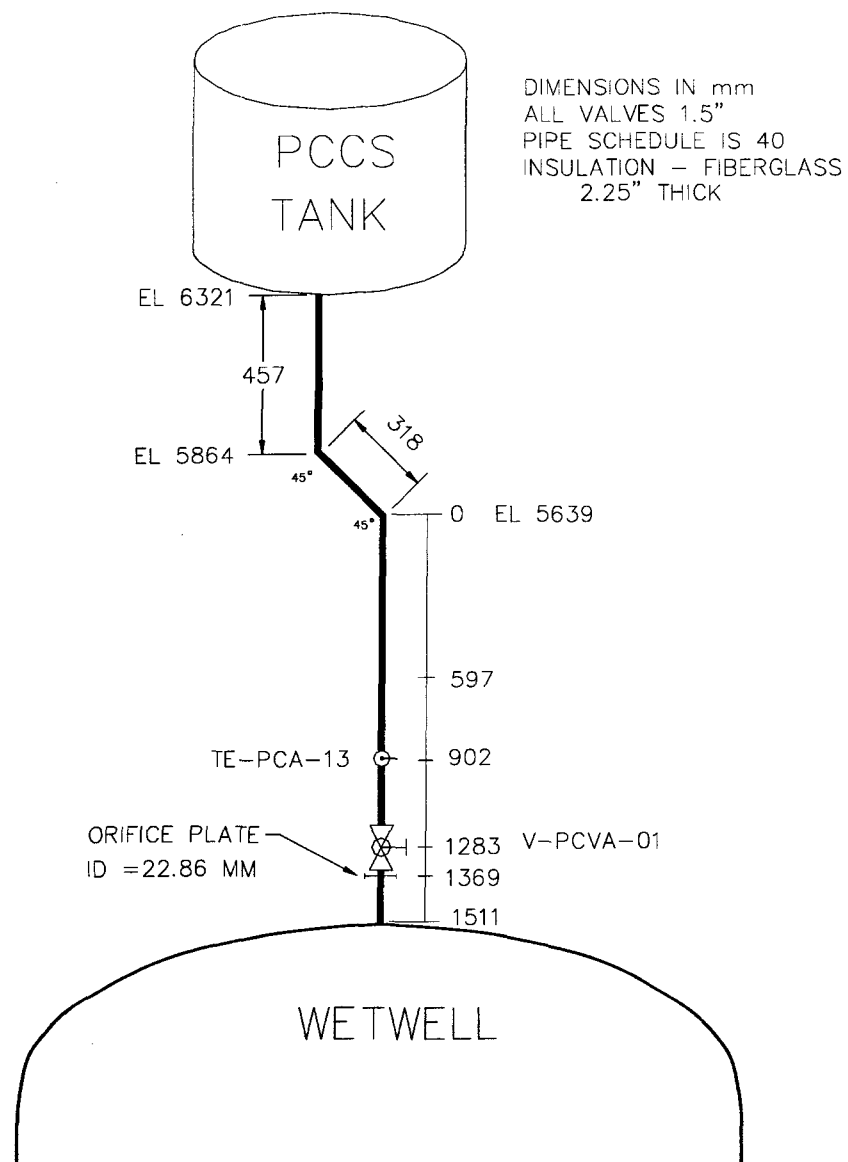
WETWELL

Figure B.9 PCCS Vent PC-VA Line from the PCCS Pool to Wetwell

PCCS CONDENSER

EL 6.321

457

EL 5.864   45°

152

45°   0 EL 5.757

TE-PCB-13   978

1372   V-PCVB-01

ORIFICE PLATE   1458

1638

DIMENSIONS IN mm
ALL VALVES 1.5"
PIPE SCHEDULE IS 40
INSULATION — FIBERGLASS
2.25" THICK
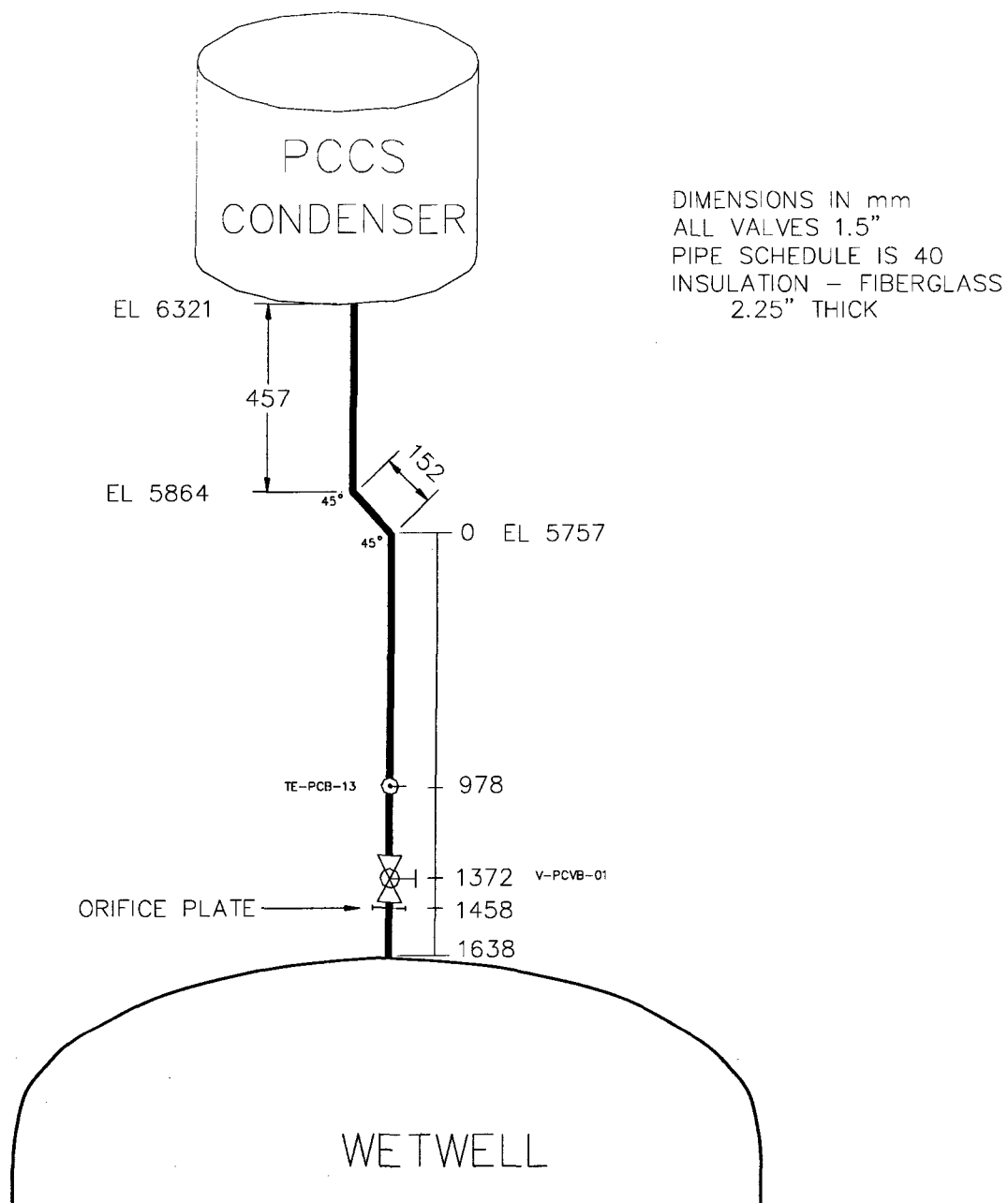
WETWELL

Figure B.10 PCCS Vent PC-VB Line from the PCCS Pool to Wetwell

PCCS CONDENSER

DIMENSIONS IN mm
ALL VALVES 1.5"
PIPE SCHEDULE IS 40
INSULATION — FIBERGLASS
2.25" THICK

EL 6321

457

940

0   EL 5864

90°   90°

TE-PCC-13   1092

1486   V-PCVC-01

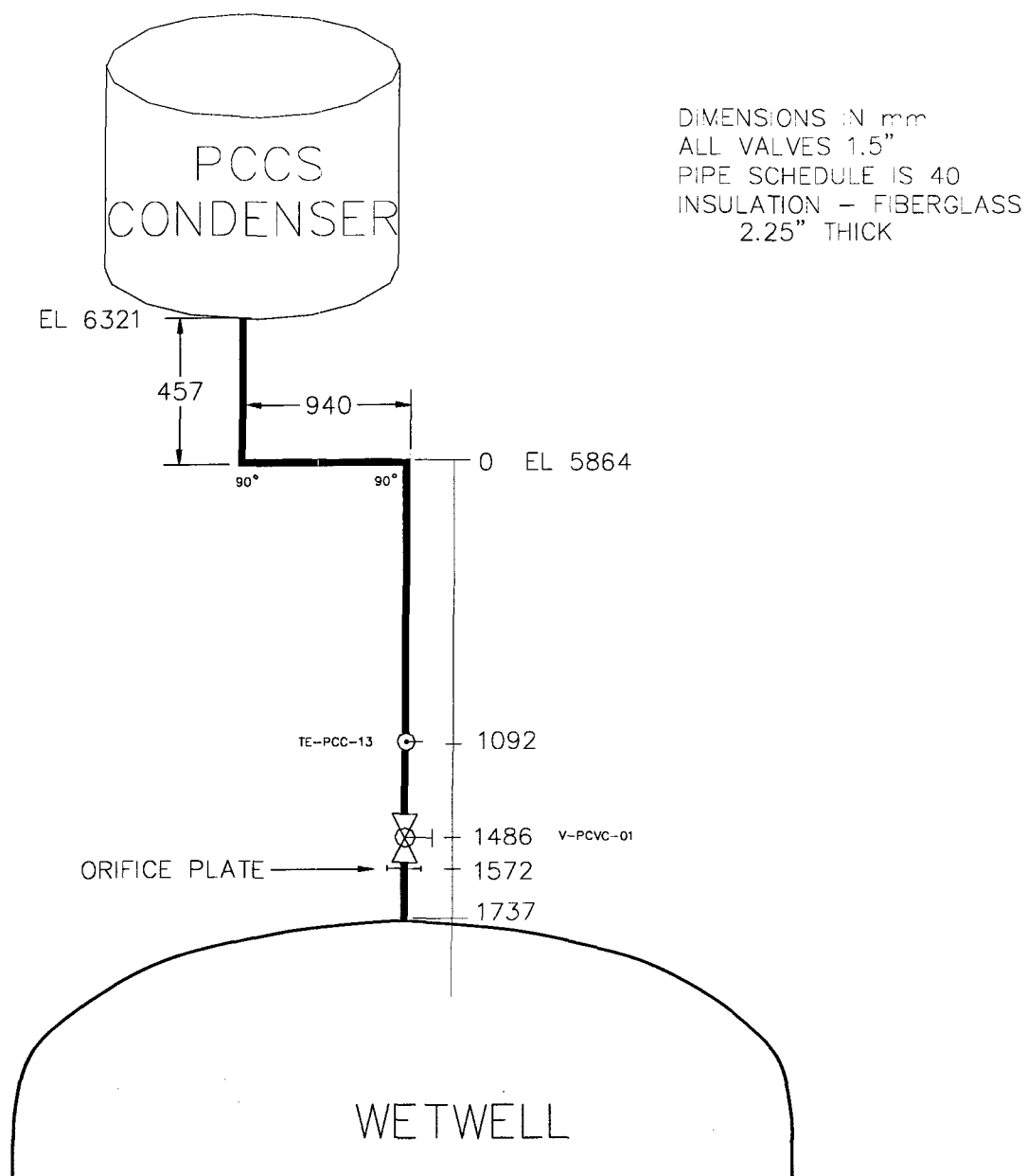ORIFICE PLATE   1572

1737

WETWELL

Figure B.11 PCCS Vent PC-VC Line from the PCCS Pool to Wetwell
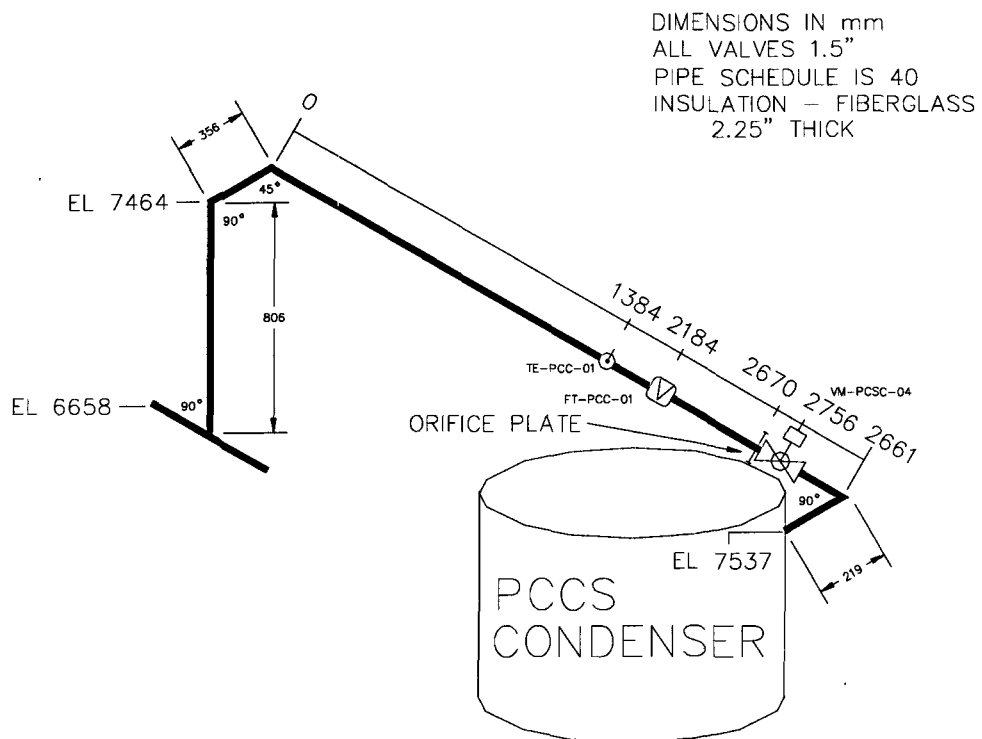
Figure B.12 PCCS Supply A Line from Drywell to the PCCS Pool

DIMENSIONS IN mm
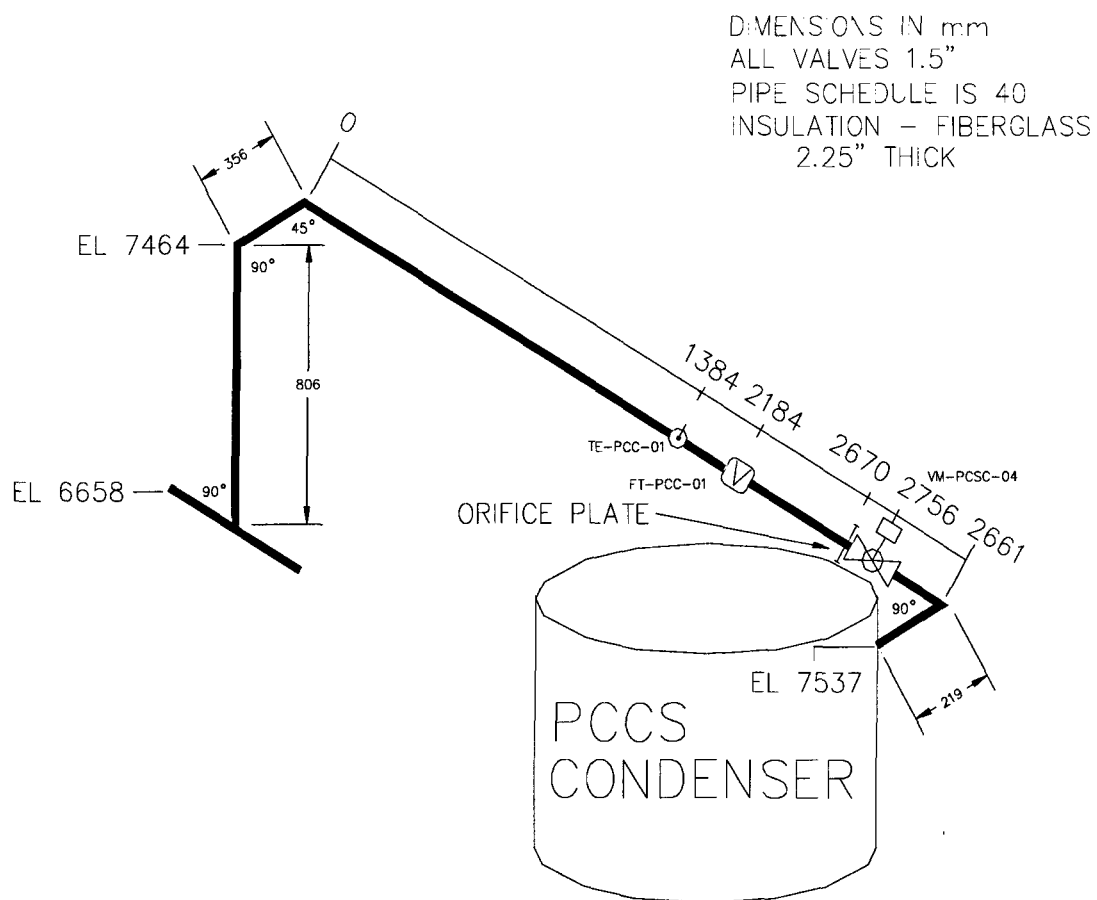ALL VALVES 1.5"
PIPE SCHEDULE IS 40
INSULATION — FIBERGLASS
2.25" THICK

O

356

EL 7464

45°

90°

806

EL 6658

90°

1384 2184

2670 2756 2661

TE-PCC-01

FT-PCC-01

VM-PCSC-04

ORIFICE PLATE

90°

EL 7537

PCCS CONDENSER

219

Figure B.13 PCCS Supply B Line from Drywell to the PCCS Pool

DIMENSIONS IN mm
ALL VALVES 1.5"
PIPE SCHEDULE IS 40
INSULATION — FIBERGLASS
2.25" THICK
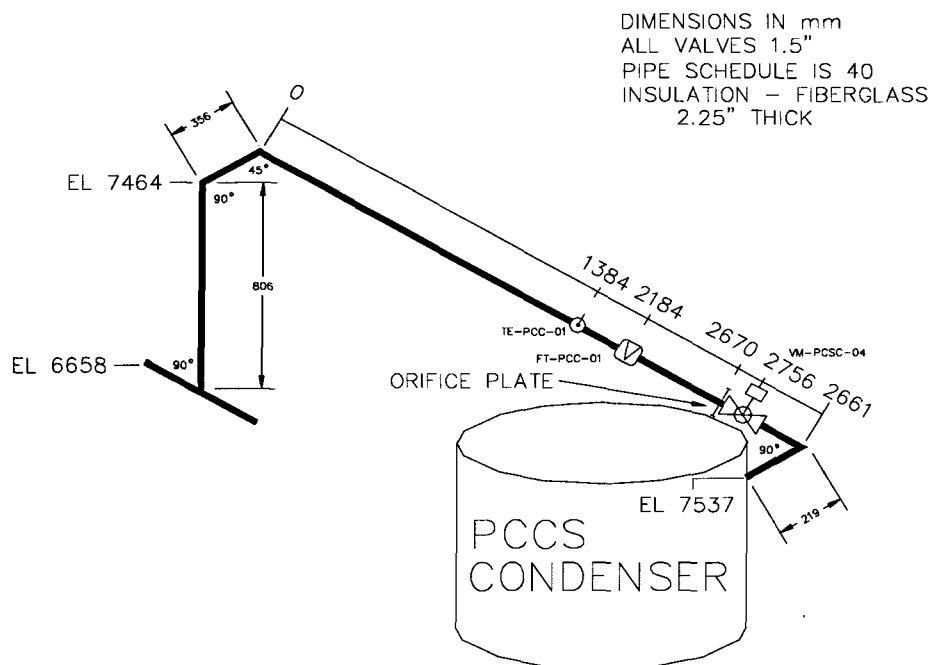
Figure B.14 PCCS Supply C Line from Drywell to the PCCS Pool

DIMENSIONS IN mm
ALL VALVES 1"
INSULATION — FIBERGLASS
     0.5" TUBE — 1.25" THICK
     1" TUBE — 1" THICK
1" TUBING O.D. = 1.0"
          I.D. = 0.86"
0.5" TUBING O.D. = 0.5"
          I.D. = 0.375"

Fig. B-15 1" PC-CA From PCCS Condenser to PCCS Drain Tank

DIMENSIONS IN mm
ALL VALVES 1"
INSULATION — FIBERGLASS
        0.5" TUBE — 1.25" THICK
        1" TUBE — 1" THICK
1" TUBING O.D. = 1.0"
            I.D. = 0.86"
0.5" TUBING O.D. = 0.5"
            I.D. = 0.375"
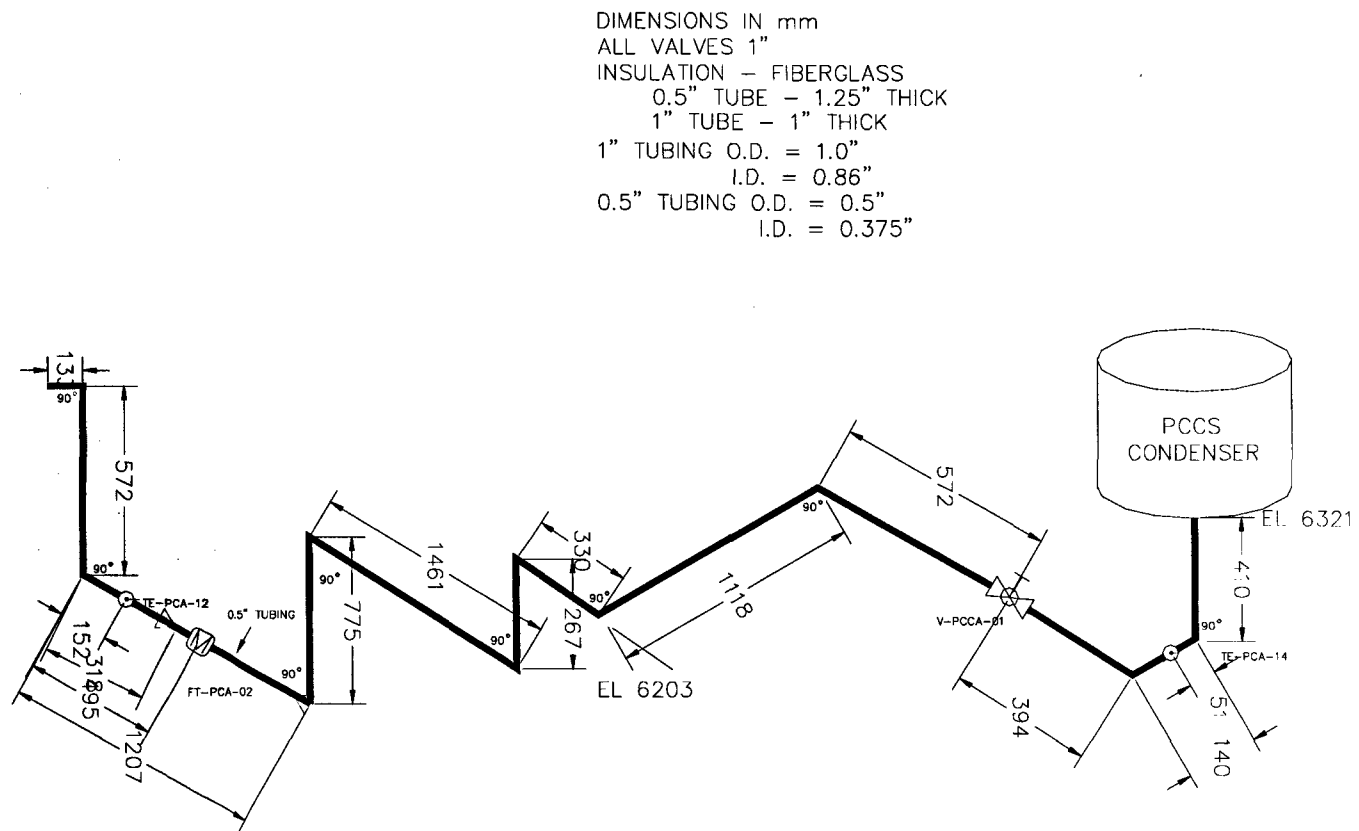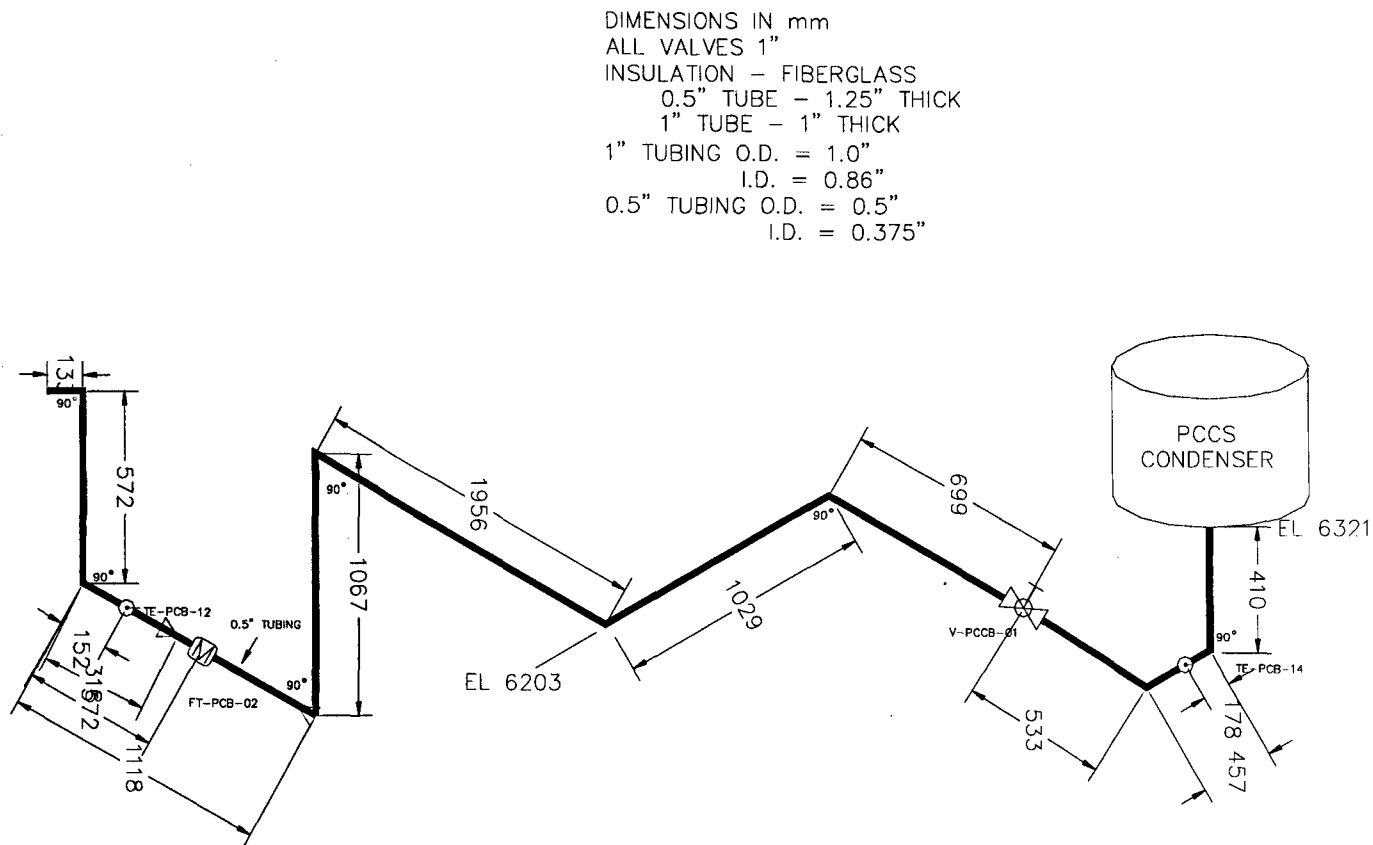
Fig. B-16 1" PC-CB From PCCS Condenser to PCCS Drain Tank

Figure.B.17 1" PC-CC from PCCS Condenser to PCCS Drain Tank

DIMENSIONS IN mm
ALL VALVES 1"
INSULATION — FIBERGLASS
    0.5" TUBE — 1.25" THICK
    1" TUBE — 1" THICK
1" TUBING O.D. = 1.0"
        I.D. = 0.86"
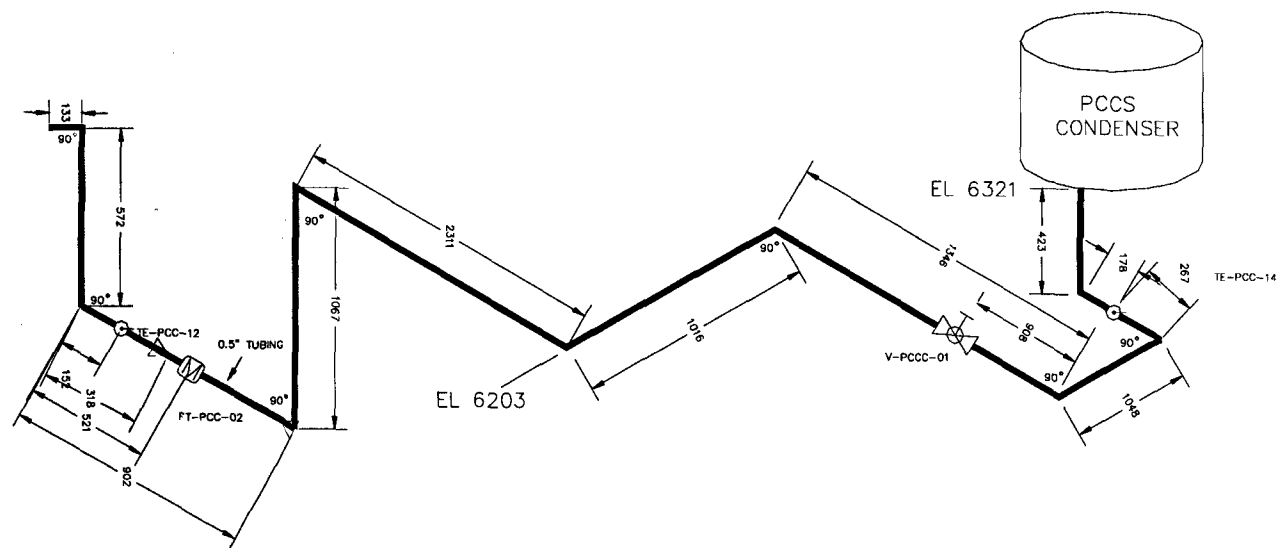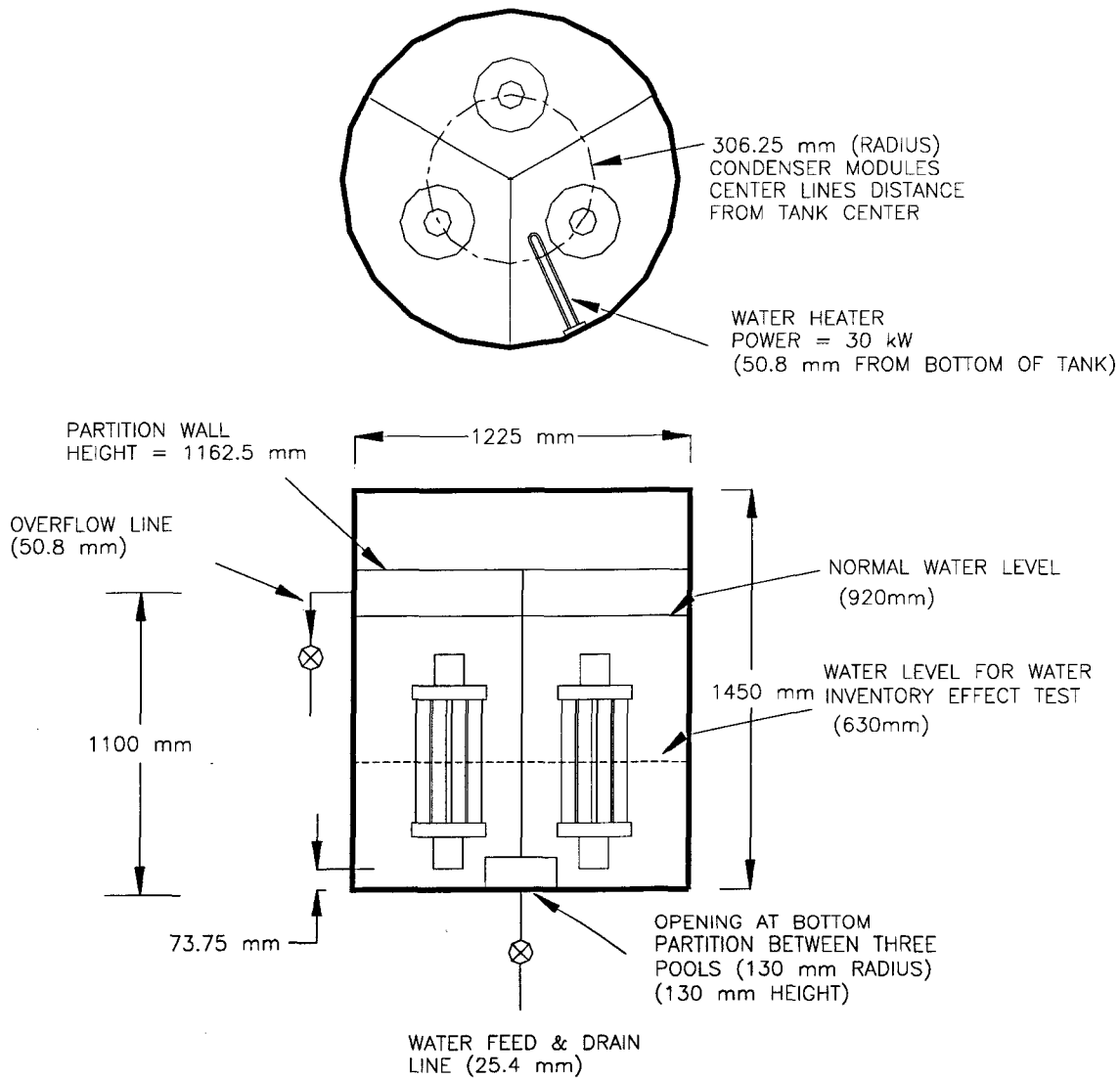0.5" TUBING O.D. = 0.5"
        I.D. = 0.375"

Fig. B-17 1" PC-CC from PCCS Condenser to PCCS Drain Tank

TOP VIEW OF PCCS CONDENSERS TANK

306.25 mm (RADIUS)
CONDENSER MODULES
CENTER LINES DISTANCE
FROM TANK CENTER

WATER HEATER
POWER = 30 kW
(50.8 mm FROM BOTTOM OF TANK)

PARTITION WALL
HEIGHT = 1162.5 mm

1225 mm

OVERFLOW LINE
(50.8 mm)

NORMAL WATER LEVEL
(920mm)

WATER LEVEL FOR WATER
1450 mm INVENTORY EFFECT TEST
(630mm)

1100 mm

73.75 mm

OPENING AT BOTTOM
PARTITION BETWEEN THREE
POOLS (130 mm RADIUS)
(130 mm HEIGHT)

WATER FEED & DRAIN
LINE (25.4 mm)

FRONT VIEW OF PCCS CONDENSERS TANK
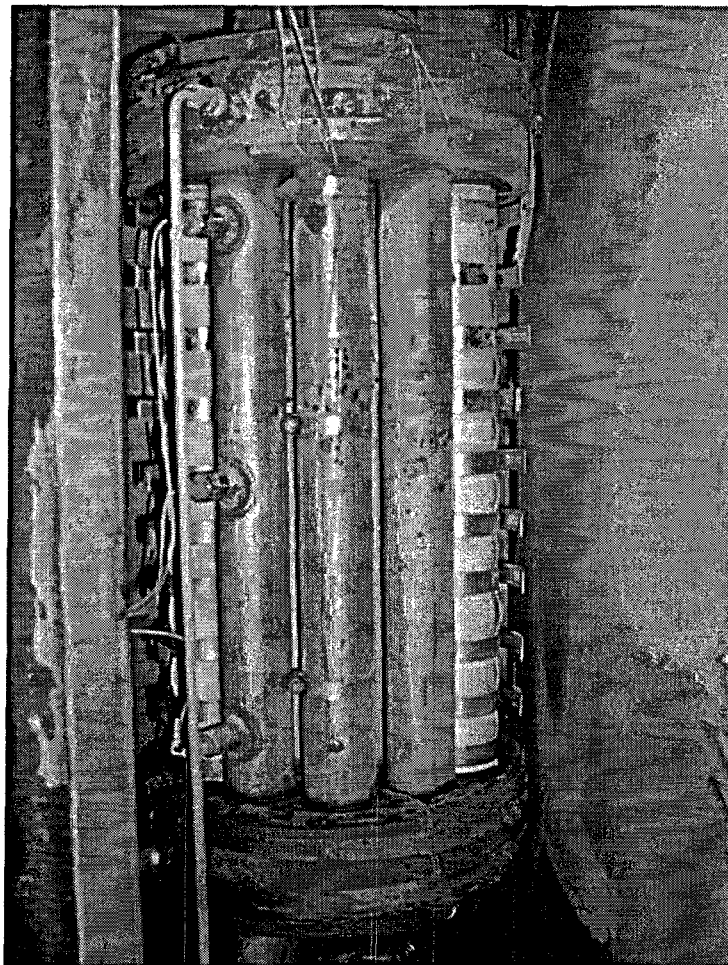
Figure B.18 Design of PUMA PCCS Pools

Figure B.19 Picture of PUMA PCCS-A unit

Appendix C. Data Review Summary

Table C.1 Data review summary

Test No.	$\dot{m}_{msl}$ (kg/Sec)	$\dot{m}_{air}$ (g/sec)	Pressure (kPa)	TE-PCB-12
LM807A	0.025	0.0	200	A
LT912A	0.026	0.0	200	A
LM807B	0.026	0.0	230	A
LT727B	0.027	0.0	230	A
LM807C	0.028	0.0	260	A
LT727C	0.028	0.0	260	A
LT823D	0.028	0.0	300	N/A
LT718B	0.020	0.0	230	A
LT711C	0.021	0.0	260	A
BL721AR	0.070	0.0	220	A
BL723D	0.062	7.5	220	A
BL731BR	0.077	0	260	A
BL723E	0.062	0.0	260	A
BL723C	0.071	0.0	300	A
BL723G	0.055	10.8	300	A
CY602A	0.031	0.0	220	N/A
CY602D	0.032	0.1	220	N/A
CY903D2	0.032	0.6	220	A
CY903D4	0.033	1.3	220	A
CY602B	0.033	0.0	240	N/A
CY602E	0.033	0.1	240	N/A
CY604E2	0.034	0.6	240	N/A
CY903C	0.033	0.0	260	A
CY604F	0.034	0.1	260	N/A
CY602F2	0.034	0.6	260	N/A
CY903F4	0.033	1.3	260	A

CH830A	0.042	0.0	220	A
CH826D2	0.040	0.6	220	N/A
CH826D4	0.040	1.3	220	N/A
CH826E4	0.041	1.3	240	N/A
CH622C	0.039	0.0	240	N/A
CH826F4	0.042	1.3	260	N/A
CM701D	0.031	0.2	220	A
CM701D2	0.030	0.6	220	A
CM810D4	0.027	1.3	220	N/A
CM616E	0.034	0.1	240	A
CM822E2	0.030	0.7	240	N/A
CM707E4	0.029	1.3	240	A
CM810E6	0.027	1.9	240	N/A
CM616C	0.031	0.0	260	A
CM822F2	0.031	0.6	260	N/A

Appendix D. Instrumentation Calibration Results

PCCS - A Drain Line

$y = 1.1944x - 0.0079$
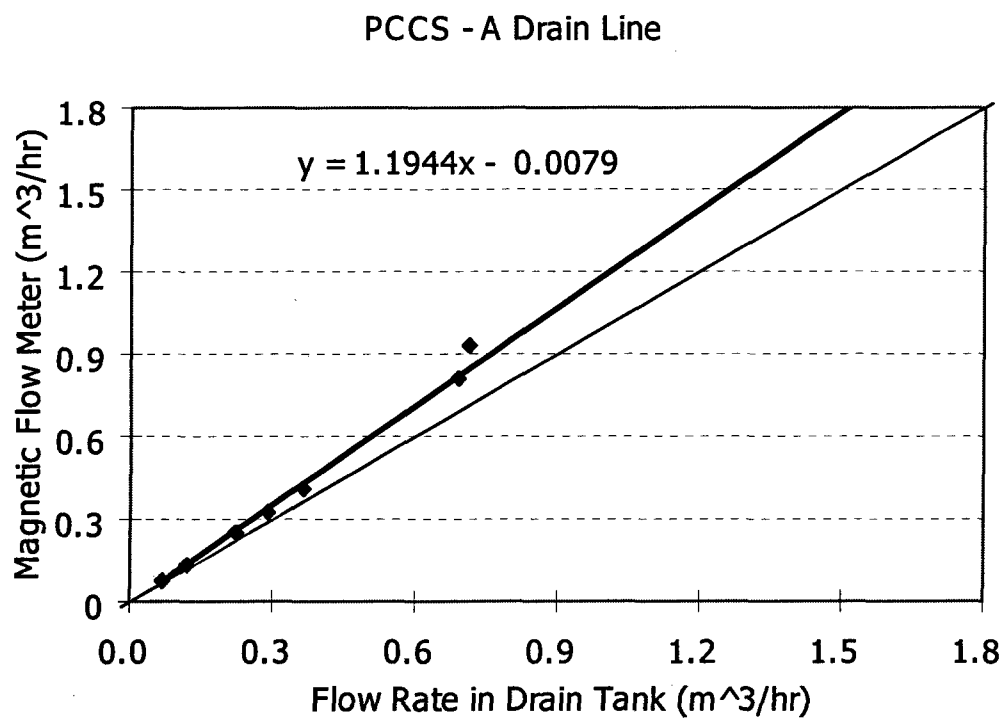
Fig.D.1. Magnetic flow meter calibration in PCCS drain line A

PCCS −B Drain Line

$y = 1.1132x + 0.0066$
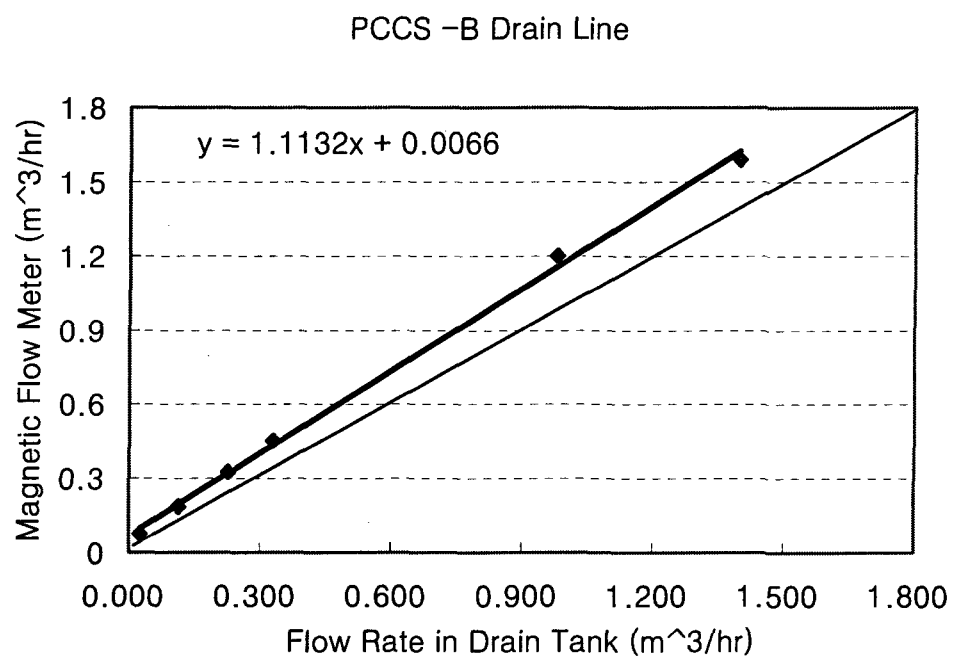
Fig D.2. Magnetic flow meter calibration in PCCS drain line B
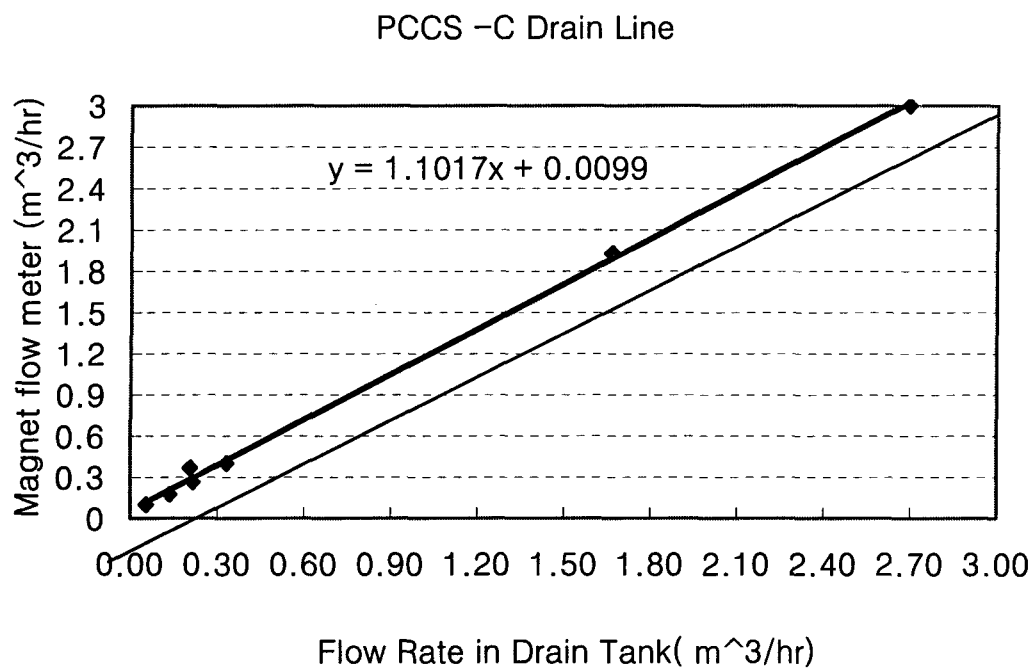
PCCS −C Drain Line

$y = 1.1017x + 0.0099$

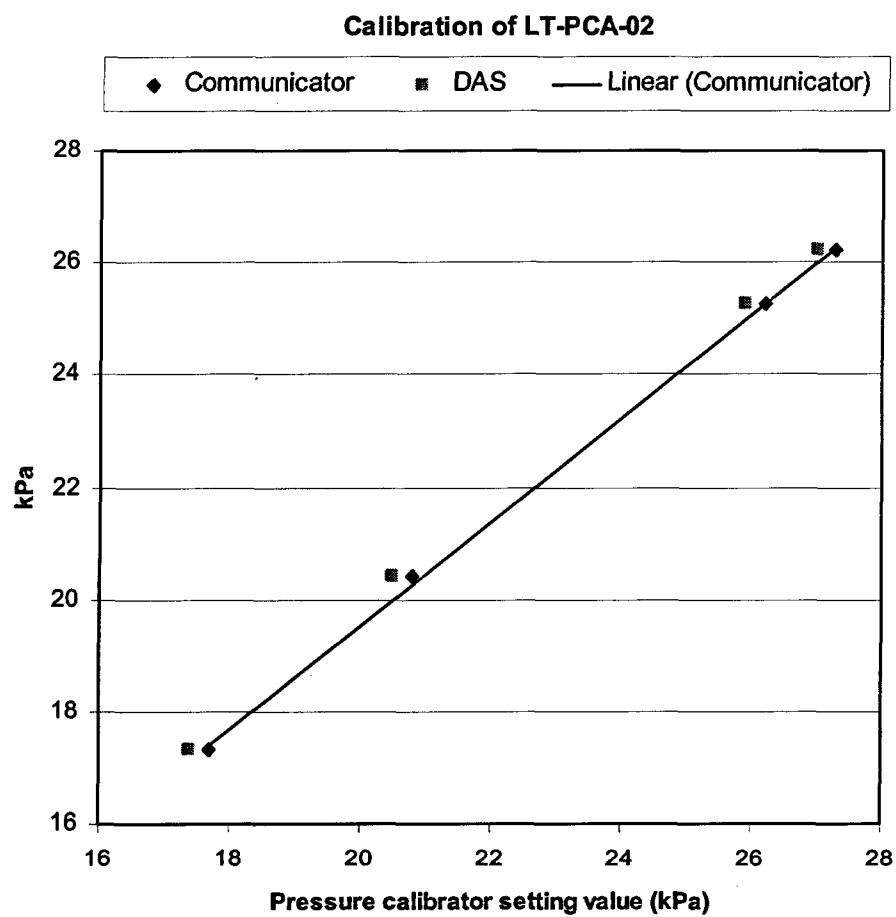Fig D.3. Magnetic flow meter calibration in PCCS drain line C
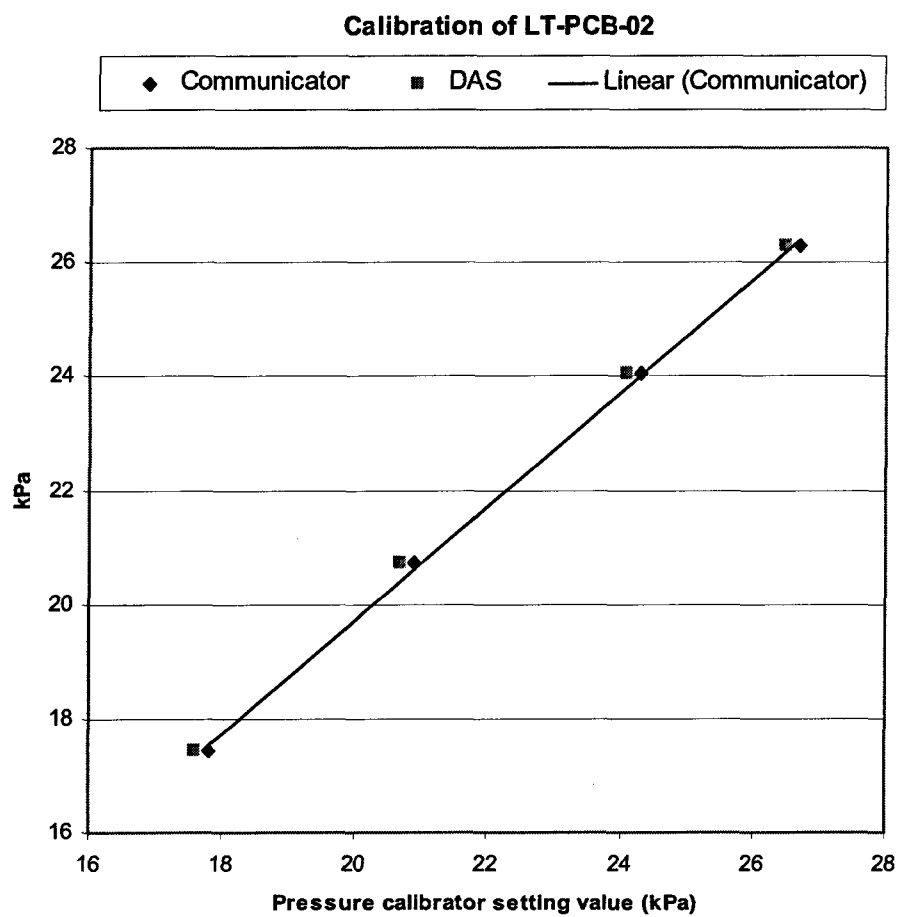
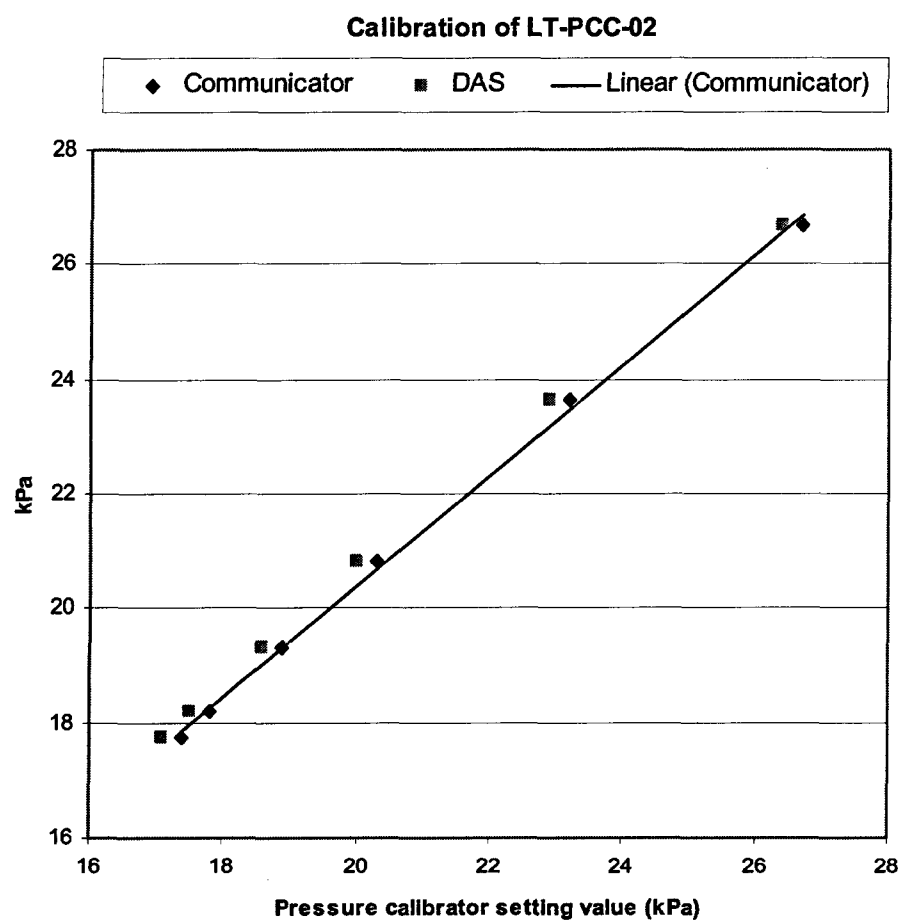Fig D.4. Calibration for LT-PCA-02

Calibration of LT-PCB-02

Fig D.5. Calibration for LT-PCB-02

Fig D.6. Calibration for LT-PCC-02